THE JOURNAL
OF
CHEMICAL PHYSICS

VOLUME 16, NUMBER 2 February, 1948

Target Chemistry of Cesium; Isolation of $Ba^{133,134}$

M. H. KURBATOV, FU-CHUN YU, AND J. D. KURBATOV
The Ohio State University, Columbus 10, Ohio

(Received July 28, 1947)

Barium ($Ba^{133,134}$) obtained by *dn* and *d2n* reactions of spectroscopically pure cesium chloride was separated in quantities of $<1\times10^{-9}$ gram without addition of common barium. The procedure studied involves adsorption of barium on hydrous ferric oxide under conditions at which cesium ions remain in solution. The effect of (a) *p*H of solution and (b) varying quantities of ferric hydrous oxide on the fraction of Ba adsorbed from solution containing $<10^{-9}$ g Ba, keeping other factors constant, showed that the fraction of Ba adsorbed, $y=k[Z(X-X_0)]^{\lambda}$, Z being the quantity of adsorbent (from 1×10^{-5} to 3×10^{-4} g atom Fe); X, the OH^- concentration in solution (from 3×10^{-9} to 3×10^{-6}); X_0, the critical concentration of OH^- necessary to maintain the adsorbent in the solid state. When *p*H was kept constant the value of λ for $y=k'Z^{\lambda}$ was found to be 0.35, and when the quantity of adsorbent was constant the λ for $y=k''(X-X_0)^{\lambda}$ was 0.33. The fact that the two experimental slopes were so nearly the same in spite of certain variations in experimental conditions is taken as support for two assumptions made in the derivation of the expression *viz.*, (1) the fraction of barium adsorbed from a very dilute solution depends on the quantity of adsorptive centers in the solid phase and (2) the quantity of adsorptive centers in the solid phase available for barium adsorption is proportional to the OH^- concentration in solution, other factors being constant. Adsorption procedure is described.

INTRODUCTION

IN previous work it has been shown that absorbents such as hydrous ferric oxide will remove part of such divalent ions as strontium, barium, and radium from their solutions at any feasible low concentration if experimental conditions are appropriate.[1,2]

Consequently it was suggested that chemisorption might be applied first, to isolation, without carriers, of minute quantities of radioactive and stable species produced by nuclear transmutations, from elements of different atomic number and, second, to determination of quantities as low as 1×10^{-11} g atom, that is, quantities less than those measurable by the most sensitive previously known schemes.[3]

The adsorption of divalent ions on hydrous ferric oxide is influenced by such variables as *p*H, salt concentration, quantities of adsorbent and adsorbate, volume of liquid phase, temperature and duration of adsorption. However, the dependence of adsorption of divalent ions in extreme dilution on the above variables is insufficiently known especially for purposes of isolation, without carriers, of species produced by nuclear transmutations.

In the present work a scheme for isolation of $Ba^{133,134}$ (produced by activation of cesium with 10.5-Mev deuterons) in quantities of less than 10^{-9} g has been studied with reference to its dependence on hydrogen ion concentration and quantity of adsorbent.

PROCEDURE

$Ba^{133,134}$ as the chlorides were separated (as described later in this paper) in quantities of less than 10^{-11} g atom from the target material; the

[1] J. D. Kurbatov, J. L. Kulp, and Edward Mack, Jr., J. Am. Chem. Soc. 67, 1923 (1945).
[2] M. H. Kurbatov and J. D. Kurbatov, J. Am. Chem. Soc. 69, 438 (1947).
[3] M. H. Kurbatov and J. D. Kurbatov, Phys. Rev. 71, 466 (1947).

TABLE I.

Fe g atom./exp.	0.1 N HCl ml	Water ml	1 N NH_4OH ml	0.1 N NH_4OH ml
6×10^{-4}	0.0	23.0	1.50	5.55
1×10^{-4}	16.7	6.3	1.60	5.90
1×10^{-5}	19.7	3.3	1.65	5.40

target being spectroscopically pure cesium chloride and the holder platinum. The purity of tracer (Ba^{133} as chloride*) was confirmed by (1) evaporation of the whole tracer in a micro beaker and weighing, with the result that no weight could be detected to 10^{-6} g (10^{-8} g atom) and (2) by adsorption procedure indicating less than 10^{-9} g atom Ba. That is, 40 percent of the tracer solution was added to 1×10^{-5} g atom Fe, the solution titrated to *p*H 8, and the fraction adsorbed found to be 25 percent. Then ten percent of the residual solution after adsorption (7.5 percent of the total) was added to a fresh portion of iron and volume and *p*H adjusted as before. The second portion adsorbed was the same fraction, i.e., 25 percent, indicating the original concentration was in the region in which the fraction adsorbed is independent of concentration.[2]

The quantity of tracer used in individual adsorption experiments did not exceed 1×10^{-4} of the total tracer obtained after bombardment, that is not more than 10^{-13} g atom Ba. Also the bombarded target was spectroscopically pure cesium chloride so it contained less than 10^{-6} g barium per 0.1 g of activated material and this in turn was diluted to less than 10^{-10} g (or 10^{-12} g atom). Considering a maximum of 2000 counts used per adsorption experiment with a counter efficiency of 9 percent the amount of radioactive Ba^{133} was of the order of 10^{-14} g atom.

The purity of the tracer with reference to radioactivity was verified by following its disintegration on an electrometer. The curve obtained corresponded to Ba^{133} ($T=38.8$ hours) and was the same as that obtained from a sample purified with stable barium carrier added.

For the adsorption studies on the effect of *p*H and quantity of adsorbent, in addition to the purified tracer solution just described, solutions of stable barium chloride, ferric chloride, hydrochloric acid and ammonia, were required. Spectroscopically pure barium chloride was diluted to 1×10^{-11} g atom/ml in 0.01*N* hydrochloric acid. Since the spectroscopic analysis indicated no impurities present to the extent of 10^{-5} g/g barium, the diluted barium could not contain more than 10^{-15} g atom/ml of impurities from the barium chloride. The water used in preparing all solutions was triple distilled and checked by *p*H measurement. The ferric chloride used as source of adsorbent was purified by repeated precipitation of the hydrous oxide at low *p*H, under which conditions divalent impurities are removed in solution.

The ammonia solutions used in titrating the samples were prepared by ammonia gas transfer from concentrated solutions into triple-distilled water in a closed vessel.

For the individual adsorption determinations under a given set of conditions a series of samples was made up of stable barium, tracer, and ferric chloride. The required volumes of these solutions having been transferred into outside ground weighting bottles, water or hydrochloric acid or both were added to adjust salt concentration and volume. Then the samples were rapidly titrated with ammonia to the predetermined *p*H and samples closed and set aside to allow adsorbent to settle. After a given time interval, portions of solution were removed by pipette, these portions evaporated in 4-cm Petri dishes, and the activity measured on a G-M counter.

More specifically, in the case of the determination of *p*H effect the factors which were held

TABLE II. Effect of amount of hydrous ferric oxide on adsorption of barium.

Constant factors: Temp. $=25°\pm1°$; total Ba $=1\times10^{-11}$ g atom, *p*H $=8.01\pm0.01$; NH_4Cl conc. $=5.4\times10^{-2}$ N; Vol. $=32.3-34.4$ ml.

Total Fe in g atom	Ba adsorbed in 4 hours g atom $\times10^{-12}$	Total Ba left in sample after 10 ml sol'n. removed g atom $\times10^{-12}$	Ba adsorbed after total of 23 hours g atom $\times10^{-12}$
1×10^{-5}	2.41	7.71	4.42
2×10^{-5}	2.88	7.87	5.51
3×10^{-5}	3.40	7.96	5.67
6×10^{-5}	4.37	8.29	6.84
1×10^{-4}	5.92	8.82	7.61
2×10^{-4}	6.85	9.11	8.40
3×10^{-4}	7.95	9.37	8.98
6×10^{-4}	9.20	9.76	9.61

* Ba^{134} is stable.

constant are shown in Table II. Each sample was made up with 1-ml barium chloride solution containing 1×10^{-11} g atom Ba in 0.01 N HCl, 1 ml $FeCl_3$ solution containing 1×10^{-4} g atom Fe, 1-ml tracer in 0.01 N HCl and 5 ml of water. Then each was titrated to a different *p*H using both 0.1 N and 0.01 N NH_4OH, so that the final volumes were all within the range of 12 to 13 ml.

In the case of the experiments using different quantities of adsorbent, the samples were made up with each containing 1 ml of barium chloride solution having 1×10^{-11} g atom Ba in 0.01 N HCl, 1 ml of tracer in 0.01 N HCl, and 1 ml ferric chloride solution containing the various quantities of iron shown in Table I. Since the varying quantities of ferric chloride meant varying amounts of acid from hydrolysis, the more dilute iron solution had acid added to compensate for the greater acidity in the more concentrated iron solutions and varying amounts of water were added to maintain constant final volume. All then were titrated to the same *p*H.

Typical samples were as shown in Table I.

DEPENDENCE OF ADSORPTION OF BARIUM IN EXTREME DILUTION ON HYDROGEN ION CONCENTRATION AND QUANTITY OF ADSORBENT

The adsorption of divalent ions on a given quantity of hydrous ferric oxide may be looked upon as competitive with all positive ions present in solution. With very dilute solutions of divalent ion the change in hydrogen ion concentration in solution—resulting from an adsorption—would not be measurable. However, as the *p*H of the solution is changed by the addition of an appropriate reagent it would be expected that the amount of adsorption would be inversely related to the hydrogen ion or directly related to the hydroxyl ion concentration in solution.

If we assume that (1) the fraction of barium adsorbed (y) depends only upon the quantity of adsorptive centers in the solid phase when other factors such as salt concentration, temperature, volume, and duration of adsorption are held constant (in dilution below 10^{-10} g atom/ml the fraction adsorbed is known to be experimentally independent of total barium) and (2) the available quantity of adsorptive centers (S) in the solid phase for a given quantity of Fe (Z) is

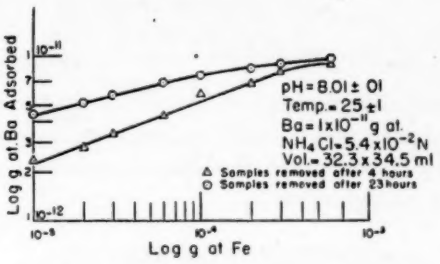
Log g of Ba Adsorbed
Log g of Fe
pH = 8.01 ± .01
Temp. = 25 ± 1
Ba = 1x10⁻¹¹ g at.
NH₄Cl = 5.4 x10⁻² N
Vol. = 32.3 x 34.5 ml
Δ Samples removed after 4 hours
○ Samples removed after 23 hours

FIG. 1. Effect of amount of hydrous ferric oxide on adsorption of barium.

inversely proportional to hydrogen ion concentration, or directly proportional to the hydroxyl ion concentration in solution, that is,

$$S/Z = C[OH^-],$$

where C is a proportionality constant; then since both S and Z refer to the solid phase the effective $[OH^-]$ is that above a critical value at which the solid phase can be maintained. This critical $[OH^-]$ is designated X_0 and the higher $[OH^-]$ as X so the above expression becomes

$$S = KZ(X - X_0).$$

If a fraction y of barium is adsorbed in the presence of a quantity S of adsorptive centers in the solid phase, then an increase of S by dS would give rise, according to (1), to a proportionate increase in y by dy. Therefore,

$$\frac{dy}{y} = k'\frac{dS}{S}.$$

Integration gives

$$\ln y = \lambda \ln[Z(X - X_0)] + \text{const.},$$

TABLE III. Effect of *p*H on adsorption of barium ion by hydrous ferric oxide.

Constant factors: Temp., 25°±1°; total Ba, 1×10^{-11} g atom; Fe, 1×10^{-4} g atom; NH_4Cl conc., 2.5×10^{-2} N; Vol., 13.3±0.3 ml. Duration of adsorption ~3½ hours.

*p*H	Activity in 5 ml of solution	Tracer in exp.	Ba adsorbed
	Counts/min.	Counts/min.	g atom$\times10^{12}$
5.48	303	878	1.02
6.00	290	882	1.45
6.53	259	884	2.32
6.89	239	858	2.79
7.48	166.5	853	4.82.
7.98	114.5	880	6.61
8.45	26.8	856	9.15

and

$$y=k[Z(X-X_0)]^{\lambda}.$$

From this expression it follows that a log-log plot of adsorbed barium against total iron present when *p*H and other factors are constant should give a straight line.

EXPERIMENTAL RESULTS

The effect of varying the quantity of adsorbent while keeping the *p*H, total barium, salt, volume, and duration of adsorption constant is shown in Table II and Fig. 1.

The range of iron quantities which could be used readily was rather limited. The lower limit was an amount which would settle well under the conditions used and the upper limit an amount which would introduce acid in quantity not too much in excess of that used in the other series of experiments (to keep salt concentration comparable). As a check on the results obtained for a four-hour interval a second portion was removed from each sample twenty-three hours after the titration.

Within the range of iron quantities from 1×10^{-5} to 3×10^{-4} g atom Fe the log-log plot of adsorbed barium *vs.* iron is an experimentally straight line, in agreement with the equation, but above this range the curve breaks. Extrapolation of the straight line would indicate 100 percent adsorption by 5.5×10^{-4} g atom of Fe but 6×10^{-4} g atom Fe does not adsorb all the barium even at the longer time interval.

The curve at 23 hours verifies the fact that the curve at 4 hours is not a straight line throughout and that the range of iron quantities which gives a straight line is dependent on duration of adsorption in addition to other factors mentioned.** In addition, from comparison of the two curves on Fig. 1, it can be seen that (with extreme dilutions of barium and limited quantities of hydrous ferric oxide) the adsorption occurs sufficiently slowly to show its dependence on time. Equilibrium is not established in a period of a few hours.

In Table III and Fig. 2 may be seen the result of changing the *p*H of the solution on barium adsorption when the total barium, iron, salt, volume, and duration of adsorption were kept constant. The log-log plot is an experimentally straight line over the range of *p*H values used (*p*H 5.5 to 8.5).

Extrapolation of this curve indicates that at *p*H 3.3 ($2\times10^{-11}[OH^-]$), the region in which iron precipitates, the amount of adsorption would be two percent, however, since the iron does not settle well enough at this *p*H for accurate measurements, the deviation from a straight line was not established. On the other end of the curve extrapolation indicates 100 percent adsorption at 3.5×10^{-6} $[OH^-]$ or *p*H 8.56 and this is experimentally not observed. An explanation of this is the time factor. So the application of the equation for *p*H effect must be considered as limited to about the range of $[OH^-]$ studied. It is to be noted that the value of X_0 (2×10^{-11}) becomes insignificant in this range.

The slope of the straight line part of the curve of the "iron effect" is 0.35 while that of the "*p*H effect" curve is 0.33. Considering the differences in volume and some experimental variations in salt concentrations and time intervals, the similarity in slopes is taken as supporting the assumptions made in the derivation of the equation.

TARGET CHEMISTRY OF CESIUM ACTIVATED WITH DEUTERONS

The bombarded cesium chloride was allowed to stand for several hours for disintegration of the radioactive chlorine.

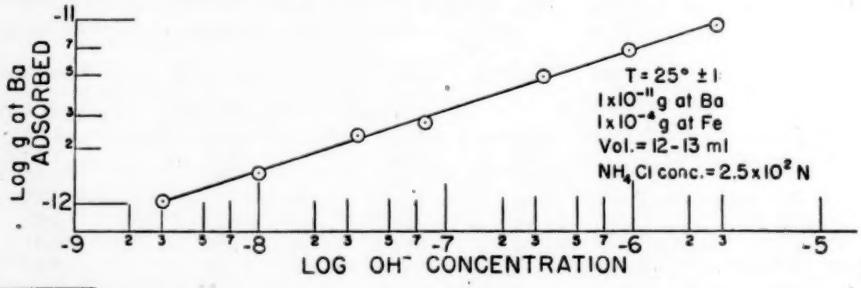

FIG. 2.

** The short half-life of the tracer required study of adsorption over short time intervals.

The target material was then washed from the platinum holder with triple-distilled water, dissolved in hydrochloric acid (pH$\sim$2) and filtered through analytical paper. The impurities insoluble in hydrochloric acid were rejected (see Fig. 3). To the acid filtrate was added 1×10^{-3} g atom iron as ferric chloride and the solution titrated with ammonia to pH 10. The filtrate from this was rejected.

The precipitate containing 91.5 percent of the active barium was dissolved in acid and the procedure repeated twice.

The additional loss of 1.8 percent of active barium was less than previously lost because of lower salt concentration and volume.

Potassium, activated by deuterons, was purified by similar adsorption procedure, and $\sim$300 counts added to the barium^{133,134} as a tracer for monovalent ions (Cs) that might be present in the barium solution.

The adsorption procedure with hydrous ferric oxide was carried out again.

Finally the iron was precipitated at pH 5.4, and the filtrate containing 83.1 percent of the initial barium activity was freed from salt by sublimation, dissolved in 0.01 N HCl, filtered, the operation repeated, the sample weighed and found to contain no weighable material.

The active material was dissolved in 0.01 N HCl and diluted 10^4 times for use as tracer. It is assumed that the tracer contained minute quantities of potassium and cesium.

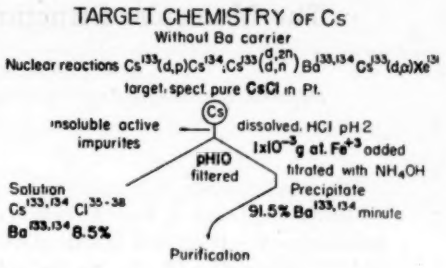

FIG. 3a.

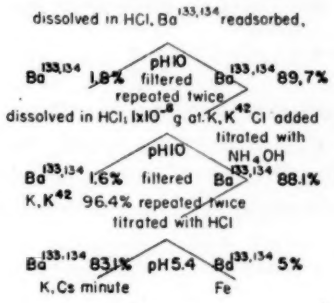
dissolved in HCl, Ba133,134 readsorbed,
Ba133,134 1.8% pHIO filtered Ba133,134 89.7%
repeated twice
dissolved in HCl; 1x10-8 g at. K, K42Cl added
titrated with NH4OH
pHIO
Ba133,134 1.6% filtered Ba133,134 88.1%
K, K42 96.4% repeated twice
titrated with HCl
Ba133,134 83.1% pH5.4 Ba133,134 5%
K, Cs minute
Fe

FIG. 3b.

ACKNOWLEDGMENT

We are deeply indebted to Professor Edward Mack, Jr. for his discussion and support which greatly facilitated this work

It is a pleasure to express our gratitude to the Ohio State University Development Fund for grants for research equipment.

The Molecular Structure of Dimethyltrisulfide, $(CH_3)_2S_3$*

JERRY DONOHUE AND VERNER SCHOMAKER
*Department of Chemistry,** California Institute of Technology, Pasadena, California*

(Received July 1, 1947)

Dimethyltrisulfide $(CH_3)_2S_3$ has been investigated by the electron diffraction method. The molecule was found to have the chain configuration, with the following interatomic distances and angles: C−H=1.09A (assumed), C−S=1.78±0.04A, S−S=2.04A, ±0.02A, ∠H−C−S =112° (assumed), ∠S−S−S=104°±5°, and ∠C−S−S=104°±5°. The results also suggest that the C−S bonds oscillate with rather large amplitude about a mean position approximately 106° out of the plane of the three sulfur atoms.

THE present electron diffraction investigation was undertaken mainly to determine whether dimethyltrisulfide is a simple trisulfide (I), a thiodisulfide (II), or a dithiosulfone (III).

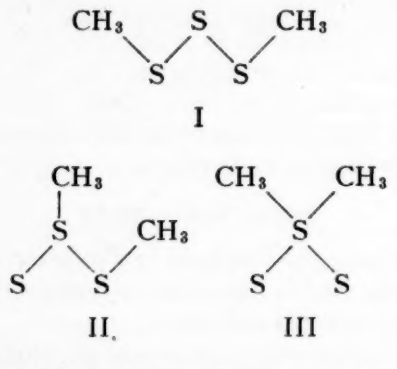

I II III

Knowledge of this structure is of interest in connection with the problems of the constitutions of the inorganic persulfides and polythionates,[1] as well as of the alkyl polysulfides,[2] and the Thiokols.[3] With the exception of the trithionate ion,[4] $O_3S-S-SO_3^=$, there is no direct structural evidence which settles the question whether the molecules of these substances have the chain configuration or are related to II or III. In the case of the disulfides H_2S_2, S_2Cl_2, and $(CH_3)_2S_2$, the existing evidence from electron diffraction favors chain structures for all three molecules.[5–7]

EXPERIMENTAL

The sample used in this investigation was provided by Professor R. C. Fuson. It was pale yellow in color and was used without further purification. Excellent electron diffraction photographs were made in the apparatus described by Brockway[8] with the use of the high temperature nozzle.[9] At the end of each run the boiler and remaining liquid were examined; no corrosion of the boiler and only slight darkening of the liquid were observed, indicating that very little decomposition occurred.

INTERPRETATION OF THE PHOTOGRAPHS

The characteristic features of the photographs are represented by curve V of Fig. 1, which was drawn in accordance with the measured ring diameters (except that the unobservable first maximum, which is not structure sensitive, was added arbitrarily), so as to have the general properties of theoretical intensity curves calculated with the simplified expression

$$I(q)=\sum_{i,j}\frac{Z_iZ_j}{r_{ij}}\exp(-b_{ij}q^2)\sin\left(\frac{\pi}{10}r_{ij}q\right).$$

* The work herein was done under Contract OEMsr-753 between the National Defense Research Committee and the California Institute of Technology.

** Contribution No. 1108 from the Gates and Crellin Laboratories of Chemistry, California Institute of Technology.

[1] D. M. Yost and H. Russell, *Systematic Inorganic Chemistry* (Prentice Hall, Inc., New York, 1944), p. 361ff.

[2] R. Connor, *Organic Chemistry* (John Wiley and Sons, Inc., New York, 1943), edited by H. Gilman, p. 864.

[3] S. M. Martin and J. C. Patrick, Ind. Eng. Chem. **28**, 1144 (1936).

[4] W. H. Zachariasen, Phys. Rev. **37**, 1295 (1931).

[5] K. J. Palmer, J. Am. Chem. Soc. **60**, 2360 (1938).

[6] D. P. Stevenson and J. Y. Beach, J. Am. Chem. Soc. **60**, 2872 (1938).

[7] P. G. Ackerman and J. E. Mayer, J. Chem. Phys. **4**, 377 (1936).

[8] L. O. Brockway, Rev. Mod. Phys. **6**, 234 (1936). Camera distance, 10.91 cm. Electron wave-length, 0.0610A calibrated with respect to zinc oxide smoke (C. S. Lu and E. W. Malmberg, Rev. Sci. Inst. **14**, 271 (1943)) and corrected for film expansion.

[9] L. O. Brockway and K. J. Palmer, J. Am. Chem. Soc. **59**, 2181 (1937).

The radial distribution integral,[10] curve *RD* of Fig. 1, was calculated by use of the formula

$$rD(r) = \sum_{q=1,2,\cdots}^{100} I(q) \exp(-aq^2) \sin[(\pi/10)qr],$$

with $\exp(-a(100)^2) = 0.1$. The integral has maxima at 1.78A, 2.04A, 2.45A, 3.02A (very broad, asymmetric peak), and 4.0A (very broad, small peak). Of these peaks the first two may be interpreted as representing, respectively, the bonded C−S and S−S distances, the third the non-bonded S...H distance, and the asymmetric fourth the non-bonded C...S and S...S interrelations. The interpretation of the weak maximum at 4.0A is discussed below.

An extensive investigation of the straight chain structure I by the correlation procedure was made. For structure I four parameters are required to define the structure if the positions of the hydrogen atoms are assumed and if the long, rotation-dependent, C...S distance is neglected. These may be chosen as: (1) bonded C−S; (2) bonded S−S; (3) non-bonded S...S; and (4) non-bonded C...S.

The first two of these parameters may be determined directly from the radial distribution integral. As a check on the accuracy of this determination, twenty-one intensity curves, some of which are shown in Fig. 1, were calculated for models with varying ratios between these two distances. In these models the S−S distance was held at 2.04A and the non-bonded C...S and S...S distances were varied in a systematic fashion so that their average was in general agreement with the broad maximum of the integral at 3.0–3.2A. Best agreement between the calculated curves and the appearance of the photographs was obtained for models with C−S = 1.78A as was expected, changes of more than 0.03A giving marked discrepancies regardless of the particular values used for the non-bonded C...S and S...S distances.

The determination of the two remaining parameters is a more difficult problem since the terms which are involved in their variation contribute only about 20 percent of the total scattering. Since the term representing the two non-bonded C...S distances and the term for the non-bonded S...S distance are of nearly equal weight, it is impossible to distinguish between them. For example, a curve calculated for a model with ∠S−S−S = ∠S−S−C = 104° is indistinguishable from one calculated for a model with ∠S−S−S = 95½° and ∠S−S−C = 115°. However, it is appropriate to choose S...S<C...S so that the sulfur bond angles ∠S−S−S and ∠S−S−C have similar values, and this is done in the following analysis.

Twenty-two scattering curves, some of which are shown in Fig. 2, were calculated for models with varying values of these distances. It was found that it is not possible to obtain theoretical scattering curves in agreement with the appearance of the photographs unless (1) a distance at 4.0A as suggested by the radial distribution integral is included in the intensity formula and (2) the S...S distance is given a rather severe temperature factor. The distance at 4.0A corresponds to the two longer non-bonded C...S distances in a non-planar model with the C−S

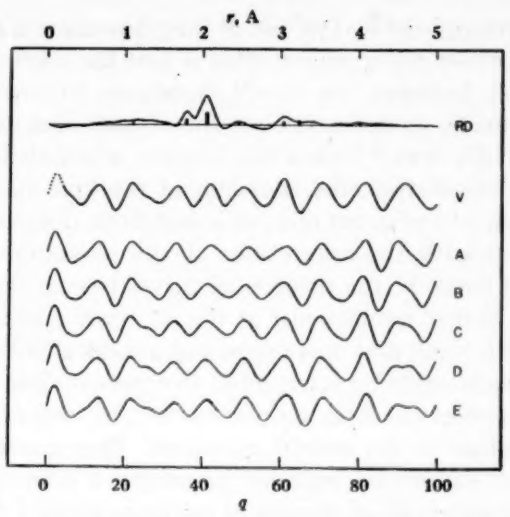

FIG. 1. Electron diffraction curves for dimethyltrisulfide. Chain models with C−H = 1.09A, S−S = 2.04A, S...H = 2.45A, C...S = 3.02A, S...S = 3.22A(∠S−S−S = 104°), and $b_{C...H} = 0.00016$; the other molecular parameters are as follows.

Model	C−S	$b_{S...H}$	(∠C−S−S)
A	1.83	0	102° 45′
B	1.81	0.0003	103° 30′
C	1.78	0.0003	104°
D	1.75	0.0003	105°
E	1.73	0	106° 30′

All other $b_{ij} = 0$. The long C....S term at 4.00A, was included with $b = 0.0009$, for models *B*, *C*, and *D*, and was omitted for the other models.

[10] a. R. Spurr and V. Schomaker, J. Am. Chem. Soc. **64**, 2693 (1942); b. P. A. Shaffer, Jr., V. Schomaker, and L. Pauling, J. Chem. Phys **14**, 659 (1946).

bonds rotated by 106° out of the plane containing the three sulfur atoms. This is just the angle of twist between the O—H bonds in hydrogen peroxide, as deduced from the crystal structure of $H_2O_2 \cdot$ urea.[11] Unless this distance is included in the calculation, the character of the first maximum and adjacent minima is in definite disagreement with the appearance of the photographs and curve V, the theoretical curves having their sharp first minima just at the observed position of the weak first maximum, and a weak shoulder (which might be interpreted as corresponding to the observed first minimum) at the observed position of the second minimum. This discrepancy cannot be regarded as merely a difficulty in interpretation, in view of our knowledge of the appearance of electron diffraction photographs and their interpretation, but must be regarded as conclusive. On the curve for the accepted model, O, on the other hand, the positions of the features corresponding to the measured first and second minima and the first maximum are satisfactory. The relative depths of the indicated first and second minima, also, are in better agreement with curve V than on the curves calculated without a 4.0A term. The agreement is not perfect either in this respect or for the magnitude of the first maximum, which on the photographs is clearly visible, although very weak, but on curve O is indicated only as a region of unusually small upward curvature; however, these discrepancies do seem to represent difficulties of interpretation.

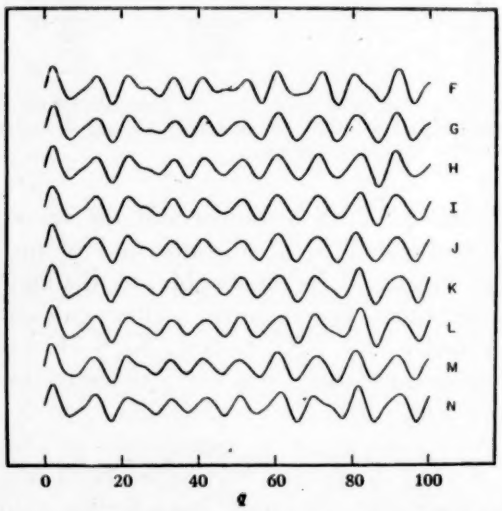

FIG. 2. Electron diffraction curves for dimethyltrisulfide. Chain models with C—H = 1.09A, C—S = 1.78A, S—S = 2.04A, S...H = 2.45A, and $b_{C...H} = 0.00016$; all other $b_{ij} = 0$ except for models *J* and *M*, for which $b_{S...S} = 0.0003$; the other parameters are as follows.

Model	C...S	S...S	(∠S—S—S)	(∠C—S—S)
F	3.10	3.10	99°	108° 20′
G	2.96	3.10	99°	101° 30′
H	2.97	3.14	100° 30′	101°
I	3.02	3.17	102°	104°
J	3.05	3.20	103°	105° 40′
K	3.02	3.22	104°	102°
M	3.05	3.25	105° 30′	105° 40′
N	3.00	3.25	105° 30′	103° 20′

The long C....S at 4.00A term was included with $b = 0.0009$, for models *J* and *M*, and was omitted for the other models.

Similar differences between the correct and the obvious interpretation of a weak inner ring—the ring appearing stronger on the photographs than would be suggested by the correct theoretical curve, or the apparent relative depths of the adjacent minima being different from that shown by the theoretical curve—have been previously observed in the case of numerous other compounds of which propane[12] is an example. Curve Z_iZ_j, for which the customary coefficients Z_iZ_j/r_{ij} were replaced by Z_iZ_j, was calculated to illustrate the notion that the apparent strength of the weak—and also relatively sharp—inner ring may be enhanced by a tendency of the eye to detect more readily the higher frequency components of the pattern.

It is evident that, in general, the appearance of the innermost rings of electron diffraction photographs cannot be so simply interpreted in terms of simplified theoretical intensity curves as can the rest of the pattern, perhaps in part because of the very rapid change of total intensity with change in scattering angle at small scattering angles, and that it is never justifiable to make important use of an inner feature—such as weak inner ring—without reference to similar features on the photographs of other substances of known structure. In addition to propane, we have here made particular reference to the photographs and curves of cyclopropane, ethylene imine, and ethylene oxide,[13] which show somewhat similar inner rings to that of dimethyltrisulfide.

[11] C. S. Lu, E. W. Hughes, and P. A. Giguère, J. Am. Chem. Soc. 63, 1507 (1941).

[12] S. H. Bauer, J. Chem. Phys. 4, 406 (1936); L. Pauling and L. O. Brockway, J. Am. Chem. Soc. 59, 1223 (1937).

[13] H. Pfeiffer, H. A. Levy, and V. Schomaker (to be published, J. Am. Chem. Soc.).

Curve O was calculated with the following values of the temperature factor b: C−H: 0.00016; S...H:0.0003; S...S:0.0003; long C....S:0.0009; all others zero, except for the remaining distances involving hydrogen, which were neglected. Curves C and P are identical with curve O except that the values zero and 0.0009, respectively, were used for $b_{S...S}$. Curve C is unsatisfactory in regard to a number of minor details in the region $35<q<60$ of which one, regarding the relative intensity of the fourth ring, can be seen most clearly in Fig. 3. Curve P is only slightly less satisfactory than curve O. This indication of a relatively large value required for $b_{S...S}$ is rather surprising. We know of no other molecules in which the temperature effect is so large for a distance between heavy atoms bonded to the same atom. The large temperature factor required for the long C....S distance, on the other hand, is quite reasonable, and indicates that only a small potential restricts internal rotation at the temperature at which the photographs were made.

Scattering curves for several of the models of type II and III which were calculated are shown in Fig. 3. The only important essential differences between these models and chain structure models are differences of amplitude of the short C...S term and the long C....S term, of which the latter is most important for our argument, the essential long C....S term having only half-strength in type II models and being absent in type III models. It is seen that these curves are quite unsatisfactory with respect to the first ring. (At large scattering angles these curves and curve O are closely similar, none having an appreciable 4.0A contribution.) Since no variation in molecular parameters whatever makes the initial portions of these curves correspond to the appearance of the photographs, we conclude that, to the accuracy of our observations of the inner rings, neither II nor III is the structure of dimethyltrisulfide.

Our final values for the parameters of the satisfactory straight chain structure are: C−H =1.09A (assumed), C−S, 1.78±0.04A, S−S =2.04±0.02A, ∠H−C−S=112° (assumed), ∠S−S−S=104°+5°, and ∠C−S−S=104° ±5°. (C...S=3.02±0.04A and S...S=3.22 ±0.04A.) The terminal CH_3−S bonds are rotated about 106° from the plane of the sulfur chain. The quantitative comparison for model O is shown in Table I.

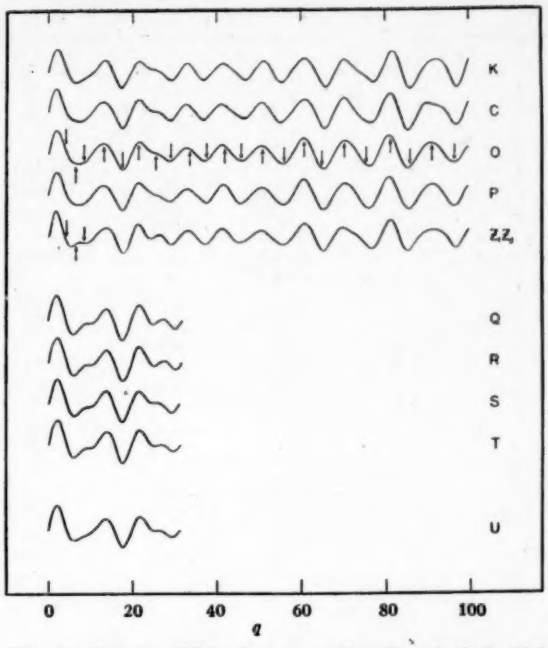

FIG. 3. Electron diffraction curves for dimethyltrisulfide. Molecular parameters for the various models are C−H =1.09A, C−S=1.78A, S−S=2.04A, S...H=2.45A, long C....S=4.00A, and $b_{C...H}=0.00016$; the other parameters are as follows.

Chain models I

Model	$b_{S...H}$	$b_{S...S}$	b long C....S term omitted
K	0	0	
C	0.0003	0	0.0009
O	0.0003	0.0003	0.0009
P	0.0003	0.0009	0.0009
Z_1Z_1	0.0003	0.0003	0.0009

C...S=3.02A and S...S=3.22A for all chain models

Dithiosulfone models III

Model	S...S	C...S	(∠C−S−C)
Q	3.02	3.12	119° 30′
R	3.12	3.02	134°
S	3.02	3.22	102°
T	3.22	3.02	132° 30′

Thiodisulfide model II

U	3.22	3.02

DISCUSSION

The chain structure found for dimethyltrisulfide is in agreement with the chain structures proposed for the three disulfides which have been previously investigated by the electron diffraction method, H_2S_2,[6] S_2Cl_2,[5,7] and $(CH_3)_2S_2$.[6] In all four molecules the bonded S−S distance is 0.02–0.03A shorter than the S−S distance 2.07A in S_8.[14] The C−S distances in $(CH_3)_2S_2$

[14] C. S. Lu and J. Donohue, J. Am. Chem. Soc. 66, 818 (1944).

TABLE I.

Min.	Max.	q_{obs}	q_{o}	q_{o}/q_{obs}
1		4.42		
	1	6.61		
2		8.52		
	2	13.35	13.2	0.989
3		17.73	17.7	.998
	3	21.59	21.6	1.000
	3′	25.70		
4		29.37	29.0	0.988
	4	33.85	33.0	.975
5		37.86	37.3	.985
	5	42.03	41.5	.987
6		45.93	46.2	1.006
	6	50.93	50.9	0.999
7		56.19	55.9	.995
	7	60.92	60.8	.998
8		65.17	65.7	1.008
	8	70.51	70.6	1.001
9		75.78	76.3	1.007
	9	81.50	81.2	0.996
10		86.12	85.8	.996
	10	91.33	91.2	.999
11		96.74	96.6	.999
			average	0.996
			average deviation	0.006

and $(CH_3)_2S_3$ are the same, and are 0.04A shorter than the distance in $(CH_3)_2S$.[15] These shortenings are probably significant although they are within the limits of experimental error in each case. When sulfur forms single covalent bonds with two other atoms, the existing data indicate the angle decreases as the electronegativity of the bonded atoms increases: the observed values are 107° in $(CH_3)_2S_2$, 105° in S_8, 104° in $(CH_3)_2S_3$, 103° in S_2Cl_2, and 101° in SCl_2.

In addition to the direct experimental evidence of the electron diffraction data, the sulfur-sulfur distance also suggests that the molecule has the straight chain structure I, inasmuch as it is approximately equal to the S−S distance in the singly bonded molecules just mentioned and is indeed just equal to the distance in $(CH_3)_2S_2$, which is agreed to have the singly bonded structure; it is about 0.15A greater than would be expected for an S−S bond of the type to be found in structure III and about 0.08A greater than the average to be expected for structure II, on the basis of the Pauling-Huggins covalent radii.[16] Although no test of these covalent-radius predictions of sulfur-sulfur multiple bonds is available, a rather close analogy can be drawn with the phosphorus-sulfur bonds in P_4S_3, in which the bonds are presumed to be single bonds, as contrasted to the phosphorus-sulfur bonds in phosphorus sulfoxide, thiophosphoryl fluoride, and thiophosphoryl chloride. The P−S distances in $P_4O_6S_4$, PSF_3, and $PSCl_3$ are 1.85A,[17] 1.85A,[18] and 1.94A,[19] respectively (the covalent radius sum for a double bond is 1.94A),[16] while in P_4S_3 the P−S single bond distance is about 2.12A[20] (radius sum 2.14A). Here the 0.2A difference between the lengths of the single and double bonds between phosphorus and sulfur is found to be valid, even though there might be some question, as there is for the special sulfur-sulfur bonds in structures II and III, as to whether the phosphorus-sulfur bond in the thiophosphoryl compounds should have the same length as that predicted in a conventional double bond.

The same conclusion is suggested by the bond angles of 104°. These bond angle values are reasonable for the singly bonded atoms in the chain structure I but they do not seem reasonable for the angles involving the doubly bonded sulfur atoms in structures II and III. For structure III, moreover, the S−S−S and C−S−S bond angles of 104° correspond to a C−S−C bond angle of greater than 130°, an unreasonably high value by a wide margin.

[15] L. O. Brockway and H. O. Jenkins, J. Am. Chem. Soc. 58, 2036 (1936).

[16] L. Pauling, *The Nature of the Chemical Bond* (Cornell University Press, Ithaca, New York, 1940), second edition, Chapter IV.

[17] A. J. Stosick, J. Am. Chem. Soc. 61, 1130 (1939).

[18] D. P. Stevenson and H. Russell, J. Am. Chem. Soc. 61, 3264 (1939).

[19] J. Y. Beach and D. P. Stevenson, J. Chem. Phys. 6, 75 (1938).

[20] O. Hassel and A. Petterson, Tids. Kjem. Bergvesen Met. 1, 57 (1941); Chem. Abs. 35, 4646 (1941).

THE JOURNAL OF CHEMICAL PHYSICS VOLUME 16, NUMBER 2 FEBRUARY, 1948

Raman Lines of Second-Order Intensity in $SnBr_4$, $SnCl_4$, and CCl_4

H. L. WELSH, M. F. CRAWFORD, AND G. D. SCOTT*
McLennan Laboratory, University of Toronto, Toronto, Canada
(Received September 9, 1947)

The characteristics of the faint Raman lines appearing in long exposures have been investigated for the molecules, $SnBr_4$, $SnCl_4$, and CCl_4. All the lines observed have been classified as overtones and combination tones of the fundamentals. The depolarizations of the second-order lines were measured by means of a Wollaston prism placed between the collimator lens and the dispersing prism of the spectrograph. The depolarizations were found to be in accordance with theory, on the assumption of tetrahedral symmetry for the molecules. The intensities of the second-order lines relative to the fundamentals were measured. For the spherically symmetrical frequencies it is shown that the observed intensities can be explained by assuming that electrical and mechanical anharmonicities are both operative; in some cases counteracting one another and in other cases enhancing the effect of each other.

INTRODUCTION

STRONGLY exposed Raman spectrograms of many substances show very faint, or second-order, Raman lines in addition to the intense, or first-order, lines due to the Raman-active fundamental vibrations of the scattering molecule. A systematic study of these lines of second-order intensity in a related group of molecules should aid in the understanding of the physical processes involved in the molecular scattering of light, and provide further information concerning the structure of molecules.

In general, Raman lines of very low intensity should be attributable to transitions that are forbidden by the first-order selection rules, but which are allowed when the anharmonicities present in the molecules are taken into account. Thus, overtones and combination tones of the fundamentals should appear, and possibly certain fundamental tones which are forbidden in the first approximation by symmetry. In some cases second-order lines occur with unusually high intensity which can be associated with accidental resonance degeneracies in the molecule. Second-order lines can also arise from multiple Raman scattering. However, the intensity to be expected for this process is negligible compared with that of the second-order lines which have been observed.

The characteristics of second-order lines that are of primary importance are: (a) the frequency shifts, (b) the intensities relative to each other and to the first-order lines, (c) the degree of depolarization, (d) the intensity contours. The frequency shift of a line identifies the transition giving rise to it. The relative intensities afford information on the electrical and mechanical anharmonicities of the molecule, although the theory is not yet sufficiently advanced to make full use of these measurements. The depolarization values can be used to test the polarizability theory and the symmetry assumed for the molecule. Finally, the intensity contours can be of considerable significance in cases in which accidental resonance degeneracies are present in the molecule.

Although overtones and combination tones of fundamental vibrations are of common occurrence in infra-red spectra, only relatively few have been observed in Raman spectra. This is probably caused by the experimental difficulties of observing these faint, second-order Raman lines. The anomalously strong overtone of the accidentally degenerate vibration, $\Delta\nu = 1550\ cm^{-1}$ in CCl_4 has been studied by a number of workers.[1,2] In addition to this overtone, two second-order lines in the spectrum of CCl_4 and one in the spectrum of $SiCl_4$ were observed by Ananthakrishnan.[3] The work on CCl_4 was ex-

* The greater part of the experimental work reported here was carried out in 1940–1941 while one of the authors (G. D. Scott) was holder of a Studentship granted by the National Research Council of Canada.

[1] L. S. Ornstein and J. J. Went, Proc. Amst. Akad. Sci. **35**, 1024 (1932).
[2] A. Carrelli and J. J. Went, Zeits. f. Physik **76**, 236 (1932).
[3] R. Ananthakrishnan, Proc. Ind. Acad. Sci. **2**, 425 (1935).

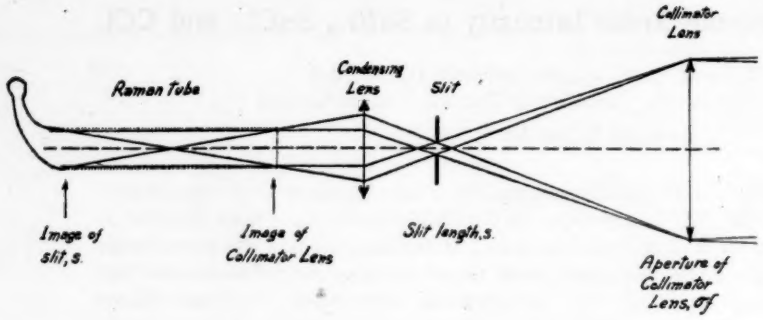

FIG. 1. Raman tube used with condensing lens.

tended by Landsberg and Malysev;[4] they also investigated $SnBr_4$ and recorded seven second-order lines. Intensity and polarization measurements have been made for the overtone $\Delta\nu = 1550$ cm^{-1} in CCl_4 by Ornstein,[1] and by Carrelli and Went.[2] Landsberg and Malysev estimated that the intensities of the second-order lines were about 3×10^{-3} of the intensity of the first-order lines. No further intensity or polarization measurements of second-order lines have been published.

EXPERIMENTAL

The Spectrograph

A double prism glass spectrograph was used. The refracting components are a constant deviation flint glass prism and a 60° crown glass prism. The collimator lens is an f:10 doublet of 75-cm focal length. Either of two camera lenses can be fitted, an f:4 triplet of 30-cm focal length or an f:10 doublet of 75-cm focal length. Both lenses give excellent definition over the Raman region of the spectrum. With the f:4 lens the dispersion is 43A/mm (225 cm^{-1}/mm) at 4358A; with the f:10 lens, it is 16A/mm (86 cm^{-1}/mm).

Raman Tubes

The Raman tubes were of conventional design with a plane window at one end and a blackened horn at the other. The standard type tube had a diameter of 1 cm and an effective length of 10 cm, and was mounted directly in front of the slit of the spectrograph. A tube 100 cm in length and 1.6 cm in diameter was also used, in this case with a condensing lens. With the same illumination per unit length of the tube, the brightness of the Raman spectrum from the 100-cm tube was approximately tenfold that from the standard tube. Both types of tubes had jackets through which a saturated solution of sodium nitrite was circulated. The solution served as a light filter and a temperature control. Most of the exposures were taken with the scattering substance at 25°C.

When a long Raman tube is used, a condensing lens placed between the window of the tube and the slit of the spectrograph is essential. It can be shown that for a given diameter the usable length of the tube is a maximum when the image of the window of the tube, formed by the condensing lens, is at the collimator lens and equal in size to its effective aperture and the image of the horn end of the tube is at the slit with a diameter equal to the slit length. Figure 1 illustrates this arrangement for a cylindrical Raman tube. The dimensions of the tube under these conditions are limited by the relation, $D^2 = L\sigma s/n$, where D is the diameter of the tube, L is its irradiated length, s is the slit length, σ is the reciprocal of the stop number of the collimator lens, and n is the index of refraction of the scattering medium. The focal length of the condensing lens is, $F = D/\sigma(1-s/\sigma f)$, where f is the focal length of the collimator lens. J. R. Nielsen[5] derived equivalent relations in 1930 and pointed out the application to Raman spectroscopy.

Mercury Lamps

The irradiating sources were low pressure mercury vapor lamps operated at 2.5 to 3.0 amperes from a 220-volt d.c. supply. They were constructed of Pyrex tubing of 9-mm bore and had an extra tungsten electrode near the anode to facilitate starting with an induction coil. In

[4] G. S. Landsberg and V. J. Malysev, C. R. (Doklady) Acad. Sci. U.S.S.R. 3, 365 (1936).

[5] J. R. Nielsen, J. Opt. Soc. Am. 20, 701 (1930).

this way, lamps with a discharge path up to 120 cm could be started on a 220-volt supply.

Lamps of different forms were used: straight lamps for polarization, and either coil or straight for ordinary spectra. In the latter case irradiation of the tube was always arranged so that the relative intensities of lines of different degrees of depolarization were not dependent on reflection losses at the faces of the dispersing prisms.

When the 100-cm tube was irradiated with a bank of eight lamps, the first-order Raman spectrum of CCl_4 was recorded in 5 seconds.

Depolarization Determinations

The essential features of the polarization technique used here are directional illumination of the Raman tube and division of the beam emerging from the collimator into two separated beams polarized in perpendicular directions. The mercury lamps are arranged so that the unpolarized light illuminating the Raman tube is confined approximately to a plane through the axis of the tube. The beam from the collimator is divided by a large Wollaston double image prism of quartz placed between the collimator and the dispersing prism. The double image prism, which can be rotated in its mount about an axis coincident with the axis of the collimator, is so oriented that the polarization of one of the emergent beams is parallel and that of the other perpendicular to the plane of irradiation. With this arrangement two adjacent spectra are recorded simultaneously, one in each of the two polarizations required to evaluate the depolarization factor ρ. Differential reflection of the two polarized beams at the faces of the dispersing prisms can be eliminated by setting the plane of irradiation at 45° to the plane of incidence at the dispersing prisms.

When the illumination of the Raman tube is not unidirectional, the ratio of the intensities of the same line in the two spectra, which is called herein the intensity ratio of the $\perp$ to the $\parallel$ component, gives only an approximate value of ρ. An accurate value of ρ can be obtained by approximating closely to the ideal arrangement in which the incident radiation is unidirectional in the scattering medium, but this necessitates much longer exposures.

An alternative method is to calibrate the experimental arrangement in which the irradiation is only approximately unidirectional by measuring the intensity ratio for a number of Raman lines whose ρ values have been determined accurately. This method does not require elimination of differential reflection of the two polarized beams because the calibration automatically corrects for the difference in reflection losses. In fact there is some advantage in setting the plane of irradiation parallel to the plane of incidence at the dispersing prisms. The intensity of the $\perp$ component is then increased relative to that of the $\parallel$ component, and for a highly polarized line their ratio can be measured more accurately. Nor is it essential, if the arrangement is calibrated, to orientate the double image prism so that the polarization of one of the emergent beams is parallel to the plane of irradiation. However, since maximum sensitivity is obtained when the double image prism is so orientated, it is not advisable to depart far from this optimum orientation.

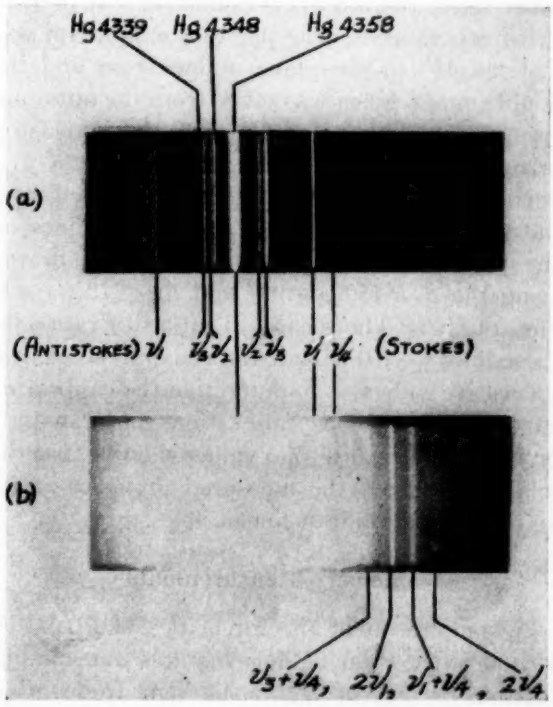

Fig. 2. Raman spectra of $SnBr_4$ excited by Hg 4358; "spectral" width of slit 3 wave numbers: (a) 1-minute exposure showing lines due to the four fundamental vibrations of the molecule; (b) 6-hour exposure showing the higher frequency overtones and combination tones.

TABLE I. Raman lines of $SnBr_4$ liquid.

	Frequency shift (cm^{-1}) Measured	Calculated	Peak intensity	Remarks
$\nu_3-\nu_2$	—	20		covered by wings
$\nu_4-\nu_1$	—	59		of Rayleigh line
ν_2	68		370	merged
ν_3	88		560	
$\nu_1-\nu_3$	134	133	3.5	*
$2\nu_2$		136		
$\nu_1-\nu_2$	151	153	1.5	*
$\nu_2+\nu_3$		156		
$2\nu_3$	176	176	0.7	*
$\nu_4-\nu_3$	193	192	6.5	*
$\nu_4-\nu_2$	—	213		*
ν_1	221		1000	sharp, symmetrical
ν_4	280		180	broad, degraded to red
$\nu_1+\nu_2$	—	289		*
$\nu_1+\nu_3$	303	309	—	*
$\nu_2+\nu_4$	—	348		
$\nu_3+\nu_4$	367	368	1.5	* broad
$2\nu_1$	442	442	2.5	sharp, symmetrical
$\nu_1+\nu_4$	502	501	0.9	degraded to red
$2\nu_4$	565	560	0.1	broad

* These lines are on the wings of fundamentals, merged with each other or merged with the fundamentals from Hg 4348 or Hg 4339; the intensities of such lines are therefore very approximate.

Since highly unidirectional irradiation would necessitate extremely long exposures for second-order lines, the alternative method was used in these experiments. The plane of irradiation was inclined 45° to the plane of incidence and the double image prism was set 8° from the optimum orientation. This orientation of the Wollaston prism makes the $\perp$ and $\parallel$ components of a depolarized line equal in intensity and facilitates the visual identification of depolarized lines on the spectrogram. The arrangement was calibrated using the $\Delta\nu=459(\rho=.05)$ and $\Delta\nu=218(\rho=.83)$ lines of CCl_4. The measured intensity ratios for these lines were 0.33 and 1.0, respectively. These values are sufficient to determine the calibration curve since previous calibrations made with a more complete range of ρ values showed that the relation between the measured intensity ratios and ρ values is almost linear.

Intensity Measurements

A comparison of the intensities of first- and second-order Raman lines requires a technique capable of measuring, at different frequencies, intensities that differ by a factor of 2×10^4. Stepped slit spectra of a Kipp and Zonen standard lamp were used as intensity standards to calibrate the photographic plates. The spectral distribution of energy emitted by this lamp for a wide range of filament currents is known from calibration data supplied by the manufacturer. The desired range of intensities is readily obtained with this method since a 20-fold range of intensities is produced by the stepped slit and a 5000-fold change can be produced by changing the current through the lamp.

Ilford Special Lantern plates were used. Previous intensity work showed that these plates had adequate sensitivity and fineness of grain, and that plates of the same emulsion number had very uniform sensitivity characteristics. To increase their sensitivity for lines of low density the plates were prefogged in green light to a density of 0.1. The prefogging was, in general, advantageous, since the continuous background of the mercury lamps was extremely low. The backing on the plates as supplied was not sufficiently effective for very strong exposures and was replaced by Eastman Opaque which eliminated halation rings.

To eliminate errors due to reciprocity failure, the Raman spectrum and the intensity standards are usually exposed for equal times. The inconvenience of this procedure for long exposure times was obviated by photographing the stepped slit spectrum on each plate with an exposure time of 15 minutes and then making corrections

TABLE II. Raman lines of $SnCl_4$ liquid.

	Frequency shift (cm^{-1}) Measured	Calculated	Peak intensity	Remarks
$\nu_3-\nu_2$	—	25		covered by wings
$\nu_4-\nu_1$	—	35		of Rayleigh line
ν_2	106		475	merged
ν_3	131		520	
$2\nu_2$	213	212	—	
$\nu_1-\nu_3$	241	237	—	
$\nu_2+\nu_3$		237		
$2\nu_3$	—	262		covered by ν_1
$\nu_1-\nu_2$	—	262		from Hg 4339
$\nu_4-\nu_3$	—	272		
$\nu_4-\nu_2$	—	297		covered by ν_1 from Hg 4348 and by ν_4 from Hg 4339
ν_1	368		1000	sharp, symmetrical
ν_4	403		265	broad, degraded to red
$\nu_1+\nu_2$	475	473	0.9	broad
$\nu_1+\nu_3$	502	499	0.4	
$\nu_2+\nu_4$		509		
$\nu_3+\nu_4$	534	534	0.8	broad
$2\nu_1$	737	736	0.6	sharp, symmetrical
$\nu_1+\nu_4$	773	771	0.5	broad, degraded to red
$2\nu_4$	814?	806	0.05?	very faint

for reciprocity failure by means of a "master" intensity calibration for plates of the same emulsion number. Calibrations at three wavelengths, 4350A, 4500A, and 4750A, were obtained by determining the characteristic curves for exposure times of 1, 5, 15, 60, and 240 minutes. From these the relative intensity of a Raman line of any frequency shift up to 2000 cm^{-1} photographed with any exposure time from 30 seconds to 10 hours could be readily determined by interpolation or extrapolation.

A Moll recording microphotometer and later a Leeds and Northrup recording microphotometer were used to measure the photographic densities.

RELATIVE INTENSITIES

Commercial c.p. samples of CCl_4 and $SnCl_4$ were used. The $SnBr_4$ was prepared from mossy tin and bromine. Each substance was carefully purified by preliminary distillations under vacuum, and then distilled into the Raman tube. In one sample of CCl_4 one of the combination tones of CCl_4 was obscured by a stronger, highly polarized line; it was identified as the $\Delta\nu = 667$ cm^{-1} line of chloroform. No lines which could be ascribed to impurities were found in any of the other samples of the three substances.

A number of plates were taken for each substance and at least two exposures were made on each plate: a short exposure, 1 to 10 minutes, to record the fundamental frequencies with suitable densities and one or more long exposures, 30 minutes to 12 hours, to record the second-order lines (see Fig. 2). The "spectral" width of the slit was from 3 cm^{-1} to 15 cm^{-1}. With these widths approximate intensity contours could be obtained for all lines.

The frequencies and relative intensities of the observed Stokes Raman lines of $SnBr_4$, $SnCl_4$, and CCl_4 are given in Tables I, II, and III, respectively. On the assumption of tetrahedral symmetry these molecules have four fundamental modes of vibration all of which are active in Raman effect. The vibrations are designated as ν_1 for the symmetrical frequency, ν_2 for the doubly degenerate frequency, ν_3 and ν_4 for the triply degenerate frequencies. All second-order lines observed have been identified as overtones and combination tones and are designated as such in terms of the fundamentals, e.g., $2\nu_1$, $\nu_1+\nu_2$. The measured shifts for the fundamentals have been used to obtain the "calculated" frequency shifts listed for the overtones and combination tones. The frequency measurements are accurate to ± 1 cm^{-1} for strong lines and to ± 5 cm^{-1} for faint or broad lines. The relative intensities are given on a scale fixed by taking the intensity of ν_1 as 1000. The error in the intensity measurements is about ± 5 percent for the fundamentals and ± 20 percent for the second-order lines when there is no overlapping. In most cases the second-order lines were found to have half-value widths approximately equal to the sums of the half-value widths of the corresponding fundamentals.

TABLE III. Raman lines of CCl_4 liquid.

	Frequency shift (cm^{-1}) Measured	Calculated	Peak intensity	Remarks
$\nu_3-\nu_2$	94	96	—	on wing of Rayleigh line
$\nu_1-\nu_2$	143	145	—	on wing of Rayleigh line
ν_2	218		890	symmetrical
$\nu_1-\nu_2$	—	241		
ν_3	314		915	symmetrical, with faint wings
$2\nu_2$	—	436		
ν_1	459		1000	asymmetrical, faint wings
$\nu_3+\nu_2$	535	532	0.7	overlaps $\nu_4'-\nu_2$
$\nu_4'-\nu_2$	—	544		
$\nu_4''-\nu_2$	580	572	—	broad, faint
$2\nu_3$	630	628	0.7	
$\nu_1+\nu_2$	673	677	0.4	overlaps ν_4' from Hg 4339
ν_4'	762		210	symmetrical doublet
ν_4''	790		210	symmetrical doublet
$2\nu_1$	915	918	0.1	
$\nu_2+\nu_4'$	989	980	0.1	broad, diffuse
$\nu_2+\nu_4''$		1008		
$\nu_3+\nu_4'$	1072	1076	0.5	broad doublet, higher frequency component slightly sharper
$\nu_3+\nu_4''$	1110	1104	0.6	broad doublet, higher frequency component slightly sharper
$\nu_1+\nu_4'$	1221	1221	0.3	broad doublet higher frequency component slightly sharper
$\nu_1+\nu_4''$	1250	1249	0.3	broad doublet higher frequency component slightly sharper
$2\nu_4$	1540	1524 1552 1580	17	broad, asymmetrical
$\nu_2+2\nu_4$	1749	1758	0.03	very broad
$\nu_3+2\nu_4$	1860	1854	0.03	very broad
$\nu_1+2\nu_4$	1995	1999	0.04	very broad

The intensities of the second-order lines relative to the first-order lines vary widely as may be seen in Tables I, II, and III. On the average, however, the ratio in CCl_4 (excluding $2\nu_4$) and in $SnCl_4$ is about 1/1000; but in $SnBr_4$ it is larger, about 3/1000.

The relative intensities of the first-order lines of the three substances were measured in binary mixtures of known concentration. For the totally symmetrical frequency ν_1, of CCl_4, $SnCl_4$, and $SnBr_4$ the peak intensities per molecule were found to be in the ratio 1:6.7:30. This ratio

TABLE IV. Depolarizations of overtones and combination tones.

	Measured intensity ratio ⊥/∥ components	Depolarization classification (experimental)	Symmetry type of upper vibrational state	Depolarization classification (theoretical)
$SnBr_4$				
$\nu_3+\nu_4$	1.0	dp	$A_1+E+F_1+F_2$	pp
$2\nu_1$	0.3	p	A_1	p
$\nu_1+\nu_4$	1.0	dp	F_2	dp
$2\nu_4$	0.7	pp	A_1+E+F_2	pp
CCl_4				
$\nu_3-\nu_2$	0.8	dp	F_1+F_2	dp
$\nu_1-\nu_3$	0.9	dp	F_2	dp
$\nu_2+\nu_3$	1.3	dp	F_1+F_2	dp
$2\nu_3$	0.8	dp	A_1+E+F_2	pp
$\nu_1+\nu_2$	1.1	dp	E	dp
$2\nu_4$	0.5	pp	A_1+E+F_2	pp

correlates the intensities in the three tables. Since the half-value widths of the ν_1 lines for CCl_4, $SnCl_4$, and $SnBr_4$ are about 12 cm^{-1}, 9 cm^{-1}, and 5.5 cm^{-1}, respectively, the integrated intensities per molecule for this vibration are in the ratio 1:5:14. Thus, as anticipated due to the increase of polarizability with atomic number, the scattering per molecule is larger when an atom in the molecule is replaced by a heavier atom of the same chemical group.

It is interesting to note that instances of triple quantum jumps were observed, namely, the lines $\nu_1+2\nu_4$, $\nu_2+2\nu_4$, and $\nu_3+2\nu_4$ of CCl_4. These lines are extremely faint and broad. Their appearance and the high intensity of $2\nu_4$ indicate a strong anharmonicity in the ν_4 mode.**

DEPOLARIZATIONS

Polarization spectra were obtained for $SnBr_4$ and CCl_4. The intensity ratios of the ⊥ to the ∥ component for the overtones and combination tones that could be measured are given in Table IV. The lines are classified as completely polarized, if this ratio is 0.3 to 0.4, depolarized if it is 0.8 to 1.2, and partially polarized if it is between 0.4 and 0.8. The tolerances for the first two classifications are set mainly by the experimental error in the intensity ratios and not by the error in the polarization calibration. The types of vibration and the depolarizations expected on the basis of tetrahedral symmetry[6] are shown in columns four and five. The agreement between theory and experiment is complete for all the lines measured except for the $\nu_3+\nu_4$ line of $SnBr_4$ and the $2\nu_3$ line of CCl_4. Even for these two the agreement can be considered satisfactory since the experimental classification of a line as dp shows only that ρ has a value near 6/7 and the theoretical classification of a line as pp means that ρ can have any value from 0 to 6/7.

The results verify such predictions as: (1) the overtone of the polarized symmetrical frequency ν_1 is polarized; (2) the overtone of the completely depolarized triply degenerate frequency ν_4 is partially polarized; (3) the binary combinations involving the polarized frequency ν_1 with a completely depolarized frequency ν_2, ν_3, or ν_4 are completely depolarized.

DISCUSSION OF THE INTENSITIES OF SECOND-ORDER LINES

A detailed interpretation of the intensities requires some of the results of the polarizability theory of scattering.[7] The intensity of the radiation scattered by a molecule is proportional to the square of the matrix elements of the polarizability tensor, α, that is to the square of $(\alpha)_{v'}^{v}$ where v and v' are the quantum numbers of the initial and final states. α can be expanded in the usual way in terms of the normal coordinates q_i. The matrix elements in the derivative terms in the expansion of α give rise to Raman scattering. The intensity of a Raman line of frequency shift ν_i, corresponding to the ith normal mode of vibration of the molecule is proportional to the product of $\{\partial\alpha/\partial q_i(q_i)_{v_i}{}^{v_i+1}\}^2$ and the appropriate Boltzmann population factor, summed over all values of v_i. The intensity of the line is also proportional to the fourth power of its frequency.

Transitions corresponding to overtones and combination tones can occur owing to electrical anharmonicities or to mechanical anharmonicities or to both. When electrical anharmonicities are present, the derivatives in the expansion of the polarizability beyond the first are different from

** The intensity contour of $2\nu_4$ in CCl_4, especially in the polarization spectra, indicates three overlapping components with different degrees of depolarization. A detailed discussion of this and other features of the CCl_4 spectrum in relation to the resonance degeneracy will be presented elsewhere.

[6] L. Tisza, Zeits. f. Physik **82**, 48 (1933).
[7] G. Placzek, Hand. d. Radiologie, VI-2 (1934).

zero. When mechanical anharmonicities are present, the classical motion of the nuclei is not simply harmonic and hence the matrix element $(q_i)_{v'}{}^{v}$ is different from zero for transitions other than $v_i \rightarrow v_i+1$, that is, for example, for $v_i \rightarrow v_i \pm 2$ and for $v_j, v_k \rightarrow v_j+1, v_k \pm 1$. Thus, if both types of anharmonicity are present the intensity of the first overtone of the ith vibration depends on the square of matrix elements of the form:

$$\left\{\frac{\alpha}{\partial q_i}(q_i)_{v_i+2}^{v_i}+\frac{1}{2}\frac{\partial^2\alpha}{\partial q_i{}^2}(q_i{}^2)_{v_i+2}^{v_i}\right\}. \quad (1)$$

Similarly, the intensity of a combination tone involving the jth and kth vibrations will depend on the square of matrix elements of the form:

$$\left\{\left(\frac{\partial\alpha}{\partial q_j}q_j+\frac{\partial\alpha}{\partial q_k}q_k\right)_{v_j+1,\ v_k+1}^{v_j,\ v_k} +\frac{\partial^2\alpha}{\partial q_j\partial q_k}(q_jq_k)_{v_j+1,\ v_k+1}^{v_j,\ v_k}\right\}. \quad (2)$$

Of the two terms in each of the expressions, the first is the contribution of mechanical anharmonicity, the second the contribution of electrical anharmonicity. It is possible that under certain conditions the terms due to the two anharmonicities can be of opposite sign and hence combine to give a value of the intensity of the second-order line smaller than that expected for either anharmonicity alone.

The relative intensities of overtones and combination tones cannot, in general, be calculated directly with present theory. Placzek[7] derived general expressions for the intensities of overtones assuming only electrical anharmonicity; however, the derivatives of the polarizability in his expressions are undetermined. Wolkenstein[8] has recently developed a classical, semi-empirical theory based on the additivity of bond polarizabilities for calculating intensities in Raman spectra of polyatomic molecules. This theory is useful in dealing with the relative intensities of fundamental vibrations, but the expressions derived for the intensities of overtones and combination tones do not admit experimental verification.

In the special case of the spherically symmetrical vibration of an XY_4 molecule, it is possible to estimate the term due to the mechanical anharmonicity in the matrix element (Eq. (1)). Since only changes in the $X-Y$ bond length occur and the vibration is symmetrical, the potential energy can be represented by a Morse function and the known wave functions for this potential can be used in calculating $(q)_{v+2}{}^{v}$.

The potential energy takes the form,

$$V(r)=4D(1-e^{-a(r-r_e)})^2 \quad (3)$$

in which D is the $X-Y$ bond energy and a is a constant. The change in the length of the bonds is $(r-r_e)$ which can be considered as the normal coordinate q. The vibrational energy is expressible in the usual form,

$$E_v=\omega_e(v+\tfrac{1}{2})-x_e\omega_e(v+\tfrac{1}{2})^2. \quad (4)$$

If the dissociation energy, $4D$, of the molecule and the vibrational frequency, ω_e, are known, the anharmonicity constant, x_e, can be estimated from the formula:

$$x_e=\omega_e/16D. \quad (5)$$

The matrix elements $(q)_{v+1}{}^{v}$ and $(q)_{v+2}{}^{v}$ can be obtained as functions of x_e by using the method given by Dunham[9] for the calculation of the intensities of overtones in infra-red spectra. For the $0\rightarrow1$ and $0\rightarrow2$ transitions these are:

$$(q)_1{}^0=1/a(k-3)^{\frac{1}{2}} \times\left\{\log\left(\frac{k}{k-1\frac{1}{2}}\right)-\log\left(\frac{k}{k-2\frac{1}{2}}\right)\right\}, \quad (6)$$

TABLE V. Intensity ratio of the overtone to the fundamental for the symmetrical vibration in XY_4 molecules.

	Anharmonicity constant x_e	$\frac{I_0}{I_f}$ (Calculated on the basis of mechanical anharmonicity alone by Eq. (13))	$\frac{I_0}{I_f}$ (observed)
$SnBr_4$	0.00060	1/2900	1/400
$SnCl_4$	0.00085	1/2200	1/1700
CCl_4	0.00111	1/1800	1/10,000

TABLE VI. $\alpha''/\alpha' \times 10^{-8}$ cm^{-1}.

$SnBr_4$	0.78 or −1.55
$SnCl_4$	0.098 or −0.90
CCl_4	−0.29 or −0.75

[8] M. W. Wolkenstein, J. Phys. U.S.S.R. **5**, 185 (1941).

[9] J. L. Dunham, Phys. Rev. **34**, 438 (1929).

and

$$(q)_2{}^0=1/a\left(\frac{k-5}{2(k-2)}\right)^{\frac{1}{2}}\left\{(k-2)\log\left(\frac{k}{k-1\frac{1}{2}}\right)-2(k-3)\log\left(\frac{k}{k-2\frac{1}{2}}\right)+(k-4)\log\left(\frac{k}{k-3\frac{1}{2}}\right)\right\} \quad (7)$$

in which $k=1/x_e$.***

The application of these formulae is considerably simplified by expanding them in series and introducing approximations justifiable when $k(=1/x_e)$ is $\gg 1$. With this procedure (6) and (7) reduce to:

$$(q)_1{}^0=1/a(1/k^{\frac{1}{2}})\equiv 1/a(x_e^{\frac{1}{2}})\equiv b, \quad (8)$$

$$(q)_2{}^0=1/a(1/2^{\frac{1}{2}}k)\equiv 1/a(x_e/2^{\frac{1}{2}})\equiv b(x_e/2)^{\frac{1}{2}}. \quad (9)$$

Since for the Morse function $a=(8\pi^2\mu c\omega_e x_e/h)^{\frac{1}{2}}$, the constant $b=x_e^{\frac{1}{2}}/a$, introduced in the above expressions is merely the zero point amplitude of the simple harmonic oscillator of the same frequency. Thus, for this approximation, the value of $(q)_1{}^0$ is the same as that for the simple harmonic oscillator.

Since the $v=1$ level of the molecules studied is also populated to some extent at a temperature of 25°C, the $1\rightarrow 2$ and $1\rightarrow 3$ matrix elements are also required. A calculation similar to the above gives:

$$(q)_2{}^1=b\cdot 2^{\frac{1}{2}},$$
$$(q)_3{}^1=b(3x_e/2)^{\frac{1}{2}}.$$

When the ground vibrational state only is considered as the initial state and when the frequency factor is neglected, the ratio of the intensity of the overtone due to mechanical anharmonicity alone to the intensity of the fundamental can be expressed very simply in terms of the anharmonicity constant:

$$\frac{I_0}{I_f}=\frac{\{\alpha'(q)_2{}^0\}^2}{\{\alpha'(q)_1{}^0\}^2}=\frac{x_e}{2}, \quad (12)$$

where α' is written for $\partial\alpha/\partial q$.

*** S. Bhagavantam (Ind. Acad. Sci. **10A**, 224 (1939)) has used these formulae to calculate Raman overtone intensities in diatomic molecules.

When the transitions from the $v=1$ state are also taken into account and the frequency factor is included, the ratio becomes:

$$\frac{I_0}{I_f}=\frac{x_e}{2}\left(\frac{1+3e^{-\omega_e/kT}}{1+2e^{-\omega_e/kT}}\right)\left(\frac{\nu-2\omega_e}{\nu-\omega_e}\right)^4 \quad (13)$$

in which ν is the frequency of the exciting light.

Thus the determination of this intensity ratio requires only the value of x_e which can be estimated from the dissociation energy by means of (5).

In Table V are listed the calculated values of x_e and I_0/I_f, and also the experimental value of I_0/I_f. The dissociation energies used to obtain x_e were taken from the tables given by Samuel.[10] It is seen that there is no agreement between calculated and experimental results. However, this is not unexpected, as it is unlikely that mechanical anharmonicity alone is responsible for the appearance of overtones. From a comparison of the observed and calculated intensity ratios it is evident that in the case of CCl_4 the electrical and mechanical anharmonicities counteract each other, whereas in the case of $SnBr_4$ they augment each other. These two possibilities are admitted by the theory as pointed out in the discussion of expression (1).

The experimental values of the intensity ratios and the calculated values of the terms of the matrix elements of the polarizability due to mechanical anharmonicity can be used to obtain values for α''/α', the ratio of the second and first derivatives of the polarizability in the neighborhood of the equilibrium position. If for simplicity only transitions out of the ground state are considered, the intensities of the overtone and the fundamental can be given as:

$$I_0=c(\nu-2\omega)^4\{(\alpha')_{0\rightarrow 2}+\tfrac{1}{2}(\alpha'')_{0\rightarrow 2}\}^2 \quad (14)$$

and

$$I_f=c(\nu-\omega)^4\{(\alpha')_{0\rightarrow 1}\}^2 \quad (15)$$

in which c is a constant factor proportional to the intensity of the exciting light; $(\alpha')_{0\rightarrow 2}$ is written for $\alpha'(q)_2{}^0$, and $(\alpha'')_{0\rightarrow 2}$ for $\alpha''(q)_2{}^0$. Substituting from expressions (8) and (9) in $(\alpha')_{0\rightarrow 1}$ and $(\alpha')_{0\rightarrow 2}$, and putting $(\alpha'')_{0\rightarrow 2}=b^2\alpha''$ in the harmonic oscillator approximation, the intensity

[10] R. Samuel, Rev. Mod. Phys. **18**, 103 (1946).

ratio becomes:

$$\frac{I_0}{I_f}=\left(\frac{\nu-2\omega_e}{\nu-\omega_e}\right)^4\left\{\frac{b\alpha'(x_e/2)^{\frac{1}{2}}+1/2b^2\alpha''}{b\alpha'}\right\}^2$$

$$=\left(\frac{\nu-2\omega_e}{\nu-\omega_e}\right)^4\left\{(x_e/2)^{\frac{1}{2}}+1/2b\frac{\alpha''}{\alpha'}\right\}^2. \quad (16)$$

Writing the frequency factor as $\bar{\nu}^4$ and rearranging the equation we have:

$$\frac{\alpha''}{\alpha'}=\frac{\sqrt{2}}{b}\left\{\frac{\pm\left(\frac{I_0}{I_f}\right)^{\frac{1}{2}}}{\bar{\nu}^2}-\left(\frac{x_e}{2}\right)^{\frac{1}{2}}\right\}. \quad (17)$$

It is seen that the experimental value of I_0/I_f and the calculated value of x_e lead to two values for α''/α'. These are given in Table VI. If the excitation of higher vibrational levels is taken into account, these results are only slightly altered.

The absolute values of α' and α'' are not obtainable from these measurements alone. However, if the ratio of the intensities of the Raman line and the corresponding Rayleigh line were available, the value of α'/α could be found. Then, if α were known, say, from refractive index measurements the values of α' and α'' could be derived.

In conclusion, it may be said that the investigation presented here shows that overtones and combination tones in Raman scattering depend on both the electrical and mechanical anharmonicities of the molecule. In special cases the intensity of the second-order line relative to the first-order line can be used to obtain the second derivative of the bond polarizability if the anharmonicity constant of the vibration is known, and if the first derivative of the polarizability has been obtained from the intensity ratio of Raman to Rayleigh scattering. Experimental data of this kind should be of use when the theory of the polarizability of molecules is further developed.

THE JOURNAL OF CHEMICAL PHYSICS VOLUME 16, NUMBER 2 FEBRUARY, 1948

Ionization Potentials of Some Hydrocarbon Series

RICHARD E. HONIG
Research and Development Department, Socony-Vacuum Laboratories, Paulsboro, New Jersey

(Received September 29, 1947)

A new method is described which permits ionization and appearance potentials to be determined reproducibly, within ±0.02 volt, by electron impact in a conventional 180° mass spectrometer. The energy spread of the ionizing electrons, while not eliminated, is accounted for in an analytical expression that describes the ionization efficiency curve of argon near the initial upward break. It is shown that an ionization or appearance potential can be determined graphically by drawing a tangent of critical slope to the efficiency curve which has been plotted on a semilog scale. Absolute values are obtained by referring the unknown to the ionization potential of a calibrating gas (usually krypton). For the monatomic gases studied, electron impact and spectroscopic values agree within the experimental uncertainty. For some known polyatomic molecules, the "vertical" impact values exceed the "adiabatic" spectroscopic potentials by 0.02 to 0.2 volt, depending on molecular complexity. Paraffins, 1-olefins, and 2-olefins show a systematic reduction in potential with chain length. A similar decrease is observed when the mono-olefins are arranged according to the number and size of substitutions on the basic ethylene structure.

I. INTRODUCTION

IONIZATION potentials of organic molecules are not only of theoretical interest, but may also be applied to practical problems, such as the identification of isomers. A large volume of work has been published on critical potentials of individual molecules by electron impact[1,2] and by Rydberg series in the ultraviolet,[3] but, with one exception,[4] no systematic survey of any particular series has been made so far. The

[1] For recent work on hydrocarbons see: D. P. Stevenson and J. A. Hipple, J. Am. Chem. Soc. **64**, 1588, 2766, 2769 (1942); **65**, 209 (1943).

[2] V. H. Dibeler, J. Research Nat. Bur. Stand. **38**, 329 (1947).

[3] For work by W. C. Price, D. M. Simpson, T. M. Sugden, W. T. Tutte, and A. D. Walsh see: Nature **148**, 373 (1941); Proc. Roy. Soc. **A174**, 207, 220 (1940); **179**, 201 (1941); **185**, 176 (1945); Trans. Faraday Soc. **41**, 35, 76, 381, 498 (1945).

[4] R. S. Mulliken, Rev. Mod. Phys. **14**, 265 (1942); see also W. C. Price, Chem. Rev. **41**, 257 (1947).

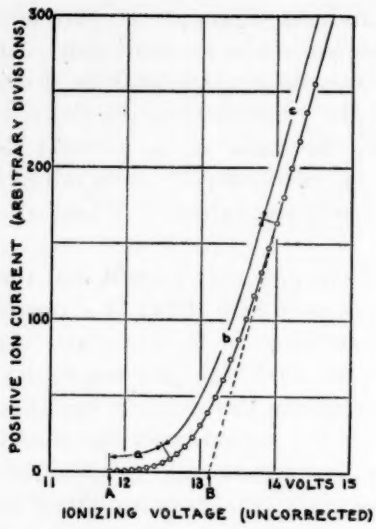

FIG. 1. Lower portion of a typical ionization efficiency curve (argon). Section *a* is exponential in character, section *b* is intermediate, and section *c* is essentially straight. Point *A* denotes the initial upward break, while point *B* is located at the extrapolated straight-line intercept.

present work is a mass spectrometric study of the variation of ionization potential with carbon number and molecular structure.

In any electron impact method employing a hot filament, the spread of electron energies makes the exact experimental determination of potentials difficult. Only for the Hg ionization potential have attempts been made to eliminate the energy spread by a magnetic filter.[5] In mass spectrometric work where such filtering would meet with practical difficulties, various methods have been devised to permit exact determinations without removing the cause of the spread.

In his study of the CH_4 molecule,[6] L. G. Smith used the initial "upward break" of the efficiency curve (point *A* in Fig. 1) to compare the potentials in question with a reference potential "under conditions of similar sensitivities" by adjusting the ordinate scales of all curves until their straight portions were parallel. Since different processes have different absolute cross sections, there is no theoretical justification for adjusting sensitivities in this manner, and considerable personal factors are involved in deciding where the curve first breaks away. However, Stevenson and Hipple showed in their comparison of argon and neon potentials[7] that this method yields values that are within 0.15 volt of the spectroscopic difference, whereas the extrapolation of the straight-line portion (point *B* in Fig. 1) will yield erroneous results. The initial onset method has been used almost exclusively ever since. One of the few exceptions is found in a paper on $SiCl_4$ by Vought.[8] He attempts to show that the appearance potential curves of molecular fragments have a shape that can be explained by the transition probability from the ground state to the antibonding branch of the ionized state, and that the extrapolated straight-line intercept should be used. This reasoning

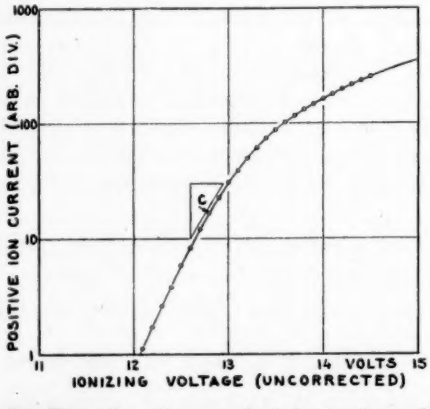

FIG. 2. Semilog plot of a typical ionization efficiency curve (argon). *C* denotes the empirical critical slope.

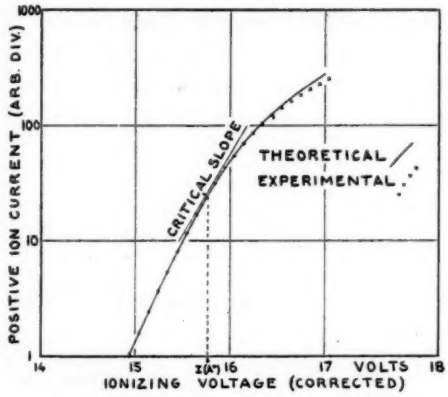

FIG. 3. Comparison of theoretical expression (using $n=2$ in Eq. (4)) with experimental values for the ionization efficiency curve of argon. Agreement is satisfactory to about 0.8 volt above the ionization potential.

[5] W. B. Nottingham, Phys. Rev. **55**, 203 (1939).

[6] L. G. Smith, Phys. Rev. **51**, 263 (1937).

[7] D. P. Stevenson and J. A. Hipple, Phys. Rev. **62**, 237 (1942).

[8] R. H. Vought, Phys. Rev. **71**, 93 (1947).

does not take into account the formation of molecular fragments by the transition to the bonding branch of the ionized state. It extrapolates from the simple two-dimensional case of H_2 to the unknown potential surfaces of a complex molecule, such as $SiCl_4$, and it is based on the simple but doubtful assumption that the probability of transition is a linear function of the excess energy above the required minimum.

This paper will present a new approach to the evaluation of ionization and appearance potentials, check the experimental accuracy obtained against the well-known ionization potentials of rare gases, and apply the new method to organic molecules.

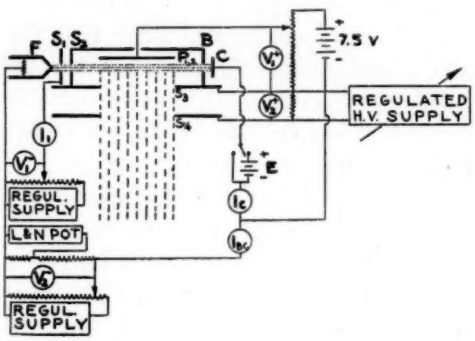

FIG. 4. Schematic diagram of electron and ion gun circuits of mass spectrometer. F—filament, S_1S_2—electron accelerating plates, B—back wall, ionization chamber, C—catcher, P_1P_2—pushers, S_3S_4—ion accelerating plates, and E—battery used for elimination of secondaries or (in reverse) for retarding potential measurements.

II. THEORY*

If the ionization efficiency curve shown in Fig. 1 is redrawn on a semilog scale (Fig. 2), the exponential character of the lower portion becomes evident. Since the energy distribution of electrons emitted from a hot filament can be described by an exponential expression, it is of interest to investigate how the shape of an efficiency curve would be modified by a given distribution. An expression will be derived that is essentially exponential below the critical energy V_c, but reflects the shape of the original efficiency curve above V_c.

Assuming a quasi-Maxwellian energy distribution and a transmission coefficient of unity

* The writer is greatly indebted to G. H. Wannier for a detailed derivation of the analytical expression presented in this section.

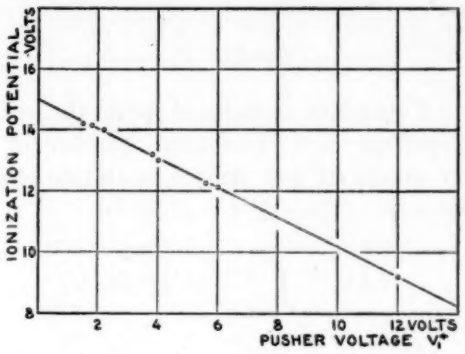

FIG. 5. Variation of the uncorrected ionization potential of argon with cross-field.

(i.e., all electrons with thermal energies U larger than the work function W leave the filament), the number of electrons of energy U leaving the filament per second,

$$N_e(U)=\frac{4\pi mA}{h^3}U\exp\left[-\frac{W-\eta+U}{kT}\right], \quad (1)$$

where m = electronic mass in g, A = surface area in cm², h = Planck's constant = 6.62×10^{-27} erg sec., U = thermal energy in ergs, W = work function in ergs, η = Fermi limit in ergs, k = Boltzmann constant = 1.38×10^{-16} erg/°K, and T = absolute temperature in °K. This expression, when integrated over all energies, yields Richardson's equation.

Before reaching the ionizing region, the electrons of thermal energy U pass through an electric accelerating field so that their total

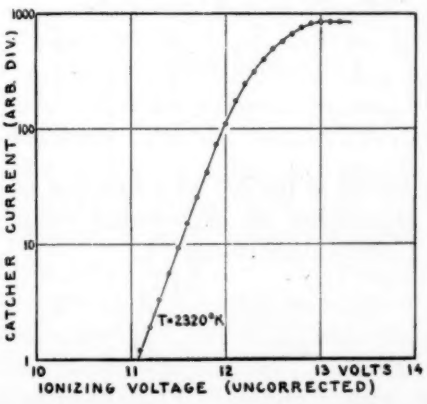

FIG. 6. Typical retarding potential plot: electron current to catcher (I_c) *vs.* ionizing voltage (V_2^-). The slope of the exponential straight line yields a distribution temperature of 2320°K. Magnet current I_m = 0.4 amp.

energy

$$E=U+V, \tag{2}$$

where V=energy associated with the accelerating voltage V/e. The total number of ions $N_i(V)$ produced per second with an electron accelerating voltage V/e is given by

$$N_i(V)=\int_{U=0}^{\infty} N_e(U)p(E)dU, \tag{3}$$

where $p(E)$=probability that an electron of total energy E produces an ion which reaches the collector. Until now, this probability has not been determined theoretically near the critical energy V_e. If it is permissible to use the empirical relation

$$\begin{aligned} &p(E)=0 \quad \text{for } E\leqslant V_e, \\ &p(E)=C_1(E-V_e)^n \quad \text{for } E\geqslant V_e, \end{aligned} \tag{4}$$

then Eq. (3) can be evaluated by substituting Eqs. (1) and (4). To date, a linear probability function ($n=1$) has been generally used.[6] In the present study it was found empirically (see below) that the best agreement between experimental and computed values is obtained for $n=2$, yielding

$$\begin{aligned} N_i(V)&=2C_2kT^3[(V_e-V)+3kT] \\ &\quad\times\exp\left[-\frac{W-\eta+V_e-V}{kT}\right] \\ &\qquad\qquad \text{for } V\leqslant V_e, \\ N_i(V)&=C_2T^2[6k^2T^2+4kT(V-V_e) \\ &\quad+(V-V_e)^2]\exp\left[-\frac{W-\eta}{kT}\right] \\ &\qquad\qquad \text{for } V\geqslant V_e. \end{aligned} \tag{5}$$

If now $\ln(N_i)$ is plotted as a function of V, the curve approaches an exponential straight line below V_e with a final slope

$$\frac{d}{dV}(\ln N_i)_F=\frac{1}{kT}. \tag{6}$$

For the critical energy $V=V_e$, the critical slope

$$\frac{d}{dV}(\ln N_i)_e=\frac{2}{3kT}. \tag{7}$$

Thus, if all the simplifying assumptions made above were valid, the ionization potential or critical energy could be determined by applying a tangent of critical slope $2/3kT$ to the semilog plot. Modifications of these assumptions will change the absolute value of the critical slope, but it will always be a certain fixed fraction of the final slope. For the most general case ($n=n$ in Eq. (4)), the critical slope can be shown to occur at

$$\frac{d}{dV}(\ln N_i)_e=\frac{n}{n+1}\frac{1}{kT}. \tag{8}$$

In order to test Eq. (5) derived above, a typical ionization efficiency curve obtained experimentally for argon was compared to the theoretical curve computed from Eq. (5). An electron distribution temperature $T=2340°$K was used (see Section III), and the two curves were matched empirically. Figure 3 shows the excellent agreement obtained over a range of several volts and presents some justification for using the relation $n=2$. It is to be noted that $n=1$ does not lend itself to such a check.

It thus appears that by plotting ion yield curves on a semilog scale and by drawing tangents of a given empirical slope to the unknown and reference curves, potential differences can be determined accurately from the horizontal separation of tangent points. Since this method depends on the location of curves drawn through at least 20 points, its reproducibility should be considerably better than that attainable by the initial onset method which depends on a few points close to the x axis.

III. EXPERIMENTAL PROCEDURE

All measurements were made on a consolidated mass spectrometer[9] which employs a 180° momentum filter. Electrons are emitted by the hot tungsten filament F (see Fig. 4), pass through a hole in shield S_1, enter the ionizing region through slit S_2, and are collected at the back wall of the ionization chamber B and on "catcher" C. Secondary electrons can be eliminated by connecting battery E into the catcher circuit, but this method introduces undesirable irregularities in the potential curves which presumably are

[9] H. W. Washburn, H. F. Wiley, S. M. Rock, and C. E. Berry, Ind. Eng. Chem. Anal. Ed. 17, 74 (1945).

due to ions formed near the catcher. Since this investigation was primarily concerned with the onset of ionization where the effects of secondaries are negligible, chamber and catcher were run at the same potential. A small cross-field (about 10 volts/cm) between "pushers" P_1, P_2 and the first ion slit plate draws some of the ions formed through slit S_3 into the strong field (about 1000 volts/cm) between S_3 and S_4. Those ions that pass S_4 are analyzed magnetically and recorded in the usual manner.

Electron energies are measured on a Leeds & Northrup No. 7655 potentiometer which had been high voltage insulated to permit safe operation as all the electron gun circuits are at high potential. In conjunction with a calibrated potential divider of proper size, the potentiometer will measure absolute voltages to better than ± 0.1 percent. The measured "ionizing voltage" V_2^- is attained by the electrons when they pass through S_2 and does not include the energy contribution from the cross-field. This contribution is variable since it depends on where in the ionizing region the ion is formed, and will contribute to the electron energy spread. Preliminary experiments were carried out to determine the maximum cross-field contribution. In Fig. 5, the uncorrected argon potential is plotted as a function of V_1^+, the pusher potential. The slope of the straight line obtained measures directly the maximum contribution as $0.49 V_1^+$. Its intercept on the y axis yields an argon potential (15.00 volts) that differs from the spectroscopic value (15.77 volts) by a thermal energy contribution and a certain contact potential difference.

The energy distribution in the electron beam is principally a function of filament temperature. Pyrometric measurements reported by H. W. Washburn[10] point to a filament temperature range of 1650–2000°K; these apparent values are not corrected for the unknown emissivity of the W_2C layer which is believed to cover the treated filament. Two other factors increasing the energy spread are the potential drop along the filament (estimated as about 0.2 volt[10]) and the cross-field, as mentioned above.

The total energy distribution was determined empirically by applying a fixed retarding potential to the catcher (see Fig. 4) and measuring the catcher current I_c as a function of ionizing voltage V_2^-. A typical semilog plot (Fig. 6) yields, by the slope of its straight-line portion, a fictitious distribution temperature of about 2320°K. A number of experiments were made to determine which of the many instrumental parameters would affect the energy spread. As expected, a decrease in filament current, and therefore filament temperature, reduces the spread. When gas is introduced, the change in work function of the filament surface shifts the entire curve shown in Fig. 6 horizontally. Since this gas effect is not reproducible, it is seen that in potential measurements the calibration gas must be introduced simultaneously with the unknown. Figure 7 shows that the fictitious distribution temperature increases as the magnet current is reduced below 0.3 amp. This results from the fact that at low field values the electron beam collimation is poor. Thus electrons that were emitted from high or low potential sections of the filament are able to pass the slit system. For this reason, special precautions must be taken when potentials of light compounds, such as H_2, D_2, and He, are to be determined.

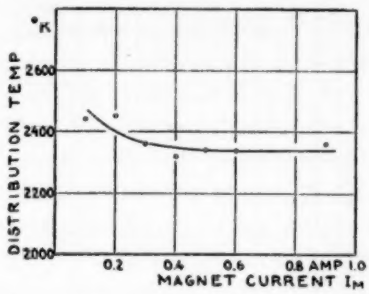

FIG. 7. Variation of temperature of electron energy distribution with magnet current I_m.

All ionization potential measurements were carried out under the following, strictly controlled conditions which have been found to yield optimum reproducibility: first electron accelerating potential, $V_1^- = 40$ volts; cross-field potential (average), $V_1^+ = 4.8$ volts; second ion accelerating potential, $V_2^+ = 600$ volts; current to ionization chamber and catcher, $I_{B+C} = 47.0\ \mu$A; magnet current I_m, adjusted to focus ion in question; reservoir gas pressure, up to 250 microns total for calibrating gas and unknown. Measurements were taken by reducing the ion-

[10] H. W. Washburn, two private communications.

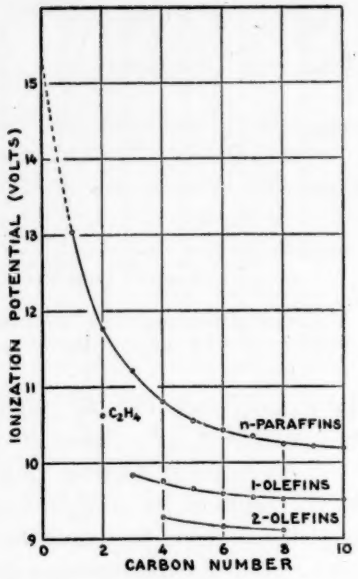

FIG. 8. Ionization potentials of some members of the normal paraffin and 1- and 2-olefin series.

izing voltage V_2^- in the critical range in steps of 0.1 volt and scanning each peak electrically several times in succession. The slight change in V_2^+ necessary to produce this sweep (about 10 volts) did not materially alter conditions in the source. To test the effect of pressure reduction in the reservoir on the curve shape, a number of experiments were made by first reducing and then increasing V_2^- and averaging the values. No differences between this and the simpler routine could be detected for all compounds tested.

The calibration gases found to be best suited for simultaneous introduction with hydrocarbons in the C_1 to C_5 range were argon and krypton, while xenon and benzene were used with all other unknowns. These four reference gases were carefully intercalibrated, and all values quoted below are based on the spectroscopic krypton potential of 14.01 volts[11] as a single primary standard.

IV. RESULTS AND DISCUSSION

The results given in Table I show that ionization potentials can be determined reproducibly by the slope method. On a typical semilog plot (see Fig. 2), a smooth curve can be drawn which will fall within ±0.01 volt of all experimental points, and the point where the critical slope is tangent to the curve can be reproduced graphically to ±0.01 volt. If the reference gas is introduced simultaneously with the unknown, repeat runs will yield absolute potentials that generally agree within 0.03 volt. Where different reference gases were used for the same compound, the maximum spread is occasionally 0.04 volt, while *n*-decane with its unusually low sensitivity is the only example of a 0.05-volt spread. Thus the experimental reproducibility of a given potential may be expressed as ±0.02 volt.

To test the reliability of absolute values obtained by the slope method, the potentials of the monatomic gases A and Xe were determined with Kr serving as reference. It is seen that for these gases the impact values agree with the spectroscopic values within the reproducibility of the measurements.

For some of the polyatomic molecules shown in Table I, spectroscopic ionization potentials computed from Rydberg series are available for comparison with the electron impact values which are based on krypton as a primary standard. In every case, the impact values, which represent "vertical" transitions favored by the Franck-Condon principle, are higher than the spectroscopic potentials ("adiabatic" transitions between vibrational levels $V'=0$ and $V''=0$)[1] by

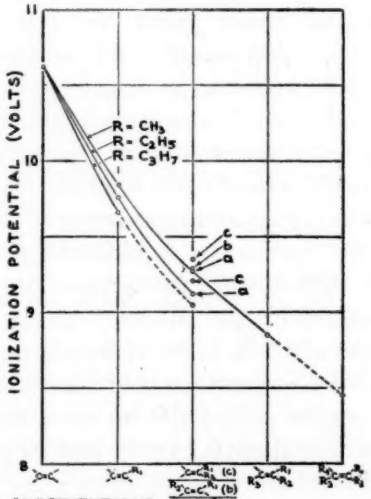

FIG. 9. Plot of ionization potential *vs.* ethylene substitutions. The last point on the methyl curve was recomputed from Price's value (see reference 3).

[11] Recomputed, using the new conversion factor 8067.49 $cm^{-1}=1$ v, from R. F. Bacher and S. Goutsmit, *Atomic Energy States* (McGraw-Hill Book Company, Inc., New York, 1932).

0.02 to about 0.2 volt. This difference seems to be a function of the molecular complexity as it is smallest for diatomic molecules and largest for benzene. According to the Franck-Condon principle, the difference between the vertical and adiabatic transitions depends on how the minima of the potential surfaces representing the ground and ionized states are located relative to each other. Since the geometry of these potential surfaces is known exactly only in the simple case of H_2, it is not possible to predict theoretically such differences. However, the problem might be avoided by comparing the molecule in question to a known molecule with a similar ionization probability rather than to a known monatomic gas.

The potentials of some members of the normal paraffin and olefin series are plotted as a function of carbon number in Fig. 8. Even though all absolute values are probably high by about 0.1 volt, the smooth curves clearly indicate that all potentials within any one series are self-consistent. The normal paraffin curve shows a systematic reduction of potential with chain length which is still noticeable in the C_{10} range. The potentials published in earlier electron impact studies[1,6] for CH_4, C_2H_6, and C_3H_8 agree, within their experimental uncertainties, with the present values. On the other hand, Stevenson and Hipple's value[1] for $n-C_4H_{10}$ (10.4_2 volts, based on $I(A^+)=15.77$ volts) lies approximately 0.4 volt below the value determined in this research and cannot be reconciled wit'. the paraffin curve. When extrapolated to zero carbon number, the paraffin curve yields the H_2 potential. Since the H−H, C−H, and C−C bonds are all believed to be similar[16] in that a σ electron is removed for the ionization of H_2, CH_4, and

TABLE I. Ionization potentials of standards, paraffins, and mono-olefins. The new conversion factor 8067.49 $cm^{-1}=1$ volt was used for recomputing the literature values.

Compound	Mass	Ionization potential in volts Individual values					Ave.	←Literature→ ←Spectroscopic→ Value	Diff.	Ref.	←"Mass Spec." Value	Ref.	Remarks
Krypton	84						*14.01*	14.01	—	(11)			Primary standard
Argon	40	15.78	15.76	15.76			15.77	15.77	0.00	(11)			Secondary standard
Xenon	132	12.14	12.16	12.17	12.16		12.16	12.14	+0.02	(11)			Secondary standard
Nitrogen	28	15.59	15.62	15.59	15.60		15.60	15.58	+0.02	(13)	15.7	(14)	
Carbon dioxide	44	13.85	13.84	13.85			13.85	13.79	+0.06	(3)			
Acetylene	26	11.44	11.43	11.42			11.43	11.40	+0.03	(3)	11.2_8	(12)	
Benzene	78	9.43	9.44	9.42	9.45	9.43	9.43	9.24	+0.19	(3)	9.8_8	(15)	Secondary standard
Methane	16	13.02	13.05				13.04				13.1_8	(6)	
Tetradeuteromethane	20	13.19	13.22				13.21						
Ethane	30	11.74	11.77				11.76				11.6_8	(1)	
Propane	44	11.22	11.20	11.22			11.21				11.2_3	(1)	
n-Butane	58	10.82	10.81	10.78	10.78		10.80				10.4_2	(1)	
n-Pentane	72	10.54	10.56				10.55						
n-Hexane	86	10.42	10.44				10.43						
n-Heptane	100	10.34	10.36				10.35						
n-Octane	114	10.24	10.24				10.24						
n-Nonane	128	10.23	10.19				10.21						
n-Decane	142	10.21	10.16				10.19						
Ethylene	28	10.60	10.63				10.62	10.51	+0.11	(3)	10.8_8	(12)	
Propene	42	9.84	9.84				9.84	9.6_8	+0.2(?)	(3)	9.7_7	(1)	Spectroscopic value uncertain
1-Butene	56	9.76	9.76				9.76				9.6_8	(1)	
1-Pentene	70	9.67	9.65				9.66						
1-Hexene	84	9.59	9.60	9.59			9.59						
1-Heptene	98	9.52	9.55				9.54						
1-Octene	112	9.51	9.53				9.52						
1-Decene	140	9.49	9.52				9.51						
cis-2-Butene (Penn)	56	9.31	9.28	9.29			9.29						
trans-2-Butene (Penn)	56	9.26	9.28	9.26			9.27	9.2_8	+0.02(?)	(3)			Spectroscopic value uncertain
cis-2-Butene (NBS)	56	9.31	9.31	9.30	9.30		9.31				9.4_1	(2)	
trans-2-Butene (NBS)	56	9.28	9.29	9.27	9.30		9.29				9.1_8	(2)	
trans-2-Hexene	84	9.15	9.17				9.16						
2-Octene	112	9.10	9.11				9.11						
2-M-Propene	56	9.34	9.35				9.35				8.8_7	(1)	
3-M-2-Butene	70	8.86	8.84				8.85	8.79	+0.06	(3)			
2-E-1-Butene	84	9.20	9.22	9.21			9.21						
trans-3-Hexene	84	9.11	9.13	9.12			9.12						

[12] P. Kusch, A. Hustrulid, and J. T. Tate, Phys. Rev. **52**, 843 (1937).
[13] G. Herzberg, *Molecular Spectra and Molecular Structure.* I. *Diatomic Molecules* (Prentice-Hall, Inc., New York, 1935).
[14] H. D. Hagstrum and J. T. Tate, Phys. Rev. **59**, 354 (1941).
[15] A. Hustrulid, P. Kusch, and J. T. Tate, Phys. Rev. **54**, 1037 (1938).

higher paraffins, respectively, it is not too surprising that H_2 fits so well into the paraffin scheme. The substantial potential difference (about 0.17 volt) between CD_4 and CH_4 will be treated in detail in another paper.

The results shown in Table I for the various mono-olefins may be represented graphically in several ways. Figure 8 shows that the 1- and 2-olefins arrange themselves into two smooth, parallel curves that lie about 0.43 volt apart; the potentials are seen to decrease in regular fashion with increasing carbon number. It is generally postulated[16,17] that an olefin is ionized by the removal of a π-electron from the C=C bond. Thus it seems logical to treat olefins as substituted forms of the basic ethylene structure, and to study how the number, size, and position of substitutions affect the ionization potential.

The top curve of Fig. 9 shows the marked and regular decrease of potential with the number of methyl substitutions in the series ethylene, propene, *trans*-2-butene, 3-methyl-2-butene, and 2,3-dimethyl-2-butene, which confirms Mulliken's tabulation[4] of W. C. Price's data. Since the last named compound was not available at the time of this research, Price's recomputed value was used to complete the curve. It is seen that the ethylene potential fits such a sequence far better than the 1-olefin series of Fig. 8. For the three possible cases of double methyl substitution, the potential decreases slightly with increasing symmetry in the sequence 2-methyl-propene (9.35), *cis*-2-butene (9.31), *trans*-2-butene (9.29). In a recent paper, Dibeler[7] quoted the *cis*- and *trans*-potentials as $9.4_1 \pm 0.1$ and $9.1_3 \pm 0.1$ volts, respectively. In view of the symmetry sequence given above, Dibeler's *cis-trans* difference appears too large to be real, but can be brought in line if his experimental error is larger than quoted. In the present research, two *cis-trans* pairs (Source: Penn State and NBS) were run a sufficient number of times to establish that the *cis-trans* difference measured (0.02 ± 0.01) is real.

The curves obtained for the ethyl and propyl substitution series lie below the methyl curve. Unavailability of pure compounds prevented their completion. Two cases of double ethyl substitution show again that the most symmetric structure has the lowest potential (2-ethyl-1-butene: 9.21; *trans*-3-hexene: 9.12). 4-octene was unobtainable to serve as an example of double substitution in the propyl series. However, an admittedly rough estimate of this point may be had by using the 2-octene value and applying a downward correction that is somewhat larger than the difference between 2- and 3-hexene. For single substitutions, the systematic lowering of potential with radical size has already been pointed out by the 1-olefin curve of Fig. 8. Similar tendencies for the double substitution sequence methyl-ethyl-propyl are apparent from Fig. 9.

Earlier electron impact studies agree, within their experimental uncertainty, with the present values for propene and 1-butene,[1] but their ethylene[12] and 2-methyl-propene[1] potentials are, respectively, too high and too low to fit into the general olefin scheme.

The experimental data presented graphically in Figs. 8 and 9 show that all paraffin and olefin potentials are self-consistent, although they may be as much as 0.1 volt higher than the spectroscopic values.

ACKNOWLEDGMENTS

The writer is greatly indebted to G. H. Wannier for the derivation of the analytical expression, and to J. R. White for fruitful discussions. It is a pleasure to acknowledge the untiring assistance of the Mass Spectrometer Research Group, especially J. G. Mollet, H. Sobcov, and Miss M. A. Eaton, in operating the instrument, reading records, and plotting data.

[16] E. J. Bowen, *The Chemical Aspects of Light* (Oxford University Press, New York, 1946), Chapter III.
[17] A. D. Walsh, Trans. Faraday Soc. 42, 779 (1946).

THE JOURNAL OF CHEMICAL PHYSICS VOLUME 16, NUMBER 2 FEBRUARY, 1948

Time-Dependence of Surface Tension of Solutions

CHARLES M. BLAIR, JR.
Petrolite Corp. Ltd., Tretolite Co. Division, Webster Groves, Missouri

(Received October 3, 1947)

The slow rate of change of surface tension observed by Addison with aqueous solutions of fatty alcohols cannot be explained by diffusion alone. It is assumed that the adsorption of non-electrolyte solutes in the surface film is opposed by a constant potential energy barrier, and, on this basis, a relation between spreading pressure and surface age is developed. With the resulting equation, the experimental data of Addison are employed to evaluate the energy term. Nearly constant values for the assumed barrier are obtained, the actual calculated values, in calories per mole at 20°C, being about 1900 for isoamyl alcohol, 1300 for *n*-hexyl alcohol, and 700 for *n*-heptyl alcohol. A second relation between spreading pressure and surface age is derived on the assumption that the energy barrier is a linear function of spreading pressure. The use of Addison's data for isoamyl alcohol in this relation indicates that the spreading pressure-dependent portion of the barrier is small and of the same order of magnitude as the energy required to compress the surface film sufficiently to admit the entering solute molecule.

THE curious slow attainment of surface tension equilibrium of solutions has often been observed.[1,2] In solutions of organic electrolytes this variation of surface tension with time is much slower than with solutions of non-electrolytes. Addison,[3–5] employing the vibrating jet technique, has measured the surface tension of fatty alcohol solutions as a function of time, and has found that the final steady value is reached in times of less than one second.

Repeated attempts[2,6–8] to describe this phenomenon in terms of rate of diffusion of solute molecules to the surface have been unsuccessful. Ross[7] was forced to the untenable conclusion that a polymolecular layer was formed on the surface of alcohol solutions, while Addison[5] concluded that the "migration velocity" of the solute molecules *increased* with increasing molecular weight. It appears that even with the non-electrolytes the rate of change of surface tension is much less than can be accounted for by diffusion alone. Doss[2] made the reasonable suggestion that an energy barrier may account for the phenomenon of slow adsorption in high molecular weight electrolyte solutions and attempted, in the case of these solutions, to describe the barrier qualitatively in terms of electrical effects at the surface.

With solutions of non-electrolytes, electrical double layer effects would presumably be absent. The results of Addison, particularly with isoamyl alcohol, thus present an opportunity to explore the nature of the adsorption barrier in a relatively simple system.

In the somewhat similar problem relating to the evaporation of water through compressed monolayers, Langmuir and Schaefer[9] were able to describe the very low evaporation rates observed by the concept of an energy barrier of the form:

$$\lambda = (A + BF)kT, \qquad (1)$$

where A and B are constants, and F is the surface film pressure. By analogy, it might be expected that a similar form of barrier would appear in the formation of a surface film from solutions. In this instance, however, since the solute molecules need not go entirely through the surface film, it would seem reasonable to expect the coefficient B in Eq. (1) to be smaller than in the process studied by Langmuir and Schaefer. If B is small, it would be difficult, in the absence of extremely accurate experimental

[1] N. K. Adam and H. L. Shute, Trans. Faraday Soc. **31**, 205 (1935); *ibid.* **34**, 758 (1938).
[2] K. S. G. Doss, Kolloid Zeits. **84**, 138 (1938); *ibid.* **86**, 205 (1939).
[3] C. C. Addison, J. Chem. Soc., 535 (1943).
[4] C. C. Addison, J. Chem. Soc., 252 (1944).
[5] C. C. Addison, J. Chem. Soc., 98 (1945).
[6] W. N. Bond and H. O. Puls, Phil. Mag. [7] **24**, 864 (1937).
[7] S. Ross, J. Am. Chem. Soc. **67**, 990 (1945).
[8] A. F. H. Ward and L. Tordai, J. Chem. Phys. **14**, 453 (1946).
[9] I. Langmuir and V. J. Schaefer, J. Frank. Inst. **235**, No. 2, 119 (1943).

TABLE I. Values of constants of Eq. (7) for various alcohols at 20°C.

Alcohol	J ($cm^2 \times 10^{16}$)	L	D ($cm^2\ sec.^{-1} \times 10^6$)
Isoamyl	16.7	0.827	7.9
n-Hexyl	19.7	0.710	7.1
n-Heptyl	18.4	0.600	6.4

data, to differentiate between a constant energy barrier and one varying with film pressure.

Depending upon the equation of state describing the surface film and the form of the assumed barrier function, a number of different relations between spreading force and time are obtained. We shall herein derive two such relations, employing an equation of state applicable to films of soluble alcohols and two simple potential functions of the Langmuir type. The extent to which either of these relations can be fitted to the experimental results will serve to indicate the *possible* correctness of assumptions involved.

CASE I

A constant energy barrier and a surface film obeying the two-dimensional Amagat equation are assumed.

Solutions of many soluble substances, including the fatty acids and alcohols, form surface films obeying the equation[10]

$$F = N(FJ + LkT), \tag{2}$$

TABLE II. Energy barrier to adsorption of alcohols in surface film (at 20°C).

Conc. of solution (Wt. %)	$F_{\frac{1}{2}}$ (dynes cm^{-1})	$t_{\frac{1}{2}}$ (sec. $\times 10^3$)	$\exp(\lambda/kT)$	λ (cal. $mole^{-1}$)
		Isoamyl alcohol		
0.122	4.3	12.4	27.6	1930
0.203	6.1	8.0	28.2	1940
0.325	9.3	5.7	28.4	1950
0.406	10.4	5.3	31.6	2010
		n-Hexyl alcohol		
0.050	5.4	24	10.4	1360
0.100	9.0	9.5	8.9	1270
0.150	11.4	6.0	9.3	1300
0.200	13.2	4.9	10.3	1350
		n-Heptyl alcohol		
0.020	6.1	36	3.30	690
0.040	10.0	17	3.31	700
0.060	12.6	10	3.38	710

[10] N. K. Adam, *The Physics and Chemistry of Surfaces* (Oxford University Press, London, 1941), p. 118.

where N is the number of molecules of solute per cm^2 of surface and J and L are constants.

Ward and Tordai[8] have shown that diffusion theory leads to the following expression for the rate of arrival of diffusing solute molecules at one cm^2 of surface of a solution,

$$\partial M/\partial t = Dn_0/(\pi Dt)^{\frac{1}{2}}, \tag{3}$$

where n_0 is the bulk concentration of solute and D is the diffusion constant.

We have assumed, however, that the actual adsorption of molecules in the surface film is opposed by a constant barrier of height λ. Therefore, the rate of adsorption of solute is given by

$$\partial N/\partial t = \partial M/\partial t \exp(-\lambda/kT). \tag{4}$$

Hence,

$$N = 2n_0(Dt/\pi)^{\frac{1}{2}} \exp(-\lambda/kT). \tag{5}$$

Combining Eq. (5) and Eq. (2), we obtain the desired relation between spreading pressure and time:

$$F/FJ + LkT = 2n_0(Dt/\pi)^{\frac{1}{2}} \exp(-\lambda/kT), \tag{6}$$

which may be written in the form,

$$\exp(\lambda/kT) = 2n_0(FJ + LkT)(Dt/\pi)^{\frac{1}{2}}/F. \tag{7}$$

Equation (3) was originally obtained by neglecting any backward diffusion of solute molecules from the surface, and accordingly can only be correct at times short of equilibrium. In order to test Eq. (7), therefore, we shall consider the times required for the surface pressure to go only half of its way to equilibrium. The work of Addison[4,5] on the rate of change of surface tension of solutions of isoamyl alcohol, *n*-hexyl alcohol, and *n*-heptyl alcohol furnishes enough experimental data to permit calculation of the approximate values of the energy barriers by Eq. (7).

The required values of J and L may be obtained from the data given by Addison on the equilibrium surface tension and the rate of change of surface tension with concentration for solutions of the above mentioned alcohols. The diffusion constants (at 20°C) were taken from the curve of Ward and Tordai.[8] Table I gives the numerical values of the various constants of Eq. (7) so obtained, at 20°C.

Table II gives the spreading force-time data for the three alcohols as interpolated from

Addison's experimental results, and the values of the energy barriers as calculated from these data and those of Table I by insertion in Eq. (7). In Table II, $F_{\frac{1}{2}}$ denotes the spreading force of the surface film when the surface tension has proceeded one-half of its way toward equilibrium, and $t_{\frac{1}{2}}$ is the time required for the spreading force to reach this value. $F_{\frac{1}{2}}$ and $t_{\frac{1}{2}}$ are used for F and t in Eq. (7) for the reason previously cited.

It is evident that with each alcohol the calculated energy barrier values are essentially constant within the range of accuracy of the spreading force measurements. However, there is a consistent suggestion in the trend of calculated values that the barrier may increase slightly with increasing film pressure, or, in other words, that B of Eq. (1) should have a small positive value rather than the value of zero assumed in this case. It is also found that the height of the barrier decreases markedly with increase in molecular weight of the alcohol, a result which may be related to the fact that the lateral adhesion of the molecules in a surface film increases rapidly with increasing hydrocarbon chain length.

CASE II

An energy barrier of the Langmuir type, and a surface film obeying the two-dimensional Amagat equation are assumed.

Expressed formally, these assumptions are that

$$\lambda=(A+BF)kT^{*}$$

and

$$F=N(FJ+LkT).^{**}$$

Therefore,

$$dN/dt=LkT/(FJ+LkT)^{2}(dF/dt).$$

Substituting these values and Eq. (3) in Eq. (4), we obtain

$$\exp(BF)dF/(FJ+LkT)^{2}=n_{0}(D/\pi t)^{\frac{1}{2}}\exp(-A)/LkTdt. \quad (9)$$

Integration of Eq. (9) leads to the desired relation between spreading pressure and time, namely

$$\exp(A)-LkT\exp(A+BF)/FJ+LkT+BLkT/J\{Ei[B(FJ+LkT)/J]-Ei[BLkT/J]\}\exp(A-BLkT/J)=2n_{0}J(Dt/\pi)^{\frac{1}{2}} \quad (10)$$

where Ei is the exponential integral function.[11]

When the coefficient B has the value of zero, the conditions are those of Case I, and Eq. (10) reduces to Eq. (7).

For accurate evaluation of the constants A and B, the use of Eq. (10) is somewhat cumbersome, and, in addition, requires more precise experimental data on the relation between spreading pressure and time than are now available for non-electrolyte solutions. However, in the case of isoamyl alcohol, the appropriate constants from Table I and the experimental data from Table II have been employed in Eq. (10) to obtain approximate values of A and B. These are found to be 3.2 and 0.040, respectively. Therefore, for the adsorption of isoamyl alcohol in the surface of its aqueous solution at 20°C, the apparent energy barrier is given by

$$\lambda=(3.2+0.040F)kT$$

or, in calories per mole at 20°C,

$$\lambda_{\text{cal./mole}}=1860+23F. \quad (11)$$

This result conforms with the indicated slow increase of the energy barrier value with increasing spreading pressure observed in Case I.

DISCUSSION OF RESULTS

The results of calculations presented in Table II and under Case II show that the concept of a potential energy barrier, of reasonable magnitude, hindering the adsorption of solute molecules in the surface is sufficient to describe the slow attainment of surface tension equilibrium in solutions of some organic non-electrolytes. For more accurate determinations of the energy barriers and their dependence on spreading pressure, more precise experimental data on the relation between surface tension and time would

* See Eq. (1).
** See Eq. (2).

[11] Numerical values of the exponential integral function are given by E. Jahnke and F. Emde, *Tables of Functions* (Dover Publications, New York, 1943), p. 6 *et. seq.*; and by A. N. Lowan, *Tables of Sine, Cosine, and Exponential Integrals* (Works Progress Administration, New York, 1940), Vols. I and II.

be desirable. Also, experiments on this relation at different temperatures would be helpful in evaluating the barrier.

In considering the possible origin of a potential barrier to adsorption of a solute molecule, there immediately appears the work required to compress the surface film sufficiently to make space for the molecule entering the film from solution. This energy requirement would be roughly equal to Fa, where a is the effective area occupied by the entering solute molecule. Such a potential barrier would, of course, be directly proportional to the spreading pressure and would increase with increasing molecular weight of solute. We have found, for the fatty alcohols discussed above, only a very slight dependence of λ on F and a smaller value of λ for the higher alcohols. The value of Fa will also be far too small, in general, to account for the λ values calculated. Taking isoamyl alcohol as an example, and using a molecular cross-sectional area calculated from its density at 20°C, we find Fa to have a value of about $57F$ cal. per mole. This is of the same order of magnitude as the spreading pressure-dependent portion of the potential barrier calculated for isoamyl alcohol and given in Eq. (11). It thus appears that, at most, the work of compressing the surface film can only account for the small portion of λ which is dependent on spreading pressure.

Although in carrying out the present calculations, $F_{\frac{1}{2}}$ and $t_{\frac{1}{2}}$ values have been employed in Eq. (7) and Eq. (10), it should be pointed out that the use of other corresponding F and t values up to the point where F is at least 80 percent of its equilibrium value yields essentially the same values of λ. Therefore, it appears that back diffusion from the surface probably leads to no important errors in the calculations, within the range of F values used.

THE JOURNAL OF CHEMICAL PHYSICS VOLUME 16, NUMBER 2 FEBRUARY, 1948

Search for Near Ultraviolet Bands in Borazole*

LOIS E. JACOBS, J. R. PLATT
Physics Department, University of Chicago, Chicago, Illinois
AND G. W. SCHAEFFER
Chemistry Department, University of Chicago, Chicago, Illinois

(Received October 1, 1947)

Borazole, $B_3N_3H_6$, shows no absorption bands in the region 2000A–4600A, at pressures of about 2 atmospheres in a 4-cm cell. Since bands analogous to those of benzene are expected on theoretical grounds, it is concluded that the analogues of the benzene 2600A and 1830A bands are the borazole 1995A and 1720A bands, with the analogues of the benzene 2080A bands perhaps being hidden in between.

AN attempt has been made to find bands in triborine-triamine or borazole, $B_3N_3H_6$, corresponding to the 2600A bands in benzene—that is, having the same general appearance as the latter bands and lying, like these, in the quartz ultraviolet. Pressures of about 2 atmospheres, higher than any previously used in this experiment, were obtained but with a 4-cm path no bands were found in the region 2000A–4600A.

This experiment was suggested by Dr. E. H. Hutten. He attempted earlier to detect these bands in this laboratory, but only enough borazole was available at that time to obtain vapor pressures of about 20 cm in a 4-cm cell. His work was the result of the belief that the ring structure and electronic structure of borazole are very similar to those of benzene (see Bibliography in reference 1).

In support of this belief was later work from this laboratory on borazole solutions[1] in which bands at 1995A and a peak at 1720A seemed to be similar to the benzene bands at 2080A and

* This work was assisted by the Office of Naval Research under Task Order IX of Contract N6ori-20 with the University of Chicago.

[1] J. R. Platt, H. B. Klevens, and G. W. Schaeffer, J. Chem. Phys. 15, 598 (1947).

the strong $N \rightarrow V$ transition peak at 1830A, respectively. Also, Dr. R. S. Mulliken has shown that on theoretical grounds "a one-to-one correspondence and close resemblance between the electron configuration and over-all states of borazole and benzene are to be expected" (footnote 12 of reference 1). In these solution experiments the bands similar to the 2600A benzene bands were not found even when concentrations 20 times that necessary for detecting these bands in benzene were used.

For the present work, $2.4_3 \times 10^{-3}$ moles of borazole were heated to 77°C, or until all the material appeared to be in the vapor state, in a quartz cell of 4-cm length and approximately 35.4-cc volume, giving a concentration of $6.8_7 \times 10^{-2}$ m/l. The borazole was prepared by the method indicated in reference 1. Plates taken on the small University of Michigan vacuum fluorite spectrograph[1] showed no bands in the 2000–4600A region. The benzene 2600A bands observed in a matching cell were still distinctly visible when the side arm was at a temperature of −68°C, corresponding to a pressure of about 0.042 mm. It was estimated that they would be barely visible at pressures about five times lower, corresponding to a concentration of 6.8×10^{-7} m/l. This would indicate that if bands like the 2600A benzene bands occur in borazole in the 2000–4600A region, their intensity must be less than that of benzene by the factor of at least 10^5. Therefore, one might conclude that no bands exist in borazole corresponding to the 2600A benzene bands, or that if they do exist, they have shifted to shorter wave-lengths and the upper state has become so mixed with other states that the bands are unidentifiable as such.

Another explanation which seems more plausible in view of the theoretical reasons for expecting such bands, is that the 1995A borazole bands should not be identified, as was done in a former paper,[1] with the 2080A benzene bands, but are instead themselves the analogs of the 2600A bands. On this view, it would be the analogues of the 2080A benzene bands which are concealed, perhaps being hidden by the strong $N \rightarrow V$ peak at 1720A. This interpretation would reduce the spread of the states of the upper electronic configuration from its value of about 15,000 cm^{-1} between the $^1B_{2u}$ and $^1E_{1u}$ states in benzene to about 5000 cm^{-1} between the $^1A_2'$ and $^1E'$ states of borazole, but it would preserve the sequence of corresponding states in the compounds. Also the comparative weakness of the 1995A bands, which was a difficulty in the former interpretation making them analogous to the rather strong 2080A benzene bands, now becomes quite reasonable, as they are several times as strong as the 2600A benzene bands. Their strength and their diffuseness may then be the result of their closeness to the strong $N \rightarrow V$ transition.

The whiteness of boron nitride crystals, which was commented on in the former paper, also becomes somewhat more understandable on this interpretation. The resonance interaction which produces the spread in energies among the states of the upper electron configuration now appears to be only one-third as strong in a B_3N_3 ring as it is in a C_6 ring. Consequently it is no surprise that in a lattice of B_3N_3 hexagons the resonance interactions do not produce even the 20,000- or 30,000-cm^{-1} spread necessary to give a visible color, even though in the corresponding carbon lattice of graphite the states are spread throughout 60,000 cm^{-1} or more and the compound is black.

We are indebted to Mr. Riley Schaeffer for the preparation of the borazole used in the experiment.

Molecular Orbital Treatment of the Ultraviolet Spectra of Benzene and Borazole†

C. C. J. ROOTHAAN* AND R. S. MULLIKEN
The University of Chicago, Chicago, Illinois

(Received October 1, 1947)

The ground state and the first excited states of benzene and borazole are treated according to the semi-empirical molecular orbital method. Comparing the observed spectra with the computed energies, a spectroscopic value of -2.6 ev for the bond integral β is obtained in the case of benzene. In the case of borazole this procedure includes one more parameter, which takes care of the difference in electronegativity of boron and nitrogen. Taking a reasonable value for this parameter, a value of -2.3 ev for the bond integral between boron and nitrogen, β^*, is obtained in fair agreement with theoretical expectations.

THE benzene molecule has been treated according to the molecular orbital method by Mayer and Sklar.[1] These authors made a completely theoretical computation. For the Hamiltonian, they took for the field of the core the field of six carbon atoms minus six $2p\pi$ electrons, then fed these six electrons into this field and calculated the energies of the ground state and the first excited states. The only empirical value they used was 1.40A for the C−C distance.

In the present paper a semi-empirical method is used. The procedure is equally simple for benzene (C_6H_6) and borazole ($B_3N_3H_6$), the only difference being the occurrence of one more parameter in the case of borazole.

Neglecting interactions of non-neighbor ring atoms, we can write the secular equations for the six approximate molecular orbitals, derivable as linear combinations of $2p\pi$ atomic orbitals of the ring atoms, in the form;

$$\begin{vmatrix} A & 1 & 0 & 0 & 0 & 1 \\ 1 & A & 1 & 0 & 0 & 0 \\ 0 & 1 & A & 1 & 0 & 0 \\ 0 & 0 & 1 & A & 1 & 0 \\ 0 & 0 & 0 & 1 & A & 1 \\ 1 & 0 & 0 & 0 & 1 & A \end{vmatrix} = 0 \text{ (benzene)},$$

$$\begin{vmatrix} A' & 1 & 0 & 0 & 0 & 1 \\ 1 & A'' & 1 & 0 & 0 & 0 \\ 0 & 1 & A' & 1 & 0 & 0 \\ 0 & 0 & 1 & A'' & 1 & 0 \\ 0 & 0 & 0 & 1 & A' & 1 \\ 1 & 0 & 0 & 0 & 1 & A'' \end{vmatrix} = 0 \text{ (borazole)},$$

where

$$A=\frac{\alpha-E}{\gamma-SE}, \quad A'=\frac{\alpha'-E}{\gamma^*-S^*E}, \quad A''=\frac{\alpha''-E}{\gamma^*-S^*E},$$

$$\alpha=\int \bar{\psi}_C{}^1 H \psi_C{}^1 d\tau, \quad \alpha'=\int \bar{\psi}_B{}^1 H^* \psi_B{}^1 d\tau,$$

$$\alpha''=\int \bar{\psi}_N{}^1 H^* \psi_N{}^1 d\tau,$$

$$\gamma=\int \bar{\psi}_C{}^1 H \psi_C{}^2 d\tau, \quad \gamma^*=\int \bar{\psi}_B{}^1 H^* \psi_N{}^2 d\tau,$$

$$S=\int \bar{\psi}_C{}^1 \psi_C{}^2 d\tau, \quad S^*=\int \bar{\psi}_B{}^1 \psi_N{}^2 d\tau.$$

The ψ's are atomic $2p\pi$ orbitals, the subscripts referring to the kind of atom, the superscripts to the location in the ring. H and H^* are the one-electron Hartree-field Hamiltonian operators for benzene and borazole, respectively. Substituting

$$\begin{gathered} \alpha-E=-X, \\ \gamma-S\alpha=\beta, \\ \gamma^*-S^*\alpha=\beta^*, \\ \alpha'-\alpha=\delta', \\ \alpha''-\alpha=\delta'', \end{gathered}$$

we get

$$A=\frac{-X}{\beta-SX}, \quad A'=\frac{\delta'-X}{\beta^*-S^*X}, \quad A''=\frac{\delta''-X}{\beta^*-S^*X}.$$

† This work was assisted by the Office of Naval Research under Task Order IX of Contract N6ori-20 with the University of Chicago.

* At present at the Catholic University of America, Washington, D. C.

[1] M. G. Mayer and A. L. Sklar, J. Chem. Phys. 6, 645 (1938). See also V. Griffing, J. Chem. Phys. 15, 421 (1947).

The α's, γ's, and β's are known to be negative quantities. The α's are electronegativity parameters, and can be taken proportional (with reversed sign) to the absolute electronegativities.[2] In Pauling's electronegativity scale,[3] the electronegativity increases by approximately a constant amount for successive members in the second row of the periodic table. We therefore assume $-\delta'=\delta''=\delta(<0)$.

By a suitable similarity transformation[4] the secular equations can be reduced to the forms:

$$\begin{vmatrix} A & 2 & 0 & 0 & 0 & 0 \\ 2 & A & 0 & 0 & 0 & 0 \\ 0 & 0 & A & 1 & 0 & 0 \\ 0 & 0 & 1 & A & 0 & 0 \\ 0 & 0 & 0 & 0 & A & 1 \\ 0 & 0 & 0 & 0 & 1 & A \end{vmatrix} = 0,$$

$$\begin{vmatrix} A' & 2 & 0 & 0 & 0 & 0 \\ 2 & A'' & 0 & 0 & 0 & 0 \\ 0 & 0 & A' & 1 & 0 & 0 \\ 0 & 0 & 1 & A'' & 0 & 0 \\ 0 & 0 & 0 & 0 & A' & 1 \\ 0 & 0 & 0 & 0 & 1 & A'' \end{vmatrix} = 0.$$

(The equation for benzene could be reduced completely by a different transformation based on the higher symmetry of benzene; however, in the given form the similarity between benzene and borazole comes out more clearly.) The molecular orbitals corresponding to the roots $A=-2$ and $A=-1$ (twice), in benzene, or the corresponding orbitals in borazole, are each occupied in the ground state by two electrons. The average height above the ground state of the first group of excited states[1,5] (three singlets and three triplets), corresponding in benzene to the excitation of one electron from one of the $A=-1$ orbitals to one of the $A=+1$ orbitals, is given by the difference X_2-X_1 of the two roots of

$A^2-1=0$, i.e., of $X^2-(\beta-SX)^2=0$;

namely

$$X_2-X_1=-\frac{2\beta}{1-S^2}$$

for benzene; and for borazole, of

$A'A''-1=0$, i.e. of $X^2-\delta^2-(\beta^*-S^*X)^2=0$;

namely

$$X_2-X_1=-\frac{2\beta^*}{1-S^{*2}}(1+(1-S^{*2})d^2)^{\frac{1}{2}},$$

where $d=\delta/\beta^*(>0)$.

The overlap integrals S and S^* can easily be evaluated if we use Slater $2p\pi$ orbitals. The results are:[6,7]

$$S=\left(1+x+\frac{2}{5}x^2+\frac{1}{15}x^3\right)e^{-x}$$

for like atoms, with $x=Z'R/n^*$, where $Z'=$effective nuclear charge (3.25 for carbon), $n^*=$effective quantum number (2 for $2p$ orbitals), and $R=$internuclear distance, in atomic units.

$$S^*=\left\{\frac{(ab)^{\frac{1}{2}}}{\frac{1}{2}(a+b)}\right\}^5\frac{1}{\eta^2}\left\{\cosh\eta x+\frac{1}{\eta}\sinh\eta x+3\left(1-\frac{1}{\eta^2}\right)\frac{1+x}{x^2}\left(\cosh\eta x-\frac{1}{\eta x}\sinh\eta x\right)\right\}e^{-x}$$

for unlike atoms, with

$a=Z'/n^*$, $b=Z''/n^*$, $Z'=2.60$ for boron,

$x=\frac{1}{2}(a+b)R$, $Z''=3.90$ for nitrogen,

$\eta=\dfrac{a-b}{a+b}$, $n^*=2$.

The actual internuclear distances in benzene and borazole are 1.39A and 1.44A,[8] respectively. With these values we get $S=0.25$, $S^*=0.22$, and for the mean energies from the ground state to the first excited states:

benzene: $E_2-E_1=-2.13\beta$,

borazole: $E_2-E_1=-2.10\beta^*(1+0.952d^2)^{\frac{1}{2}}$.

As was mentioned above, corresponding to the mean energy E_2, a group of six electronic states

[2] R. S. Mulliken, J. Chem. Phys. **2**, 782 (1934); **3**, 573 (1935).

[3] L. Pauling, *The Nature of the Chemical Bond*, (Cornell University Press, Ithaca, New York, 1940), p. 65.

[4] These transformations will be treated in a future publication.

[5] See footnote 12 in J. R. Platt, H. B. Klevens and G. W. Schaeffer, J. Chem. Phys. **15**, 598 (1947).

[6] Handbuch der Physik, Vol. XXIV$_1$, p. 643.

[7] A. L. Sklar, J. Chem. Phys. **7**, 991 (1939).

[8] S. H. Bauer, J. Am. Chem. Soc. **59**, 1804 (1937).

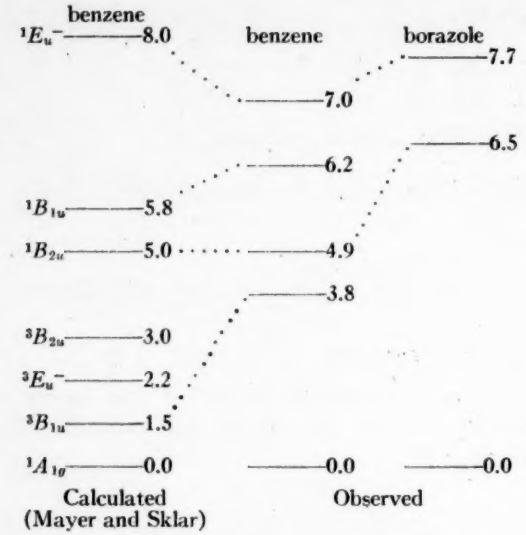

FIG. 1. Calculated and observed electronic energy levels, for vertical excitation (that is, all internuclear distances remaining fixed during the excitation process).

(three triplet and three singlet states) is expected theoretically for each of the two molecules.[1,5]

In Fig. 1 we give the results of the calculations of Mayer and Sklar on benzene, and the energy levels for benzene and borazole based on observed spectra.[9–11] Since the present calculations apply to vertical excitation, that is, to electron jumps without change in nuclear configuration, the frequencies of the intensity maxima of the band systems in the observed spectra correspond to our energy levels. (For those spectra which were observed in liquid or solution, we have estimated and corrected for the resulting red shift.) The energies above the ground state are given in ev. The group theory notation is essentially that of Placzek and Mulliken, slightly modified by Sponer and Teller.[12]

For transitions from the ground state (^1A_g in benzene, $^1A_1'$ in borazole) to the six excited states, group theory gives the following selection rules; corresponding states are listed side by side:

Benzene	Borazole	
To $^1E_u^-$	$^1E'$	(strongly[13]) allowed
$^1B_{1u}$	$^1A_1'$	electronically forbidden, but (weakly) allowed in combination with vibrations of species E_g^+, E' (or B_{2g}, A_2'')
$^1B_{2u}$	$^1A_2'$	electronically forbidden, but (weakly) allowed in combination with vibrations of species E_g^+, E'
$^3B_{2u}$	$^3A_2'$	electronically and spin forbidden
$^3E_u^-$	$^3E'$	spin forbidden
$^3B_{1u}$	$^3A_1'$	electronically and spin forbidden

The observed benzene spectrum shows a strong band system at 7.0 ev, two weaker ones at 6.2 and 4.9 ev, and a very weak one at 3.8 ev (the energies given are those for peak absorption in each case). In obtaining these values, besides the liquid or solution correction already mentioned, we subtracted one vibrational quantum of the E_g^+ or E' vibration which made the transitions from the ground state to the B or A' levels allowed.

The 7.0-ev band system is the allowed transition;[14] the 6.2- and 4.9-ev band systems are the transitions to the $^1B_{1u}$ [14] and $^1B_{2u}$ [15,15a] levels, respectively. The identification of the 4.9-ev band system has been thoroughly established by a careful vibrational structure analysis.[9,15a] The 3.8-ev band system[15,16] must be interpreted as the transition to the $^3B_{1u}$ [15] (or the $^3B_{2u}$ [17]) level,

[9] For benzene: H. Sponer, G. Nordheim, A. L. Sklar and E. Teller, J. Chem. Phys. **7**, 207 (1939), where numerous references on experimental data are given; H. Sponer, J. Chem. Phys. **8**, 705 (1940).

[10] For borazole: J. R. Platt, H. B. Klevens and G. W. Schaeffer, J. Chem. Phys. **15**, 598 (1947).

[11] For borazole: L. Jacobs, J. R. Platt, and G. W. Schaeffer, J. Chem. Phys. **16**, 116 (1948).

[12] R. S. Mulliken, Phys. Rev. **43**, 279 (1933); H. Sponer and E. Teller, Rev. Mod. Phys. **13**, 75 (1941): see Table VII.

[13] R. S. Mulliken, J. Chem. Phys. **7**, 984 (1939).

[14] The present interpretations of the 6.2- and 4.9-ev systems were first suggested as a possibility by Mayer and Sklar (reference 1). The definite interpretations were first given by G. Nordheim, H. Sponer, and E. Teller, J. Chem. Phys. **8**, 455 (1940), as modified by R. S. Mulliken (see footnote 9 in the paper of Nordheim, Sponer, and Teller).

[15] A. L. Sklar, J. Chem. Phys. **5**, 669 (1937).

[15a] The vibrational analysis shows that the 4.9-ev transition is electronically forbidden, and vibrations of symmetry E_g^+ which make the transition allowed, can be indicated. This proves that the electronic level is either $^1B_{1u}$ or $^1B_{2u}$. A transition to a $^1B_{1u}$ level should also be made allowed by a vibration of symmetry B_{2g}; the presence of such a vibration in the band would establish the symmetry of the electronic level as $^1B_{1u}$ for certain, its absence would make $^1B_{2u}$ probable. A more detailed vibrational analysis of the 4.9-ev band might confirm or disprove the labeling $^1B_{2u}$.

[16] G. N. Lewis and M. Kasha, J. Am. Chem. Soc. **67**, 994 (1945).

[17] From the numerical values of the integrals computed by Mayer and Sklar, the $^3B_{1u}$ level should be the lowest, the

since the low intensity in absorption and the long phosphorescence lifetime[18] indicates a doubly forbidden transition, and its appearance in phosphorescence shows that it must be from the lowest triplet level.[16,19] Since no other band systems have been found in the visible or near ultraviolet, and the transition to the $^3E_u^-$ state is expected to be about 10^3 times stronger than the observed singlet-triplet transition, the $^3E_u^-$ level must be at least as high as 4.7 ev; the transition to this level could then be masked by the 4.9-ev band system, which is expected to be 10^2 times stronger.[20] Since a larger shift is improbable, we shall in estimating the locations of the unobserved levels assume 4.7 ev for the $^3E_u^-$ level. For the remaining unobserved $^3B_{2u}$ (or $^3B_{1u}$) level we shall assume 5.6 ev, since Mayer's and Sklar's calculations give equal separations among the three triplet levels. The fact thus probably established, that the $^3B_{2u}$ (or $^3B_{1u}$) level must be above the lowest singlet level, means that the calculations of Mayer and Sklar not only give numerical values of some interaction integrals in disagreement with experiment, but even with the wrong sign. However, as these authors pointed out, any orbital type of approximate calculation tends to give triplet states somewhat too low compared to singlet states.

The observed spectrum of borazole, if we accept the interpretation given in reference 11, shows the allowed transition at 7.7 ev, and the equivalent of the 4.9-ev transition in benzene at 6.5 ev. To complete the picture of the energy levels, we assume the splittings of the six levels to be proportional to the splittings in benzene.

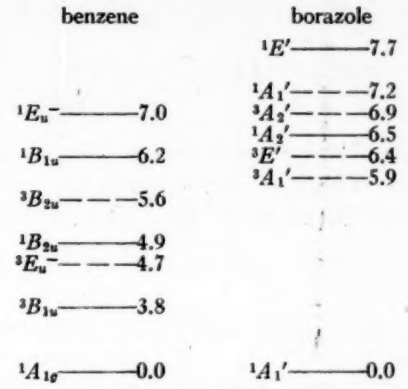

FIG. 2. Observed and (dashed lines) estimated electronic energy levels, for vertical excitation. In benzene it is fairly likely that the labels of the two ^3B levels should be interchanged, and similarly for the two ^3A levels of borazole. Similar reversals may also be needed for the corresponding singlet levels.[15a]

The final results for both molecules are shown in Fig. 2.

In the formulas which we derived for the energy difference E_2-E_1 between the first excited states and the ground state in terms of the bond integral β, E_2 refers to the average of the energies of the six levels we have just been discussing (in averaging, each E level must be taken with double weight since these levels are orbitally doubly degenerate; corresponding singlet and triplet levels are, however, given *equal* weight, a procedure whose correctness can be seen by referring to ref. 1). The resulting averages are 5.5 ev for benzene and 6.8 ev for borazole. (These averages do not depend on a change in labels of the B or A levels.[15a,17].)

The formula then gives for benzene, if we designate by β_{spec} the spectroscopically determined β, $\beta_{\text{spec}}=-5.5/2.13=-2.6$ ev. From spectroscopic data on ethylene, the value $\beta_{\text{spec}}=-3.0$ ev is obtained,[21] again for a $2p\pi$ C−C bond although for a somewhat smaller internuclear distance. From resonance energy data another β value van be obtained for benzene:[21] $\beta_{\text{res}}=-3.1$ ev.

For borazole, we find

$$\beta_{\text{spec}}{}^*=-6.8/2.1(1.95)^{\frac{1}{2}}=-2.3 \text{ ev}$$

if we assume $d=1.0$,

$^3B_{2u}$ level the highest, among the triplet states. However, if the true values of the integrals should be somewhat different, the $^3B_{2u}$ might be the lowest, the $^3B_{1u}$ the highest. In any event, the theoretical prediction that the $^3E_u^-$ should lie in the middle is independent of the numerical values of the integrals.

[18] 4.0 sec. (private communication from M. Kasha). This agrees roughly as to order of magnitude with the lifetime of about 0.1 or 0.2 sec. calculated from the observed absorption. (The absorption f value, estimated from Fig. 13 on p. 1000 of reference 16, is about 1.2×10^{-8}.)

[19] G. N. Lewis and M. Kasha, J. Am. Chem. Soc. 66, 2100 (1944).

[20] The transition to $^3B_{1u}$ is about 10^{-5} times as strong as that to $^1B_{2u}$; since the transition to $^1B_{2u}$ is about 10^{-3} times as strong (see J. R. Platt and H. B. Klevens, Chem. Rev. 41, 301 (1947)) as that to $^1E_u^-$, we expect the transition to $^3E_u^-$ to be about 10^3 times stronger than that to $^3B_{1u}$ and thus about 10^2 times weaker than the $^1B_{2u}$ transition.

[21] R. S. Mulliken and C. A. Rieke, Rev. Mod. Phys. 14, 259 (A) (1942); and full papers to be published shortly, in which the significance of bond integrals from spectroscopic and other data will be discussed.

or

$$\beta_{spec}^{*} = -6.8/2.1(3.14)^{\frac{1}{2}} = -1.8 \text{ ev}$$

if we assume $d = 1.5$.

This gives for δ the respective values -2.3 and -2.7 ev. The first choice gives the closest resemblance between benzene and borazole and gives at the same time what is probably a reasonable value for δ.[2]

It can be seen from the formulas for $E_2 - E_1$ that the main reason for the higher frequency of the borazole spectrum as compared with benzene is the appearance of the parameter d in the formula for borazole.

THE JOURNAL OF CHEMICAL PHYSICS VOLUME 16, NUMBER 2 FEBRUARY, 1948

The Effect of Certain Column Variables on Thermal Diffusion

H. G. DRICKAMER, V. J. O'BRIEN, J. C. BRESEE, AND C. E. OCKERT
Noyes Laboratory of Chemistry, Urbana, Illinois

(Received October 3, 1947)

Tests have been made on two thermal diffusion columns with different annular spacing. The results indicate that the dependence of the separation on temperature and annular spacing predicted by Furry, Jones, and Onsager holds. The dependence on pressure is slightly different than was predicted. The possibility that the index of repulsive force may depend on the pressure is pointed out.

NOMENCLATURE

C_v = specific heat at constant volume
D_{12} = coefficient of ordinary diffusion
D_T = coefficient of thermal diffusion
g = gravitational constant
L = column length
p = pressure in atmospheres
q = separation factor $(X_1^T X_2^B / X_2^T X_1^B)$
T = absolute temperature, °K
$\bar{T}$ = arithmetic average temperature, °K
ΔT = temperature difference between hot and cold walls
v_1, v_2 = convection velocity of species 1, 2
X_1, X_2 = mole fraction of species 1, 2 in feed
X_1^T, X_2^T = mole fraction of species 1, 2 in top reservoir
X_1^B, X_2^B = mole fraction of species 1, 2 in b.t.m. reservoir
w = one half of annular spacing
α = thermal diffusion ratio $= (D_T/D_{12})$
δ, ϵ = empirical constants
η = viscosity
λ = thermal conductivity
ρ = density
ν = index of repulsive force in $F = -(K_{12}/r^{\nu})$

INTRODUCTION

THERMAL diffusion—the transport of molecules caused by a temperature gradient, was predicted theoretically by Enskog[1] in 1911 and independently by Chapman[2] in 1916. Its existence was confirmed experimentally by Chapman and Dootson[3] in 1917. With the development of the thermal diffusion column with hot wire by Clusius and Dickel[4] and the refinement to a concentric tube column by Brewer and Bramley,[5] it became a practical process for isotope separation.

Furry, Jones, and Onsager[6] and later Furry and Jones[7] have presented an extensive analysis of the theory of the column. This paper reviews their results briefly and compares the predicted effect of certain column variables on the separation with experiment.

THEORY

Furry, Jones, and Onsager[6] use the defining equation:

$$X_1 X_2 (v_1 - v_2) = -D_{12} \operatorname{grad} X_1 + D_T \operatorname{grad} \ln T, \quad (1a)$$

[1] D. Enskog, Physik. Zeits. **12**, 56, 533 (1911).

[2] S. Chapman, Phil. Trans. **216A**, 279 (1916).

[3] S. Chapman and F. W. Dootson, Phil. Mag. **38**, 248 (1917).

[4] K. Clusius and G. Dickel, Naturwiss. **26**, 546 (1938).

[5] A. K. Brewer and A. Bramley, Phys. Rev. **55**, 590(A) (1939).

[6] W. H. Furry, R. C. Jones, and L. Onsager, Phys. Rev. **55**, 1083 (1939).

[7] W. H. Furry and R. C. Jones, Rev. Mod. Phys. **18**, 219 (1946).

or

$$X_1X_2(v_1-v_2) = D_{12}(-\text{grad}X_1+X_1X_2\alpha \text{ grad } \ln T), \quad (1')$$

for the thermal diffusion coefficient, D_T, and thermal diffusion ratio, α. Applying the Navier Stokes Law for viscous flow to a simplified hydrodynamical model of the column, a general differential equation is obtained expressing the flux of one component in terms of the molecular properties of the gas and the constants of the column.

To solve this equation it is necessary to know the temperature dependence of the molecular properties and, therefore, to select a satisfactory molecular model. One of the simplest models giving approximately satisfactory results is the point source of repulsive force model,

$$F=(-K_{12}/r^\nu). \quad (2)$$

For this model Chapman and Cowling[8] give the following relationships for the gas coefficients:

$$\eta=\Omega(T, m, \nu)=\Omega' T^{(\nu+3)/2(\nu-1)}, \quad (3a)$$

$$D_{12}=\psi(T, m, x, \nu, p)=\psi'\frac{T^{(3\nu+1)/2(\nu-1)}}{P}, \quad (3b)$$

$$\lambda=\gamma(\nu)\eta C_v, \quad (3c)$$

$$\alpha=\varphi(\nu, m, x)(\nu-5/\nu-1), \quad (3d)$$

$$D_T=X_1X_2\alpha D. \quad (3e)$$

It should be pointed out that more accurate molecular models indicate that α depends on the temperature.

The general equation cannot be solved, but if one ignores vertical diffusion the equation simplifies and can be solved using (3a)–(3d). A correction for vertical diffusion can then be appended to the solution. The solution is particularly simple if one considers that the temperature dependence of D_{12}, η, and λ is that of Maxwellian molecules ($\nu=5$). For many gases this simplification adds little inaccuracy.

One then obtains for the separation factor $q=(X_1^TX_2^B/X_2^TX_1^B)$ the relationship

$$\ln q=\frac{63L\alpha D_{12}\eta f(\Delta T/\bar{T})}{2\omega^4\rho g}\times\left[\frac{1}{1+5670(D_{12}\eta\bar{T}/\omega^2g\rho\Delta T)^2}\right]. \quad (4)$$

The factor in the brackets is the correction for vertical diffusion.

The quantity $f(\Delta T/T)$ is essentially equal to one for $(\Delta T/T)\leqslant 0.50$.

Solving Eq. (4) for the thermal diffusion coefficient one obtains

$$D_T=\frac{2}{63}\frac{X_1X_2\omega^4\rho g \ln q}{L\eta}\times\left[1+5670\left(\frac{D_{12}\eta\bar{T}}{\rho g\omega^4\Delta T}\right)^2\right]. \quad (5)$$

It is the purpose of this paper to consider the effect of certain column variables on the separation and to compare predicted values with experiment.

Assuming the Maxwellian temperature dependence of D_{12}, and η, α independent of temperature, and the ideal gas law, one obtains for (4)

$$\ln q=\frac{C_1\bar{T}^4}{\omega^4P^2}\left[\frac{1}{1+(C_2\bar{T}^{10}/P^4\omega^6)}\right], \quad (4')$$

where C_1 and C_2 are independent of T, p, and W. Equation (4′) can be maximized with respect to p, T, or W at constant values of the other two variables. Figure 1 shows $\ln q$ plotted against pressure, with temperature and W as parameters. For this case the following values were assumed for the different variables:

$L=250$ cm
$D_{12}=0.1\times10^{-6}T^2$
$\eta=0.3\times10^{-6}T$
$\rho=0.488(T/P)$
$\alpha=0.012$

Different values for these functions would merely shift the curves without changing the qualitative relations discussed below.

From this diagram it is convenient to study variations of $\ln q$ with (1) p and T at constant W, (2) p and W at constant T, (3) T and W at constant p.

[8] S. Chapman and T. G. Cowling, *The Mathematical Theory of Non-Uniform Gases* (The Cambridge University Press, New York, 1939).

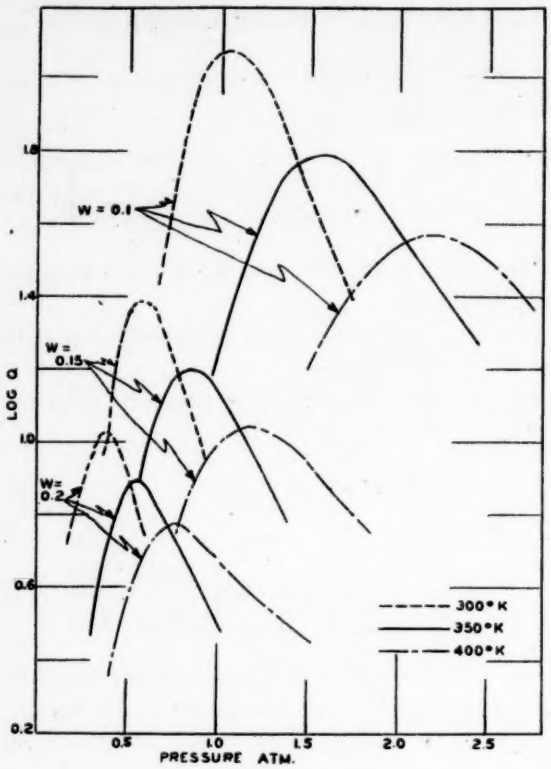

FIG. 1. Effect of temperature, pressure, and annular spacing on separation factor q.

The first category corresponds to the problem of establishing optimum operating conditions in an existing column. The second or third would be involved in design considerations where the temperature or pressure were fixed within narrow limits by external circumstances.

At constant W one can always improve the separation by decreasing the temperature and pressure approximately in such a manner that $(C_2\bar{T}^{10})/(W^6p^4)$ always equals one.

At constant temperature the separation can always be improved by increasing p and decreasing W, subject to a similar limitation.

Likewise, at constant pressure the separation can be improved by decreasing $\bar{T}$ and W as above.

The possibility of improving the separation by adjusting the above variables is subject to further limitations, as pointed out by Furry and Jones,[7] because of remixing due to asymmetry, remixing due to turbulence, and unduly long separation times.

The possibility of asymmetry in construction, which would cause remixing currents, increases with decreasing W and therefore limits the feasibility of moving indefinitely in this direction.

The Reynolds number, which is a measure of turbulence, is defined by Onsager and Watson[9] as proportional to $(W^3p^2\Delta T/\bar{T}^5)$. This limits the possibility of large pressure increases except at very small values of W, very high temperature, or very low values of ΔT. These factors are subject to further limitations discussed below.

The relaxation time is roughly proportional to $(\bar{T}^{10}L)/(W^7p^5(\Delta T)^2)$. This imposes a limitation on the feasibility of decreasing W, p, or $\Delta\bar{T}$ indefinitely, or of operating at very high temperature. It also limits the practical length of a column. These problems, including the practicality of multi-stage and continuous operation are discussed in detail by Furry and Jones.[7]

The following sections present the results of experiments performed on two single-stage batch columns connected to reservoirs on each end, to test certain of the relationships described above.

TABLE I. Constant pressure data $p = 1.118$ atmos.

Column I Run No.	Av. Temp.°K	Percent CO_2 Feed	Top	B.t.m.	$\ln q$
1	382	54.41	57.72	48.38	0.376
1	382	54.41	57.59	48.85	0.352
2	362	54.22	56.91	49.11	0.314
2	362	54.22	55.98	48.52	0.299
3	334	58.34	57.83	50.86	0.281
3	334	58.34	57.44	50.66	0.273
4	379	57.07	59.48	49.40	0.408
4	379	57.07	59.65	49.56	0.409
5	356	56.89	58.10	49.73	0.337
5	356	56.85	56.90	49.60	0.295
6	311	55.47	56.38	51.54	0.195
6	311	55.47	55.77	50.94	0.194
7	334	57.57	59.76	53.95	0.237
7	334	57.57	59.66	53.79	0.237
8	357	53.50	56.67	49.38	0.293
8	357	53.50	56.41	49.09	0.294
9	398	52.68	57.45	48.10	0.376
9	398	52.68	57.20	48.96	0.376
Column II					
10	405	58.22	77.73	36.29	1.813
10	405	58.22	79.44	35.06	1.968
11	379	55.29	74.29	35.55	1.576
11	376	55.30	73.51	36.46	1.304
12	355	55.83	68.94	37.64	1.317
12	353	55.84	68.82	37.17	1.320

[9] L. Onsager and W. W. Watson, Phys. Rev. **56**, 474 (1939).

EXPERIMENTAL EQUIPMENT AND PROCEDURE

Experiments were performed on two concentric tube columns each 244 cm long and connected to 200-cc reservoirs at each end. Column I had an annular spacing of 0.456 cm ($W=0.228$) and column II an annular spacing of 0.308 cm ($W=0.154$ cm).

The outside wall was cooled by circulating cooling water through a jacket. The water was maintained at 16.5±1°C and never gained over 1°C in passing through the column. The inner wall was heated by radiant energy from a hot wire passed up the inside tube and held in place by ceramic spaghetti and spacers. The inside tube was sealed off and evacuated to eliminate convection currents.

The inside wall temperatures were measured by means of thermocouples inserted in the inside tube from each end and held in place by spring steel rings. The whole thermocouple, except for the head which was protected by the ring, was insulated to prevent exposure to radiation.

On the average, the top and bottom temperature differed by 6°C with a maximum difference of 12°C. It is felt that this difference represents errors in thermocouple readings due to exposure to radiation rather than actual differences in wall temperature.

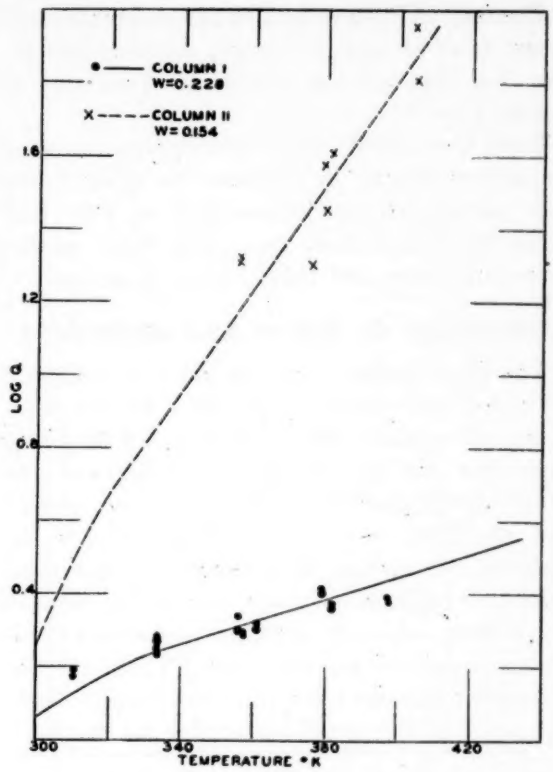

FIG. 2. Comparison of experimental and predicted separation factor as a function of temperature and annular spacing.

TABLE II. Constant temperature data $T=380$°K.

Column II Run No.	Pressure (Atmos.)	Percent CO_2 Feed	Top	B.t.m.	$\ln q$
1	1.116	56.15	74.61	37.03	1.610
2	0.836	55.02	72.80	36.92	1.520
2	0.845	55.02	72.42	37.34	1.483
3	0.625	51.02	64.98	38.95	1.068
3	0.631	51.02	64.48	38.24	1.076
4	0.397	50.07	56.48	43.47	0.523
4	0.390	50.07	55.68	42.36	0.536
5	0.998	53.21	70.95	34.81	1.521
6	0.682	51.47	65.50	36.97	1.175
6	0.686	51.47	65.24	36.13	1.199
7	1.410	55.16	67.23	40.20	1.112
7	1.395	55.16	67.43	39.51	1.154
8	0.510	51.30	62.39	42.84	0.795
8	0.510	51.30	62.79	42.37	0.831
9	0.744	53.63	67.34	34.64	1.359
9	0.744	53.63	66.69	34.71	1.326
10	1.593	57.44	67.87	42.96	1.032
10	1.590	57.44	67.66	43.08	0.994
11	1.248	56.48	71.03	40.08	1.299
11	1.247	56.48	71.70	40.12	1.330
12	0.312	55.14	56.24	48.75	0.301
12	0.309	55.14	56.21	49.13	0.285
13	1.805	49.58	62.97	41.99	0.854
13	1.805	49.58	63.01	42.40	0.839
14	1.153	53.49	68.97	36.01	1.374
14	1.143	53.49	68.91	35.14	1.409
15	1.082	53.49	69.59	34.67	1.462
15	1.082	53.49	69.51	34.96	1.445
16	0.924	53.49	69.66	34.21	1.485
17	0.433	51.08	58.56	43.31	0.615
17	0.439	51.08	58.40	41.67	0.676

The gases used were carbon dioxide obtained from the Ohio Chemical Company and 99.9 percent propane obtained from the Matheson Company. The method of purification and analysis followed closely that described by Wall and Leaf,[10] making use of a Zeiss portable interferometer for analyses, with purified propane being the reference gas.

The two columns were operated over a range of average temperature of 311°K–405°K at 1.118 atmospheres pressure. The average temperature was considered to be the arithmetic average of the hot and cold wall temperatures. Then column II was operated at pressures from 0.309–1.805 atmospheres with a constant average temperature of 380°K.

[10] F. T. Wall and B. Leaf, J. Phys. Chem. 46, 820 (1942).

The feed analysis was maintained substantially constant at 55 percent carbon dioxide throughout. The experimental results are presented in Tables I and II.

Runs were continued until samples indicated no further change in analyses. In general, the first sample was not taken until at least four times the approximate relaxation time, as discussed by Furry and Jones,[7] had elapsed.

COMPARISON OF THEORY AND EXPERIMENT

The first constant pressure runs on column I indicated that the best value of v for the point source of repulsive force model was 6.15. Using this value and the equations of Chapman and Cowling,[8] Chapters 9 and 10, to predict α and D, and the data of Trautz and Kurz[11] for the viscosity of carbon dioxide-propane mixtures, values of $\ln q$ were calculated from Eq. (4). In Fig. 2 these values are compared with the experimental values of $\ln q$ taken from Table II. The agreement obtained for the two columns indicates definitely that the dependence of $\ln q$ on W is correctly predicted by Eq. (4). Also, the equation appears to predict the correct dependence of $\ln q$ on the temperature over the temperature range covered. It should be pointed out that since the cold wall temperature was fixed, it was not possible to vary the average temperature, $\bar{T}$, independently of ΔT.

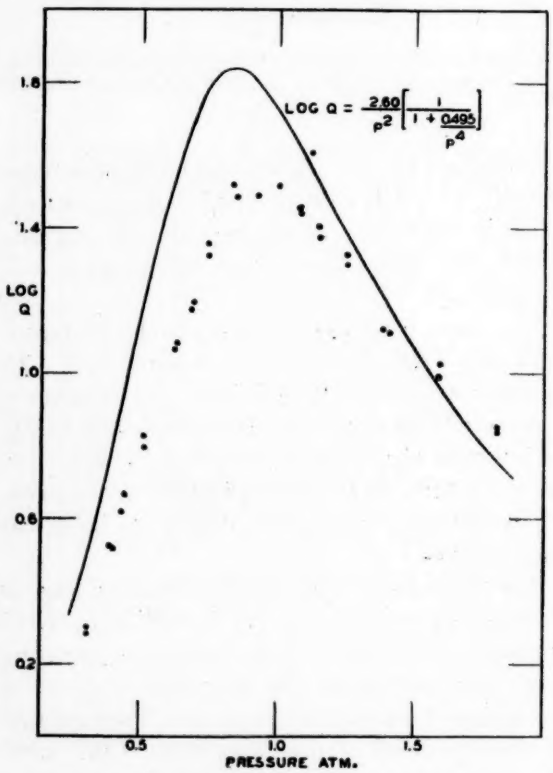

FIG. 3. Comparison of experimental and predicted effect of pressure on the separation factor.

[11] M. Trautz and F. Kurz, Ann. d. Physik 9, 981 (1931).

Seventeen runs were made at different pressures using column II. Since these data were the last obtained, after operating and analytical techniques had been perfected, it is felt that these runs are the most reliable ones.

Evaluating the constants in Eq. (4) from data in the literature or in the case of α and D_{12} from theory (using the 6.15 point source model) one obtains an equation for $\ln q$

$$\ln q = \frac{2.60}{P^2}\left[\frac{1}{1+(0.495/P^4)}\right]. \qquad (6)$$

Figure 3 compares experimental values of $\ln q$ with those predicted from Eq. (6). It can be seen that the general shape of the two curves is the same, but that the agreement is quantitative only in the pressure region around 1.2 atmospheres where the value of $v=6.15$ was first established from experiment. Further, it can be seen that no adjustment of the non-pressure dependent variables will bring the curves into agreement.

Possible reasons for the discrepancy include: (1) Some consistent experimental error. (2) The lack of spherical symmetry of the molecules, whereas the equations are derived for spherically symmetrical molecules. (3) The use of the inverse power model and of the Maxwellian model for D_{12}, η, and λ. (4) The method of solution of the differential equation for diffusion used by Furry, Jones, and Onsager,[6] first ignoring vertical diffusion and then appending a correction for it. (5) The possibility that v and, therefore, α may depend on the pressure. Considering these in order, no source of consistent error in the experimental work was discovered.

The second possibility can only be tested by the use of spherically symmetrical molecules, such as the rare gases. There appears, however, to be no *a priori* reason why the lack of spherical symmetry should affect the pressure dependence at these low pressures.

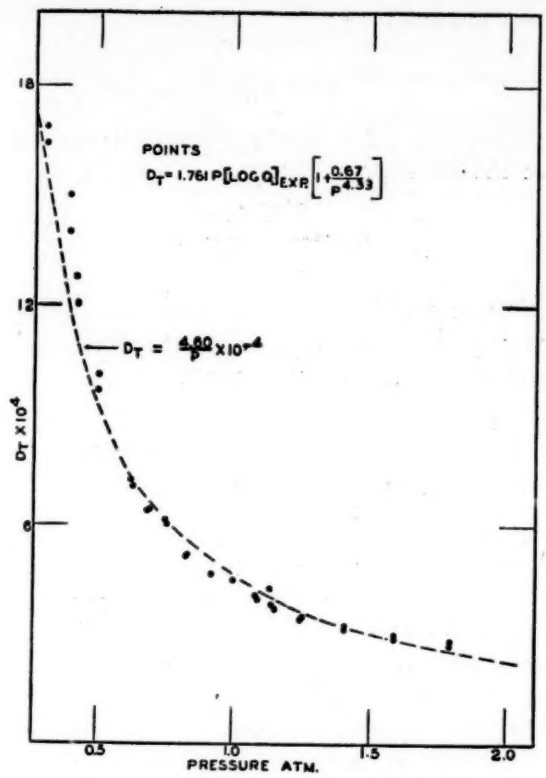

FIG. 4. Comparison of theoretical values of D_T with those predicted from empirical Eq. (8).

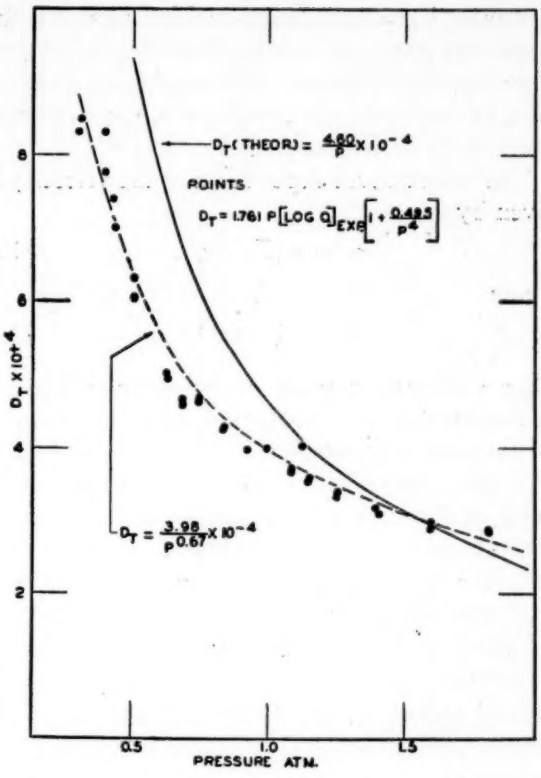

FIG. 5. Comparison of values of D_T predicted from Eq. (5) with values obtained from Eq. (13) when V is taken to be a function of pressure.

Third, the inverse power model is known to be somewhat crude. However, the more refined models so far studied do not predict any different pressure dependence for the gas coefficients.

The fourth possibility is not so easily disposed of. The fact that Eq. (4) predicts the correct temperature and W dependence for $\ln q$ indicates that its form is correct. If one considers an empirical equation of the form:

$$\ln q = \frac{2.60}{P^2}\left[\frac{1}{1+(\delta/P^{\epsilon})}\right], \tag{7}$$

values of δ and ϵ can be obtained from experimental values of $\ln q$, and Eq. (7) becomes

$$\ln q = \frac{2.60}{P^2}\left[\frac{1}{1+(0.67/P^{4.33})}\right]. \tag{7'}$$

Equation (5) for D_T, calculated from experimental data, is then modified

$$[D_T]_{\text{exper.}} = 1.761 \times 10^{-4} P\left[1+\frac{0.67}{p^{4.33}}\right][\ln q]_{\text{exper.}}. \tag{8}$$

Using the relations of Chapman and Cowling,[8] one obtains the equation

$$D_T = (4.60\times 10^{-4})/p, \tag{9}$$

with the 6.15 inverse power model. Figure 4 compares values of D_T predicted from Eq. (9) with those calculated from Eq. (8). Since the 6.15 model was used in obtaining α for Eq. (7') the agreement is to be expected.

The fifth possibility has no direct theoretical basis. If the inverse power model were really adequate, ν would be independent of temperature and pressure. However, in comparing viscosity data with theory it is found that ν must be considered a function of temperature to obtain agreement between theory and experiment. There is evidence from viscosity investigations at elevated pressures that ν may increase with pressure. Chapman and Cowling[8] point out that the solid elastic spherical model ($\nu=\infty$) gives a better fit for nitrogen at high pressures than at atmospheric pressure where $\nu=8.8$. The data of

Comings, Egly, and Mayland[12] indicate that for numerous gases the temperature dependence of the viscosity decreases with increasing pressure even at relatively low pressures in the neighborhood of 10–20 atmospheres.

The temperature dependence of the viscosity is given by

$$\eta_2/\eta_1=(T_2/T_1)^S, \tag{10}$$

where

$$S=\tfrac{1}{2}+(2/\nu+1). \tag{11}$$

So a decreasing value of S corresponds to an increasing value of ν and, thus, to a "hardening" of the molecular model with increasing pressure. If ν were only slightly pressure dependent, the value of S would not vary noticeably with pressure at ordinary pressures, but α, which is very sensitive to changes in ν, might vary appreciably.

If one substitutes Eq. (3d) for α in Eq. (4), considering $\varphi(\nu)$ as a constant to be evaluated at a pressure where the theoretical and experimental values of $\ln q$ coincide, one obtains as an approximate equation for ν over the pressure range covered:

$$\nu=\frac{5-0.206p^{0.333}}{1-0.206p^{0.333}}. \tag{12}$$

Using this value in the theoretical equations one obtains approximately

$$D_T=\frac{3.98\times10^{-4}}{p^{0.67}}. \tag{13}$$

The values of D_T predicted from this equation agree closely with those calculated from experiment by Eq. (5), which becomes

$$D_T=1.761p[1+(0.495/p4)]\times(\ln q)_{\text{exper.}}\times10^{-4}. \tag{14}$$

This agreement is shown in Fig. 5.

Considerably more experimental work would be necessary before one could put much reliance in Eq. (12) for ν and use it to extrapolate to higher pressures or to other systems. If such a relationship is really general it would provide an incentive for operating thermal diffusion columns at slightly elevated pressure.

The authors wish to acknowledge the encouragement and helpful suggestions of Dr. F. T. Wall of the Noyes Chemical Laboratory.

[12] E. W. Comings, R. S. Egly and J. C. Mayland, University of Illinois Exper. Stat. Bull. 354 (1944).

THE JOURNAL OF CHEMICAL PHYSICS VOLUME 16, NUMBER 2 FEBRUARY, 1948

The C–H Bond Energy in Toluene and Xylenes

M. SZWARC
Department of Chemistry, The University of Manchester, Manchester, England
(Received October 15, 1947)

The pyrolysis of toluene and the xylenes was investigated by a new technique, which made it possible to study these reactions for degree of decomposition ranging from 0.01 percent up to a few percent. It was shown that these reactions are homogeneous, unimolecular reactions. It was found that the weakest bond in these molecules is the C–H bond in the methyl group. The bond energy of that C–H bond was found to be 77.5 kcal. for toluene and meta-xylene, 75 kcal. for para-xylene and 74 kcal. for ortho-xylene. These data indicate that the resonance energy of the benzyl radical is 24.5 kcal. and that the hyper-conjugation in para-xylene decreases the C–H bond energy in the methyl group of this molecule by 2.5–3 kcal.

A RECENT investigation of the pyrolysis of benzyl iodide by C. Horrex[1] and the author revealed the great stability of the benzyl radical. This work gave rise to the suspicion that the resonance energy of the benzyl radical is much higher than was previously thought and the present study was started in the hope of further clarifying this point. It was decided to investigate the pyrolysis of toluene, and in particular the nature of the first step of its decomposition.

[1] This will shortly be published elsewhere.

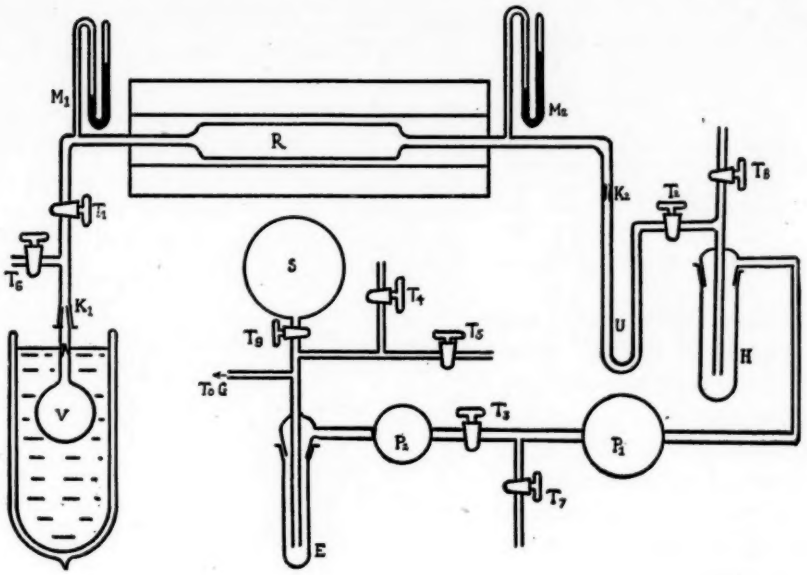

FIG. 1.

The pyrolysis of toluene and the xylenes has been investigated in the past ten years by several authors, mainly in connection with the coking process, and most of the research was devoted to studying the influence of various catalysts. It was found by Tilicheev[2] that toluene decomposes 13 times faster than benzene, and the energy of activation of this decomposition was found to be 70 kcal. It is interesting to compare this value with the value of 77.5 kcal. obtained in the present work.

Jost and Müffling[3] measured the rate of pyrolysis of a number of hydrocarbons, among them toluene, following the course of the reaction by the increase of pressure. They observed that $Hg(CH_3)_2$ had no effect on the rate of decomposition of toluene at 690°C, which indicated that the decomposition is not a chain reaction. All these investigations suffered from the common difficulty that the decomposition was carried out under conditions in which it was impossible to derive the true mechanism of the reaction, owing to the complicated mixture of products obtained.

The first successful attempt to elucidate the mechanism of the reaction was made by Hein and Mésee.[4] These authors pyrolyzed toluene in the presence of mercury vapor, using a technique similar to that developed by Rice. They succeeded in isolating mercury-di-benzyl as a product of the reaction, and followed the course of the decomposition by the determination of the quantities of the mercury compound formed. The rate of formation of this compound seemed to depend on a number of uncontrollable factors which prevented the determination of an energy of activation. Yet the authors concluded from the formation of mercury-di-benzyl that the first step in the decomposition of toluene is the rupture of the C−H bond,

$$C_6H_5\cdot CH_3 \rightarrow C_6H_5\cdot CH_2 + H \qquad (1)$$

which is followed by a reaction between benzyl radicals and mercury atoms leading to $Hg(CH_2\cdot C_6H_5)_2$. However, it would seem that the evidence for this conclusion is not definite, for it is possible to explain the formation of the benzyl radical by a mechanism involving the rupture of the C−C bond as a first step:

$$C_6H_5\cdot CH_3 \rightarrow C_6H_5 + CH_3 \qquad (12)$$

followed by the reactions:

$$C_6H_5\cdot CH_3 + CH_3 \rightarrow C_6H_5\cdot CH_2 + CH_4. \qquad (13)$$

$$C_6H_5\cdot CH_3 + C_6H_5 \rightarrow C_6H_5\cdot CH_2 + C_6H_6. \qquad (14)$$

A stronger argument, put forward by Hein and Mésee, in favor of (1) is their observation of hydrogen among the products of the decomposition. There is, however, some ambiguity about

[2] M. D. Tilicheev, J. App. Chem. U.S.S.R. 12, 741 (1939).
[3] I. W. Jost and L. v. Müffling, Zeits. f. Elektrochemie 47, 766 (1941).
[4] F. Hein and H. J. Mésee, Berichte 76B, 430 (1943).

TABLE I.

Run No.	Toluene partially pyrolysed	T°C	$K \cdot 10^{-2}$ sec.$^{-1}$	$K \cdot 10^{-2}$ sec. for 845°C	% H_2	% CH_4
70	once at 835°C	836°	1.50	2.18	59	41
71	twice at 835°C	845°	1.90	1.90	60	40
72	once at 845°C	845°	2.02	2.02	60	40
73	twice at 845°C	848°	2.02	1.78	59	41
74	three times at 847°C	852°	2.12	1.76	61	39

the origin of this hydrogen, since Hein and Mésee worked in the region of 1000°C, when according to the present study complete cracking of toluene molecules takes place.

In the present investigation the rate of pyrolysis of toluene was observed by measuring the quantity and composition of the gaseous mixture formed. The experimental conditions were so chosen that the decomposition ranged from 0.01 percent to slightly over 1 percent. It was expected that in these conditions the reaction mechanism would be simplified. The experimental results confirmed this by showing that no other gases than hydrogen and methane were produced.

APPARATUS AND TECHNIQUE OF MEASUREMENT

The pyrolysis was investigated by the flow method in the temperature range of 680°C–850°C and under a pressure of 2–15 mm Hg. The apparatus used is shown in Fig. 1. The hydrocarbon under investigation was kept in a small vessel, V, fitted with a capillary K_1. This vessel was weighed before and after every experiment, the loss of weight giving the quantity of hydrocarbon used. During runs V was kept in a Dewar vessel containing water maintained at a temperature constant to 0.1°C. By opening the tap T_1, the vapor of the hydrocarbon was led into a silica reaction vessel R heated by an electrical furnace. The temperature of the furnace was kept constant by a constant voltage transformer and measured by a double chromel P-Alumel thermocouple. The variation of temperature along the reaction vessel was ±2°C. The pressure before and after the reaction vessel was measured on two manometers M_1 and M_2 by means of a cathetometer.

The vapor leaving the furnace passed through a heated tube and heated capillary K_2 into a small trap U cooled by mixture of salt and ice to −10°C, and then through a tap T_2 into a big trap H cooled by acetone $+CO_2$ mixture. In the trap U the less volatile products such as di-benzyl, di-phenyl and others were condensed. The undecomposed hydrocarbon was condensed completely in the trap H. The trap H was connected to a system of two mercury pumps P_1 and P_2, capable of pumping all the gases into the storage vessel S. The pumps were chosen so as to maintain a vacuum of 10^{-3} mm of Hg in the trap H, while the pressure in the storage vessel S could rise up to 12 mm of mercury. The trap E placed between the pump P_2 and the storage vessel S was cooled with liquid air to trap any ethane or ethylene produced in pyrolysis. The McLeod gauge G was used to measure the pressure of the gases produced. The volume of the storage part between the taps T_3, T_4, and T_5 was exactly determined (at about 1.5 l.). The taps T_4, T_6 and T_7 were used for evacuation of appropriate parts of the apparatus. T_5 led to an analytical device and T_8 was used to let air into the Trap H. By changing the capillaries K_1 and K_2 and choosing the desired temperature of water bath, it was

TABLE II. Toluene.

Remarks	No. of run	T°C	P toluene mm Hg	Time of contact sec.	% decomp.	$K \cdot 10^2$ sec.$^{-1}$	% H_2	% CH_4
	94	738	6.4	0.310	0.0098	0.032		
	87	740	6.4	0.310	0.0114	0.037		
	88	741	6.4	0.310	0.0132	0.043		
	89	742	6.1	0.296	0.0141	0.048		
	90	742	6.0	0.291	0.0155	0.053	60	40
	91	745	5.8	0.280	0.0163	0.058		
	93	747	6.4	0.310	0.0238	0.077		
	92	749	6.4	0.310	0.0246	0.079		
	76	766	6.3	0.268	0.0336	0.125	61	39
	77	771	6.1	0.235	0.0333	0.142		
Pressure decreased	82	773	2.7	0.380	0.0600	0.158		
Time of contact increased	83	773	6.8	0.825	0.140	0.170	61	39
Surface increased 15 times	86	776	11.7	0.262	0.0344	0.131	60	40
	95	779	6.3	0.294	0.0740	0.252		
	78	792	6.2	0.256	0.0730	0.286	60	40
Pressure decreased	79	796	2.8	0.286	0.107	0.375	61	39
Time of cont. increased	81	803	5.5	0.905	0.437	0.485		
Time of cont. increased. Pressure increased	80	803	13.7	0.738	0.382	0.518	59	41
	97	819	6.3	0.284	0.244	0.860		
	98	821	6.3	0.284	0.261	0.920		
	71	845	7.6	0.306	0.581	1.90	60	40
	72	845	8.1	0.338	0.690	2.02	60	40
	73	848	5.9	0.246	0.500	2.02		
Pressure decreased	75	851	2.8	0.299	0.615	2.06	59	41
	74	852	6.3	0.246	0.520	2.12		
Surface increased 15 times	84	863	8.0	0.270	1.14	4.21	62	38
Surface increased 15 times	85	864	8.0	0.270	1.25	4.62	61	39

possible to vary both the pressure of the hydrocarbon in the reaction vessel and the time of contact.

The quantity of H_2+CH_4 produced was given by the pressure in the storage part with liquid air on the trap *E*. Changing the liquid air to the acetone $+CO_2$ bath and measuring any consequent rise in pressure, it was possible to find the quantity of any C_2-hydrocarbons present.

Numerous experiments showed that this arrangement gives exact results even where the quantities of gases produced are as low as 5.10^{-3} cc N.T.P./minute, so that this technique made it possible to follow the reaction down to as little as 0.01 percent decomposition. The H_2 to CH_4 ratio was estimated by combusting the H_2, in a known quantity of H_2+CH_4 mixture, by passage through a CuO cell. This method was tested by total combustion in oxygen and estimation of the CO_2 formed.

MATERIAL USED FOR PYROLYSIS

The first series of experiments in which toluene samples of different origins were used, showed that in spite of careful purification by shaking with sulphuric acid, distillation and crystallization, some impurities remained, the pyrolysis of which gave rise to considerable side reactions. These impurities could be removed by partial pyrolysis and the repeated partial pyrolysis of toluene produced samples of toluene, which pyrolyse at a steady rate when partial pyrolysis is repeated once or several times. This is seen from Table I. The final rate of pyrolysis we take to be that of toluene itself. Accordingly, the further work was carried out with toluene purified by twice repeated partial pyrolysis at 845°C, then distilled over sodium, using an efficient column, and collecting a fraction which passed within a range of 0.3°C.

EXPERIMENTAL RESULTS OF THE PYROLYSIS OF TOLUENE

The pyrolysis of toluene produced the two gases hydrogen and methane in the constant proportion 60 percent of H_2 to 40 percent of CH_4 (see Table II). No ethane or ethylene was observed. In addition to the gaseous product,

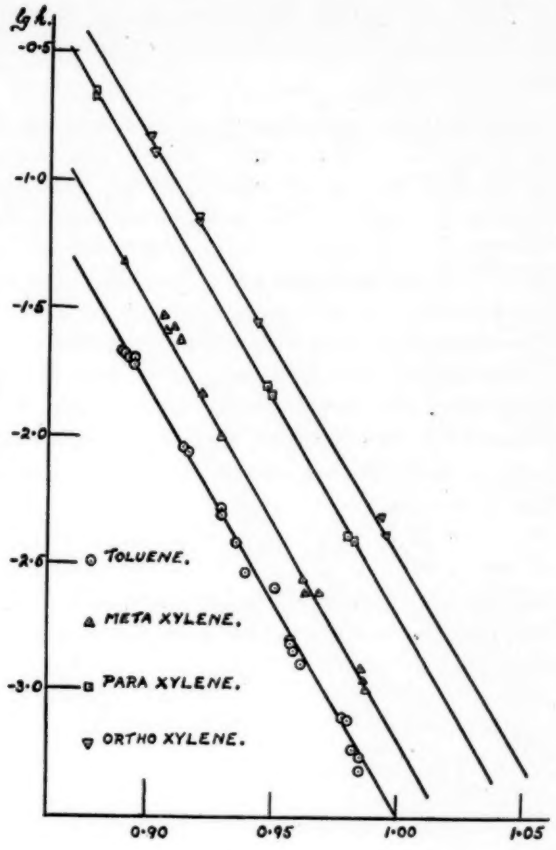

FIG. 2.

dibenzyl was isolated in quantities corresponding approximately to one mol. of dibenzyl per one mol. of gas produced. Dibenzyl was identified by its melting point and mixed melting point. The percentage of decomposition was calculated under the assumption that one mol. of gas produced corresponds to one mol. of primarily decomposed toluene. By packing the reaction vessel with silica wool which increased the surface about 15 times it was shown that the reaction is a homogeneous gas reaction (see runs 86, 84 and 85 in Table II). Reproducibility was very satisfactory, as can be seen comparing runs 89 and 90, and 71 and 72 (Table II). By changing the pressure of toluene and the time of contact, it was shown that the reaction is of the first order. The plot of $\log k$ against $1/T$ (shown on Fig. 2) can be satisfactorily drawn as a straight line, with a slope corresponding to an activation energy of 77.5 kcal. and a frequency factor of 2.10^{13}, as represented by the equation $k=2.10^{13}$

$\cdot e^{-77.5/RT}$. A further discussion of the grounds on which these constants were determined is to follow later.

MECHANISM OF PYROLYSIS OF TOLUENE

The evidence given above shows that the reaction is a homogeneous gas reaction of the first order. The fact that the frequency factor has the theoretical value of 10^{13}, as deduced by Polanyi and Wigner[5] suggests that we deal in this case with a true unimolecular reaction.

The appearance of hydrogen as one of the main products forces us to assume that the first step of the pyrolysis is the splitting of the toluene molecule into a benzyl radical and a hydrogen atom:

$$C_6H_5\cdot CH_3 \rightarrow C_6H_5\cdot CH_2 + H \qquad (1)$$

and the body of experimental evidence suggests that this step is followed by a sequence of quick reactions:

$$C_6H_5\cdot CH_3 + H \rightarrow C_6H_5\cdot CH_2 + H_2 \qquad (2)$$

and

$$\begin{cases} C_6H_5\cdot CH_3 + H \rightarrow C_6H_6 + CH_3 & (3a) \\ C_6H_5\cdot CH_3 + CH_3 \rightarrow CH_4 + C_6H_5\cdot CH_2 & (3b) \end{cases}$$

or

$$\begin{cases} C_6H_5\cdot CH_3 + H \rightarrow C_6H_5 + CH_4 & (4a) \\ C_6H_5\cdot CH_3 + C_6H_5 \rightarrow C_6H_6 + C_6H_5CH_2 & (4b) \end{cases}$$

it being assumed that the benzyl radicals are finally removed by dimerization to di-benzyl,

$$2C_6H_5\cdot CH_2 \rightarrow C_6H_5\cdot CH_2\cdot CH_2\cdot C_6H_5.$$

This mechanism accounts for the observed products (H_2, CH_4, dibenzyl and benzene) and gives the correct proportion of one mol of dibenzyl per one mol of gas produced.

We can show that the recombination of hydrogen atoms to H_2 is very unlikely under our experimental conditions, and this justifies its omission from the suggested mechanism. We do not know the energy of activation of the reactions (3a) or (4a), but we may expect these energies of activation to be smaller than that of (4b), which was estimated by Taylor and Smith[6] at 5.6 kcal. On this basis we calculate that in (3a) and (4a) at least one in ten collisions should lead to reaction. Since the chance of three body collisions should be smaller than this by several powers of ten, the recombination of H atoms in the gas phase should be negligible. The recombination at the wall should in these conditions be also of little importance, especially since at these high temperatures the accommodation coefficient is probably extremely small.[7]

The absence of recombination of H atoms at the wall was confirmed by showing that the packing of the reaction vessel caused no change in the rate of reaction, nor any increase in the proportion of H_2 produced.

The proposed mechanism leads to the result that the reaction (1) is the rate determining step and therefore the observed energy of activation corresponds to the energy of dissociation of the C−H bond in the methyl group of toluene. This conclusion makes use of the usual assumption that there is no energy of activation involved in the recombination of a bond from a free radical and a free atom. While this is not the place to re-examine this assumption, it may be stated that the theoretical reasons in its favor seem to be very strong.

Accordingly, we give for the C−H bond energy in the methyl group of toluene the value of 77.5 kcals. The difference between this value and the bond energy of C−H in methane which may be estimated at 102 kcals.[8] is to be accounted for by the resonance energy of the benzyl radical, which thus appears to have the value of 24.5 kcals.

PYROLYSIS OF META-XYLENE

The meta-xylene used was of German origin, produced by the "Gesellschaft für Verwehrtung von Kohlenteer." It was purified by repeated crystallization at −60°C, which was found to be sufficient.

The pyrolysis of meta-xylene produced hydrogen and methane in the same proportion as that of toluene (60 percent H_2, 40 percent CH_4). No

[5] M. Polanyi and E. Wigner, Zeits. f. Phys. Chem. **A139**, 439 (1928). See also S. Glasstone, M. Laidler and H. Eyring, "The Theory of Rate Processes" (1941).

[6] H. S. Taylor and J. O. Smith, J. Chem. Phys. **8**, 543 (1940).

[7] F. Paneth and K. Herzfeld, Zeits. f. Elektrochemie **37**, 577 (1931); F. Paneth, K. Hofeditz and A. Wunsch, J. Chem. Soc. (1935) p. 372.

[8] G. B. Kistiakowsky and E. B. Van Artsdalen, J. Chem. Phys. **12**, 469 (1944). D. P. Stevenson, *ibid.* **10**, 291 (1942).

TABLE III. Meta-xylene.

Remarks	No. of run	T°C	P meta-xylene mm Hg	Time of contact sec.	% decomp.	$K \cdot 10^2$ sec.$^{-1}$	% H_2	% CH_4
	121	740	3.0	0.358	0.037	0.104		
	122	741	3.0	0.360	0.040	0.111		
	123	742	3.0	0.360	0.044	0.121	60	40
	101	760	2.3	0.386	0.094	0.242		
	102	765	3.5	0.352	0.086	0.242		
	105	767	2.8	0.316	0.086	0.272	60	40
Surface increased 15 times	112	778	5.6	0.326	0.120	0.368	62	38
Pressure increased Time of cont. increased	106	802	5.9	0.840	0.825	0.98	57	43
Time of cont. increased Pressure increased	109	812	5.5	0.891	1.29	1.45	59	41
Time of cont. increased	113	815	2.5	0.910	1.37	1.50	59	41
	128	822	2.8	0.336	0.80	2.38	60	40
	129	825	2.8	0.336	0.88	2.62	60	40
Time of contact and pressure increased	107	828	5.5	0.908	2.52	2.78		
	108	829	5.5	0.876	2.60	2.96	60	40
	103	850	3.0	0.311	1.51	4.86	60	40
Pressure increased	114	851	5.8	0.320	1.60	5.00	59	41
Surface increased 15 times	110	867	4.4	0.400	3.33	8.3'	61	39
	111	867	3.7	0.410	3.54	8.75	61	39

ethane or ethylene was observed. The droplets of liquid collected in the *U* trap were identified by their boiling point as 3, 3′ di-methyl-di-benzyl.

The percentage of decomposition was calculated as before by assuming that one mol of each gas produced corresponds to one mol of meta-xylene primarily decomposed. By changing the time of contact and pressure of xylene the reaction was proved to be of the first order, and packing experiments confirmed it to be a homogeneous gas reaction. The results are summarized in Table III, and the plot of log$K$ against $1/T$ is given in Fig. 2.

The graph of log$K$ against $1/T$ demonstrates strikingly that the pyrolysis of meta-xylene is represented by a straight line parallel to that of toluene but displaced towards higher values of log$K$ by logarithm of 2. Accordingly, the activation energy is taken once more at 77.5 kcals. while the temperature independent factor is chosen as $4.0 \cdot 10^{13}$—that is twice the value for toluene. A more precise justification of these figures will be given later.

The interpretation which we place on these facts is that the mechanism of pyrolysis of meta-xylene is analogous to that of toluene. The recurrence of the same value for the energy of activation indicates the same C−H bond energy; while the twofold value of the frequency factor indicates a twice increased probability of reaction, owing to the presence of two independent methyl groups.

The recurrence of the same composition of gas in the products of the pyrolysis of meta-xylene as was observed for toluene is in itself a powerful argument for assuming the same mechanism of decomposition in both cases.

PYROLYSIS OF PARA-XYLENE

The para-xylene used was manufactured by Chance and Hunt. After purification by repeated crystallization the substance had a sharp melting point at 12.8°C, and gave steady results in repeated pyrolysis showing that it was pure enough for our purposes.

Table IV gives the experimental results, and the plot of log$K$ against $1/T$ is to be found in Fig. 2. Hydrogen and methane are once more the only gaseous products and no ethane or ethylene was observed. The gas produced is slightly richer in hydrogen than the gas obtained by pyrolysis of toluene and meta-xylene, the composition being 65 percent of hydrogen and 35 percent of methane. The packing experiments proved that the reaction is a homogeneous gas reaction. The rate of decomposition is at all temperatures three times greater than that of meta-xylene.

From these results we conclude that in the pyrolysis of para-xylene the first step is again the rupture of a C−H bond of a CH_3 group. The main result clearly consists in the fact that para-xylene is proved to decompose three times faster than meta-xylene. As a further discussion will presently show, this can be best accounted for by a reduction of the activation energy (which is the energy of the C−H bond) to 75

TABLE IV. Para-xylene.

Remarks	Run No.	T°C	P. para-xylene mm Hg	Time of contact sec.$^{-1}$	% decomp.	$K \cdot 10^2$ sec.$^{-1}$	% H_2	% CH_4
	134	745	3.2	0.419	0.158	0.378		
	135	745	3.2	0.419	0.159	0.381	67	33
	130	746	3.3	0.425	0.168	0.395		
	136	747	3.3	0.428	0.178	0.415	67	33
	138	781	2.6	0.239	0.344	1.44	67	33
Surface increased 15 times	133	782	6.2	0.715	0.365	1.35	64	36
	137	783	2.0	0.238	0.372	1.56		
	139	866	3.7	0.344	7.73	22.4		
	140	866	3.8	0.354	7.73	21.8	65	35
Surface increased 15 times	131	860	4.5	0.410	10.0	25.0	63	37

kcal; the temperature independent factor being retained at the $4 \cdot 10^{13}$.

The slight change in the proportion of hydrogen to methane is probably the result of the decrease in the C−H bond energy, as this would increase the probability of the reaction between the hydrogen atom and para-xylene molecules which leads to the production of hydrogen molecules. (Reaction 2.)

The pyrolysis of para-xylene differs from that of toluene and of meta-xylene in the following particular. The last two give rise to dimers of the free radicals primarily produced. The radical produced in the pyrolysis of para-xylene gives no dimer but only a high polymer which accumulates in trap *U* and trap *H*.

The problems arising from this polymerization are discussed elsewhere.[9] It appears that the primarily produced para-xylyl radicals disproportionate in the gas phase according to the following equation:

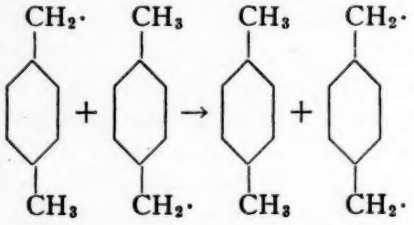

and the biradical (or its quinonoid form

polymerizes rapidly on condensation at a cooled surface.

PYROLYSIS OF ORTHO-XYLENE

The ortho-xylene used was a B.D.H. product, which was additionally purified by crystallization at −30°C, followed by a careful distillation. Since this product was not pure enough, it was further purified by partial pyrolysis. The necessity of this purification is seen from Table V. (Compare runs 153 and 150, 151 and 152, also 146 and 147 with 148 and 149.) The concordant results obtained with pyrolyzed ortho-xylene, proved that they represent the pyrolysis of ortho-xylene itself.

[9] M. Szwarc, "Discussion on labile molecules," Trans. Faraday Soc., in press.

The main features of the pyrolysis of ortho-xylene are the same as those of the previously investigated hydrocarbons. The principal gaseous products are hydrogen and methane. The rate of their formation is somewhat (about 70 percent) greater than that observed for para-xylene, the percentage of hydrogen being smaller (50 percent H_2 50 percent CH_4). In this case the formation of a small quantity of C_2 hydrocarbon was observed; about 10 percent of H_2+CH_4.

It seems reasonable to explain the formation of C_2 hydrocarbons from ortho-xylene by the presence of two adjoining methyl groups. This may also account for the low H_2/CH_4 ratio if the steric interaction of the two CH_3 groups is assumed to decrease the Ph−C bond energy and consequently increase the probability of the reaction leading to the formation of CH_4.

These considerations leave unaffected the conclusion that the main process in the pyrolysis of ortho-xylene is again the rupture of the C−H bond. The slightly higher rate of decomposition of ortho-xylene compared to that of the para isomer may be taken to indicate that the C−H bond is weaker in the former.

The values of $\log K$ are plotted against $1/T$ in Fig. 2, and are represented as lying on a straight line corresponding to an energy of activation of 74 kcal., indicating the decrease in C−H bond energy of ortho-xylene as compared to meta-xylene.

FURTHER DISCUSSION OF THE RESULTS

We shall now present the more detailed consideration on the ground of which the activation energies and the temperature independent factors

TABLE V. Ortho-xylene.

Remarks	No. of run	T°C	P ortho-xylene mm Hg	Time of contact sec.	% decomp. into H_2+CH_4	$K \cdot 10^2$ sec.$^{-1}$	% decomp. into C_2 hydrocarb.	% H_2	% CH_4
Partially pyrolyzed at 836°C	156	730	3.5	0.370	0.140	0.379	0.010		
	157	734	3.6	0.385	0.185	0.480	0.014		
	155	777	3.2	0.338	0.745	2.20	0.028		
	154	788	3.0	0.340	1.06	3.12	0.045	46	54
	150	815	3.4	0.330	2.26	6.85	0.22	52	48
	151	815	3.4	0.330	2.33	7.07	0.25		
Partially pyrolyzed at 870°C	152	815	3.5	0.339	2.30	6.90	0.20	52	48
Not pyrolyzed	153	815	3.5	0.339	3.24	9.55	2.72	42	58
Partially pyrolyzed at 836°C	148	836	4.0	0.372	4.83	13.0	0.35	52	48
	149	838	3.6	0.335	4.93	14.7	0.55	52	48
Not pyrolyzed	146	835	3.5	0.326	6.00	18.4	2.6	50	50
	147	837	3.5	0.326	6.20	19.0	2.4		

quoted above were determined. Using the method of least mean squares we obtain for the assumed linear dependence of $\log K$ on $1/T$ the parameters of the equation

$$\log K = -\frac{E}{2.3RT} + \nu$$

shown in Table VI. The standard deviations listed in the second column show that the accuracy is not sufficient to distinguish definitely between the activation energies of the reaction proceeding at different speeds. The situation can, however, be clarified further by assuming that the temperature independent factor is the same for the decomposition of *one methyl group* in each of the four investigated hydrocarbons. We note that all the results can be represented on this basis within the experimental errors. Such a representation limits the possible values of the temperature independent factor for the decomposition of *one methyl group* to $\nu_0 = 2.0 \cdot 10^{13} - 2.5 \cdot 10^{13}$. We can make use of the choice of any particular value within this range for a more accurate determination of the differences between the activation energies of the four pyrolytic reactions.

Table VII shows the calculated values for energy of activation on the basis $\nu_0 = 2.0 \cdot 10^{13}$, the following equations were used:

$$E = 2.3 \cdot RT(13.3 - \log K) \text{ for toluene.}$$
$$E = 2.3 \cdot RT(13.6 - \log K) \text{ for xylenes.}$$

Calculations are based on experiments at low temperature.

From these results we conclude that the C—H bond energy is the same in toluene and meta-xylene, while it is smaller by 2.3–2.5 kcal. in para-xylene and by 3.5 kcal. in ortho-xylene. We may recall the observations of Dobryanskii and Saprykin[10] on the relative stability of xylenes by pyrolytic isomerization. They found that meta-xylene was the most stable and did not isomerize, para-xylene isomerized only slightly to meta, while ortho-xylene isomerized very easily giving mainly meta- and partially para-xylene. These facts agree well with the sequence of activation energies derived above.

TABLE VI.

Hydrocarbon	E kcal.	Mean deviation of $E = \Delta E$ kcal.	ν
toluene	77.3	±1.3	2.10^{13}
meta-xylene	77.1	±1.9	4.10^{13}
para-xylene	76.2	±1.5	5.10^{13}
ortho-xylene	74.8	±1.1	5.10^{13}

[10] A. F. Dobryanskii and F. Y. Saprykin, J. Gen. Chem. (U.S.S.R.) 9, 1313 (1939).

TABLE VII.

No. of run	T°C	E	ΔE
		Toluene	
87	740	77.9	+0.4
88	741	77.9	+0.4
89	742	77.5	0.0
90	742	77.5	0.0
91	745	77.0	−0.4
92	749	77.1	−0.3
93	747	76.9	−0.5
94	738	78.3	+0.8
		average 77.5±0.14	
		Meta-xylene	
101	760	77.0	−0.2
102	765	77.1	−0.1
105	767	77.4	+0.2
121	740	77.4	+0.2
122	741	77.4	+0.2
123	742	77.0	+0.2
		average 77.2±0.18	
		Para-xylene	
130	746	74.9	+0.1
134	745	74.9	+0.1
135	745	74.9	+0.1
136	747	75.0	+0.2
137	783	74.5	−0.3
138	781	74.6	−0.2
		average 74.8±0.20	
		Ortho-xylene	
156	730	73.9	−0.1
157	734	73.7	−0.3
155	777	74.9	+0.9
		average 74.0±0.55	

The weakening of the C—H bond in the methyl groups of para- and ortho-xylene as compared with toluene and meta-xylene was to be expected on the assumption of hyperconjugation occurring for example in para-xylene as follows:

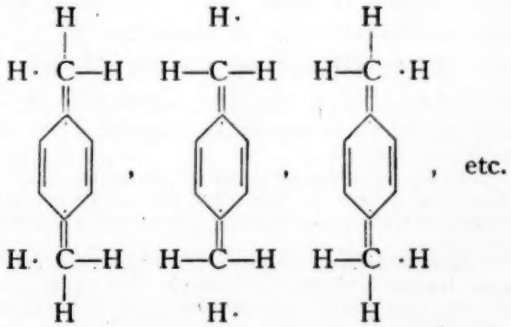

The effect of hyperconjugation weakening in the C−H bond in C_2H_6 as compared with that in CH_4 has been estimated at 7 kcals.[11] A detailed discussion of the disparity between this value and that obtained for para-xylene seems premature in view of the inaccuracy of the results obtained up to date. But we would like to emphasize that in the case of the weakening of C−H bonds in para-xylene as compared with meta-xylene we can see no other possible explanation than hyperconjugation, whereas in the case of the weakening of the C−H bond in ethane as compared with methane, the proximity of the two interacting methyl groups offers additional possibilities—for example, steric effects or dipole interactions—of an explanation.

[11] E. C. Baughan, M. G. Evans, and M. Polanyi, Trans. Faraday Soc. **37**, 377 (1941).

The author wishes to express his sincerest thanks to Professor M. Polanyi for his constant encouragement and valuable help throughout the work and the preparation of this paper. His thanks are also due to Manchester University for the I.C.I. Fellowship which enabled him to carry out this work, and to the Anglo-Iranian Oil Company for a grant.

THE JOURNAL OF CHEMICAL PHYSICS VOLUME 16, NUMBER 2 FEBRUARY, 1948

Absorption of the Alkyl Cyanides in the Vacuum Ultraviolet*

JANICE A. CUTLER**
Department of Chemistry, New York University, New York
(Received October 16, 1947)

The vacuum ultraviolet spectra of methyl and ethyl cyanide have been determined in the region 1000A to 1800A. Three members of a Rydberg series were found for methyl cyanide starting at 1292A, the limit of the series corresponding to an ionization potential of 11.96 ev. Vibrational band changes which have been found to accompany the first two members have been assigned to fundamental frequencies of the molecule by comparison with Raman data. The electronic transition, expressed by the Rydberg series, was ascribed to excitation of a π electron in the triple bond. At higher pressures, a continuous absorption appeared which was followed only to 1600A. No structure could be observed in the spectrum of the ethyl cyanide, although it paralleled that of methyl cyanide in having a stronger absorption starting at 1342A and a weaker one appearing at higher pressures and spreading to longer wave-lengths.

INTRODUCTION

THE following communication contains a study of the absorption spectra of methyl and ethyl cyanides in the vacuum ultraviolet. Previously, Herzberg and Scheibe[1] studied the spectrum of methyl cyanide down to about 1540A, finding a weak band extending from 1820A to 1600A with a maximum at about 1670A. Below 1600A, there was an indication of the beginning of a stronger absorption which would extend to shorter wave-lengths. They also observed the same indications in the spectra of the methyl halides. Price[2] extended this work on the halides to shorter wave-lengths and found discrete Rydberg series, assigning the excitation to the $p\pi$ electrons on the halide. From this it was felt that if the work on methyl cyanide were also extended to shorter wave-lengths, a Rydberg series might be identified.

EXPERIMENTAL

The far ultraviolet spectra were photographed on a Lyman continuum as a background, using hydrogen as the inert gas, by means of a vacuum spectrograph at nearly normal incidence. A lightly ruled glass grating was used, of focal length 1 meter, with 30,000 lines per inch, ruled by R. W.

* Taken from a dissertation submitted to the faculty of the Graduate School of New York University in partial fulfillment of the requirements for the degree of Doctor of Philosophy.

** Present address: Polytechnic Institute of Brooklyn, Polymer Research Institute, Brooklyn, New York.

[1] G. Herzberg and G. Scheibe, Zeits. f. physik. Chemie **B7**, 390 (1930).

[2] W. C. Price, J. Chem. Phys. **4**, 539 (1936).

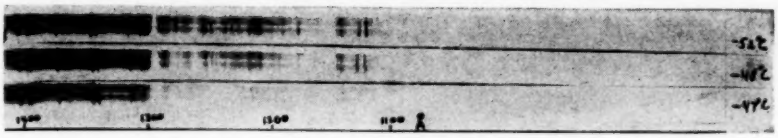

FIG. 1. Spectrum of methyl cyanide.

Wood. The dispersion was about 8.43A per mm. Eastman Kodak III-O, ultraviolet sensitized plates and Ilford Q1 plates were used. The Eastman plates were made on *x* thin glass so that they could be bent to fit the Rowland circle. Three exposures could be made on one plate, each exposure covering 500A. Discrete bands were measured from microphotometer traces using the strong Si and O lines in the source as standards. The spectrum of MeI was taken as a test plate for the region 1900–1300A since Price[2] has published an illustration of the sharp bands found in that region. The absorption spectra of the compounds were taken with the vapor filling the entire spectrograph, thus producing a total absorbing path of 2 meters. The concentration of the vapor was controlled by the temperature of an acetone bath cooled by dry ice, surrounding the distilling flask leading into the spectrograph.

METHYL CYANIDE

The material supplied by the Eastman Kodak Company was dried for several days over calcium chloride and then distilled in air in an all glass still. The main fraction came over from 81 to 81.5°C. The methyl cyanide was immediately put into a distilling apparatus connected to the spectrograph and redistilled in vacuum before being vaporized into the spectrograph.

Typical spectra of methyl cyanide are reproduced in Fig. 1 where they are enlarged about three times. This compound has a set of strong, discrete bands which start abruptly at 1292A at the lower vapor pressures studied. As the pressure is increased these discrete bands widen, and a continuous absorption appears to spread from the short wave-length end. The continuum is believed to be caused by the absorption of methane and ethane in this region, starting at 1300A and 1350A, respectively.[3,4] As the pressure is increased, the absorption no longer starts abruptly at 1290A, but a continuous absorption occurs which travels to the longer wave-lengths. At the highest temperature used, −25°C, this continuous absorption extends to 1600A. The weak band from 1820A to 1600A reported by Herzberg and Scheibe was not observed, probably because the vapor pressure was never high enough.

The spectrum of methyl cyanide (see Figs. 1 and 2) is not an ideal one for measurement and interpretation. The bands are not very sharp, and it is impossible to find indications of structure which might facilitate in the analysis. In this respect the spectrum of methyl cyanide resembles the shorter wave-length spectrum of HCN as reported by Price.[5,6] The overlapping continua extending from the shorter wave-lengths are a serious difficulty, obscuring the shorter members of the discrete banded systems. Nevertheless, it seems very probable that a Rydberg series is represented by the strongest bands 1, 7, and 10. These bands can be represented by the formula

$$\nu_0^n = 96{,}426 - [R/(n+0.40)^2].$$

The constants were chosen to fit the first member, $n=2$, since the measurement of the member corresponding to $n=3$ is made difficult by interfering O III emission lines, and the band corresponding to $n=4$ is quite broad. The agreement between observed and calculated values is shown in Table I. The convergence limit, 96,426 cm^{-1} ≡1035A, is obscured in the C−C and C−H continua; the corresponding ionization potential is 11.96 volts.

The strong bands 1 and 7 are accompanied on

TABLE I.

	Observed cm^{-1}	Calculated cm^{-1}
$n=2$	77,374	77,374
$n=3$	86,953	86,933
$n=4$	90,853	90,757

[3] A. B. F. Duncan and J. P. Howe, J. Chem. Phys. **2**, 851 (1934).
[4] W. C. Price, Phys. Rev. **47**, 444 (1935).
[5] W. C. Price, Phys. Rev. **46**, 529 (1934).
[6] W. C. Price, and A. D. Walsh, Trans. Faraday Soc. **41**, 381 (1945).

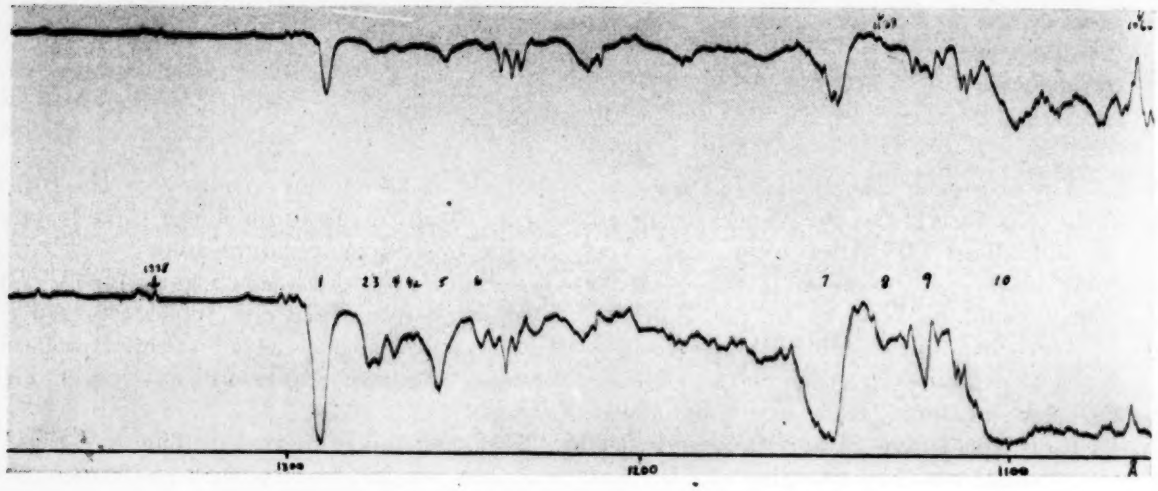

FIG. 2. Microphotometer tracing of methyl cyanide spectrum.

the short wave-length side by weaker bands which represent transitions to vibrating electronic states. The differences of the main bands of the 1292A group are listed in Table II.

There seems little doubt that the strongest vibrational band associated with the Rydberg transition of longest wave-length, with a frequency difference of 2001 cm^{-1} from the O→O band, originates in the excitation of the C≡N valence vibration (ν_2),*** of frequency 2249 in the normal state, as determined by the Raman spectrum.[7] The diminution in frequency in the excited state from its value in the normal state, indicating a diminution of bonding strength, is a common occurrence, being analogous, for example, to the change in the symmetrical C=C vibration in ethylene from its value of 1623 cm^{-1} in the ground state to 1370 cm^{-1} in its first Rydberg excited state.[8] Similarly, the band displaced by 2724 cm^{-1} from the O→O band is probably the symmetrical C−H vibration of frequency 2942 cm^{-1} (ν_1) in the ground state. The band displaced 1239 cm^{-1} from the O→O band may represent the symmetrical deformation frequency of the methyl group, 1376 cm^{-1} in the ground state (ν_3). The ground state has a totally symmetrical "C−C" frequency ν_4, at either 916 cm^{-1} or 1124 cm^{-1},*** more likely the former, and it therefore seems probable that the frequency interval 813 cm^{-1} or 968 cm^{-1}, more likely the former, represents this vibration in the excited state. Herzberg assigns the second of the frequencies just mentioned in the normal state to the degenerate rocking frequency of the methyl group (ν_7), and it is possible that the 968 cm^{-1} band represents this frequency in the excited state, although the intensity seems unusually large for a degenerate vibration. The very weak band 4*a* (Fig. 2), with a frequency separation of 1560 cm^{-1} from the O→O band, may be $2\nu_4$, and a weak band at about 4000 cm^{-1} from the O→O band may be $2\nu_2$.

The vibrational transitions associated with the second Rydberg member at 1150A are less certain because of difficulties of measurements imposed by interfering emission lines in the source. A strong band displaced 2009 cm^{-1} (band 9) from the O→O band doubtless repre-

TABLE II.

Band	cm^{-1}	Differences from O→O
1, O→O	77,374	
2	78,187	813
3	78,342	968
4	78,613	1239
4*a*	78,934	1560
5	79,375	2001
6	80,098	2724

*** Notation in G. Herzberg, *Infrared and Raman Spectra of Polyatomic Molecules* (D. Van Nostrand Company, Inc., New York, 1945), p. 333.

[7] A. W. Reitz and R. Skrabal, Monats. F. Chem. **70**, 398 (1937).

[8] W. C. Price and W. T. Tutte, Proc. Roy. Soc. London **A174**, 207 (1940).

sents the C≡N vibration (ν_2), and the frequency interval of 1107 cm^{-1} (band 8) may represent the methyl deformation vibration (ν_3).

ETHYL CYANIDE

No discrete bands could be found for ethyl cyanide. A diffuse absorption starts at 1342A and extends to shorter wave-lengths. This absorption occurs at low pressures similar to those at which the Rydberg type of absorption was predominant in methyl cyanide. At higher pressures the continuous absorption extends to longer wave-lengths similar to the continuous absorption of methyl cyanide.

DISCUSSION

The discrete Rydberg band series starting at 1292A in the case of methyl cyanide is assigned to an excitation of one of the four π electrons making up the C≡N bond. The fact that the C≡N vibration is most strongly excited lends support to this assumption. This excited electron, however, can set up methyl and C−C vibrations since its excited orbital will probably extend, to some extent, into the rest of the molecule. As in the case of methyl iodide (where the excited electron has been proved to be the $p\pi$ electron on the iodine),[2] symmetrical methyl vibrations in another part of the molecule accompany the early Rydberg members. Since only the O→1 vibrations are excited strongly in each Rydberg transition, we may conclude that the relative positions of the atoms in the molecule do not change very much by excitation.

It is interesting to note that one of the Rydberg series found by Price and Walsh[6] for methylacetylene,

$$\nu_0{}^n = 91{,}240 - [R/(n+0.48)^2],$$

has a constant in the term value denominator (0.48) which is similar to that found for methyl cyanide. Price and Walsh showed that it was a π electron from the triple bond of methylacetylene which was excited. The term values observed for methylacetylene and methyl cyanide are compared in Table III.

Although the term value for the ground state in methylacetylene is 91,240 cm^{-1} as compared with 96,430 cm^{-1} for methyl cyanide, the term values for the corresponding higher states of the

TABLE III.

	Methyl cyanide (obs.)	Methylacetylene (obs.)
$n=2$	19,052	17,643
$n=3$	9,473	9,003
$n=4$	5,573	5,488

π electron of the triple bond are very similar. The lowest members are the ones most affected by the immediate configuration of the surrounding molecule. Since the two molecules are isosteric, it is interesting to note the similarity in term values and one may probably conclude that a π electron of the triple bond is also excited in methyl cyanide.

The ionization potential of HCN is given by Sponer as 14.8 ev,[9] as compared with 11.96 ev found for methyl cyanide in these experiments. This reduction is similar to that found by Price and Walsh[6] for methylacetylene as compared with acetylene, and can be accounted for in the same way, by an inductive effect and hyperconjugation. The inductive effect transfers negative charge into the triple bond from the polarizable methyl group. In the case of hyperconjugation, the three C−H bonds behave somewhat as a triple bond and resonance occurs as in ordinary conjugation, resulting in putting more charge into the triple bond. This conjugation can be represented as:

$$H_3{\equiv}C{-}C{\equiv}N \rightleftharpoons \overset{+}{H}_3{=}C{=}C{=}\overset{-}{N}$$

or

$$\begin{matrix} & \overset{+}{H} & \\ HC & = & C=\overset{-}{N} \\ & H & \end{matrix} .$$

Hurdis and Smyth[10] explained the increase in the dipole moment of methyl cyanide (3.94 Debyes) over that of hydrogen cyanide (2.93 Debyes) on the basis of the hyperconjugation and inductive effect in methyl cyanide. Both effects would put extra negative charge into the C≡N and, therefore, the ionization potential would be lowered.

There seems to be some difficulty reconciling

[9] H. Sponer, *Molekulspektren* (Julius Springer, Berlin, 1935), Vol. I.

[10] E. C. Hurdis and C. P. Smyth, J. Am. Chem. Soc. 65, 89 (1943); N. B. Hannay and C. P. Smyth, paper presented at the American Chemical Society meeting in Atlantic City on April 9, 1946.

the value of the ionization potential of methyl cyanide as deduced in these experiments, 11.96 ev, with the value of about 13.8 ev deduced for cyanogen by Price and Walsh[6] from the difficultly measurable absorption spectrum of that compound. Methyl cyanide bears the same relationship to cyanogen as methylacetylene to diacetylene. The ionization potential of methylacetylene, deduced from a well established Rydberg series by Price and Walsh, is 11.36 ev, and that of diacetylene, similarly obtained, is 10.74 ev. This is the relationship to be expected since resonance in the normal conjugated system represented by diacetylene will lower the ionization potential more than in the hyperconjugated system, methylacetylene. Similarly, the ionization potential of cyanogen is expected to be lower than the 11.96 ev of methyl cyanide, which in turn would be lower than that of hydrogen cyanide, 14.8 ev.

The first Rydberg type band in cyanogen is at 1320A as compared with 1292A in methyl cyanide, and this suggests the possibility that the first ionization potential of cyanogen should be lower than that of methyl cyanide. Similarly, the first Rydberg band of diacetylene is at 1630A (I.P. = 10.74 ev) while the first Rydberg band of methylacetylene occurs at 1540A (I.P. = 11.26 ev). If Price and Walsh's value for the ionization potential of cyanogen is taken, then in the light of this experiment, the resonance effects among cyanogen, methyl cyanide, and hydrogen cyanide are different from those among diacetylene, methylacetylene, and acetylene.

The beginning of the absorption of ethyl cyanide at 1342A may represent the limit of the C−C absorption or it may correspond to the first Rydberg member of methyl cyanide. Its shift to longer wave-lengths would indicate a lowering in ionization potential of a few tenths of an electron volt. Since the actual members of a Rydberg series could not be measured, this evaluation is very rough. The lowering of the first ionization potential of ethyl cyanide compared to methyl cyanide may be ascribed to the increase in induction of negative charge into the triple bond from the ethyl group as compared to the methyl group. The dipole moments are 4.00 Debyes and 3.94 Debyes respectively.[10] The lack of structure in the absorption of ethyl cyanide may be due to the relatively stronger C−H and C−C continua (more C−H and C−C bonds) or low frequency vibrations may be present giving the appearance of a quasi-continuum.

In conclusion, it is a pleasure to acknowledge my indebtedness to Dr. William West for his supervision and encouragement during the course of this work and for his helpful suggestions on the preparation of this paper.

THE JOURNAL OF CHEMICAL PHYSICS VOLUME 16, NUMBER 2 FEBRUARY, 1948

Quantum Corrections to the Thermodynamic Properties of Liquids, with Application to Neon[1]

O. K. RICE[2]
Clinton Laboratories, Oak Ridge, Tennessee

(Received October 18, 1947)

The quantum correction has been expressed as a deviation η from $\ln Q_c$, where Q_c is the classical partition function. Changes in volume, energy, specific heat, etc., caused by quantization can be expressed in terms of η and certain thermodynamic quantities. η itself is expressed in terms of thermodynamic quantities. The equations obtained give for solid neon the same results, within the limits of error, as the usual treatment of a Debye solid with the aid of the Grüneisen equation. To apply the equation to liquid neon, various thermodynamic quantities have been obtained from known values for argon by use of the law of corresponding states. The difference in volume and specific heat of liquid neon from the values expected from the law of corresponding states have been computed and found to agree reasonably well with the observations. However, the melting point, and the ΔE and ΔS of fusion are found experimentally to be much closer to the classical values than one would expect from the theory. No explanation of this discrepancy is apparent.

IT has frequently been noted that the properties of neon are somewhat out of line with those of the other condensed rare gases. These deviations have been ascribed to quantum effects in neon,[3] which, it is believed, would otherwise obey the law of corresponding states. Quantum effects in the solid are easily taken care of with the help of the Debye theory; the liquid presents somewhat more of a problem.

The quantum corrections for a liquid have recently been given in a general form by Mayer and Band.[4] Their results, however, involve some multiple integrals containing distribution functions and second derivatives of the interatomic potential function. They are, therefore, difficult to evaluate, and it seems desirable to derive some rougher equations which will be more easily handled. It will be the purpose of this paper to express the magnitude of the quantum effects in terms of thermodynamic quantities which have either been measured or may be approximated from the law of corresponding states, and apply the results to neon.

I. EQUATIONS FOR A ONE-PHASE ISOTHERMAL AND ISOBARIC SYSTEM

We shall express the quantum deviation by means of a quantity η defined by the equation[5]

$$\ln Q = \ln Q_c + \eta. \tag{1}$$

Here Q is the actual partition function, and Q_c is the classical partition function of the system, at the given temperature T and molal volume V. Q_c is found by taking the limiting form of Q for high temperatures, and inserting the actual value of T in this limiting form. In calculating Q only the thermal part of the energy, E_t, and the zero-point energy, E_z, are considered. The Helmholtz free energy is therefore given by

$$A = -RT \ln Q + E_p, \tag{2}$$

where E_p is the potential energy (excluding any potential energy involved in E_t and E_z); that is, E_p is the value the energy would have with all the atoms at rest in their positions of equilibrium.[6] From Eq. (1) this may be written

$$\begin{aligned} A &= -RT \ln Q_c - RT\eta + E_p \\ &= A_c - RT\eta. \end{aligned} \tag{3}$$

[1] This document is based on work performed under Contract No. W-35-058-eng-71 for the Atomic Energy Project at the Clinton Laboratories.

[2] On leave 1946–47 from the University of North Carolina, Chapel Hill, North Carolina.

[3] See K. S. Pitzer, J. Chem. Phys. **7**, 583 (1939).

[4] J. E. Mayer and W. Band, J. Chem. Phys. **15**, 141 (1947).

[5] If η is very small we may write Eq. (1) in the form $Q = Q_c(1+\eta)$, which brings out the significance of η. However, to actually define η by this equation would be less convenient for purposes of computation than to use Eq. (1).

[6] For a solid the positions of equilibrium form a regular lattice, but this is, of course, not true for a liquid.

In this equation we assume either that E_p is the same for the classical and quantum case if the volume remains fixed, or, better, that any change is included in η. Since E_p is the energy after subtracting out all thermal and zero-point energy, it would appear that any change in it which could be caused by quantization could be referred to a change in the average coordination number caused by quantization. Such a change could occur in the liquid, but may be included in η. This, then, eventually becomes merged with the assumptions regarding η which are later made, in order to estimate it for the liquid.

The Gibbs free energy F is equal to the Helmholtz free energy if the pressure $p=0$, as is essentially the case for condensed systems around atmospheric pressure. It is to be noted, however, that, in Eq. (3), A_c is to be evaluated at the same molal volume as A, not the same pressure. If A is evaluated at zero pressure, A_c must be evaluated at that pressure, δp, at which the system would have the same volume if the classical statistics held.

Since the pressure is given by

$$p=-(\partial A/\partial V)_T, \tag{4}$$

and since δp is the pressure the system would have if Q_c were the correct partition function, we may write

$$\delta p=-(\partial A_c/\partial V)_T. \tag{5}$$

The true pressure being zero, we obtain from Eqs. (3), (4), and (5)

$$\delta p=-RT(\partial\eta/\partial V)_T. \tag{6}$$

If we let $A_{c,0}$ be the classical value of A at zero pressure, we have[7]

$$A_c=A_{c,0}+\int_0^{\delta p}(\partial A_c/\partial p)_T dp$$
$$=A_{c,0}+\int_0^{\delta p}(\partial A_c/\partial V)_T(\partial V/\partial p)_{T,c}dp.$$

Using Eq. (5), and integrating, assuming $(\partial V/\partial p)_{T,c}$ to be constant,

$$A_c=A_{c,0}-(\delta p/2)^2(\partial V/\partial p)_{T,c}.$$

Aside from the assumption that $(\partial V/\partial p)_{T,c}$ is constant, this equation is exact. If η and hence δp is a small quantity, it shows that $A_c-A_{c,0}$ is a small quantity of the second order. Such quantities may, in general, be neglected in the case of the liquid, but may not be entirely negligible for the solid. The form of the dependence of $A_c-A_{c,0}$ on δp is that which is to be expected from the fact that for $p=0$ the condition of equilibrium is that A be a minimum.

There will be a first-order effect on the volume of the system. Let V_c be the volume the system would have at zero pressure if the classical statistics held, and let V be its actual volume. A classical system at volume V would have the pressure δp. To go to zero pressure its volume must change by $-(\partial V/\partial p)_{T,c}\delta p$. We therefore have

$$V-V_c=(\partial V/\partial p)_{T,c}\delta p$$
$$=-RT(\partial\eta/\partial V)_T(\partial V/\partial p)_{T,c}. \tag{7}$$

There will also be a first-order effect on the energy. We have, in general, for the sum of the thermal energy and zero-point energy

$$E_t+E_z=RT^2(\partial\ \ln Q/\partial T)_V. \tag{8}$$

At a given volume V, therefore,

$$E_t+E_z-E_{t,c}=RT^2[(\partial\ \ln Q/\partial T)_V$$
$$-(\partial\ \ln Q_c/\partial T)_V]=RT^2(\partial\eta/\partial T)_V, \tag{9}$$

where $E_{t,c}$ is the classical thermal energy at the volume V. As noted above, quantization causes no change in E_p, since any effect is taken care of by η. However, at volume V the pressure of a classical system would, as we have seen, be δp. Going back to zero pressure the energy would change by $-(\partial E/\partial V)_{T,c}(\partial V/\partial p)_{T,c}\delta p$. Further, at zero pressure we may write $(\partial E/\partial V)_{T,c}$ $=T(\partial S/\partial V)_{T,c}=T(\partial p/\partial T)_{V,c}$. Therefore, for fixed zero pressure we may write (using Eq. (6))

$$E-E_c=RT^2(\partial\eta/\partial T)_V-RT^2(\partial\eta/\partial V)_T$$
$$\times(\partial p/\partial T)_{V,c}(\partial V/\partial p)_{T,c}$$
$$=RT^2[(\partial\eta/\partial T)_V$$
$$+(\partial\eta/\partial V)_T(\partial V/\partial T)_{p,c}]. \tag{10}$$

Provided the differential coefficients are constant, both Eqs. (7) and (10) are exact.

The quantum contribution to the specific heat, δC_p, can be obtained by differentiating Eq. (10). We note that $(\partial/\partial T)_p=(\partial/\partial T)_V$ $+(\partial V/\partial T)_p(\partial/\partial V)_T$. This expression is to be

[7] We use, in general, a subscript c to designate the classical value of any quantity.

applied to the true quantized system rather than a hypothetical classical one, so the $(\partial V/\partial T)_p$, which appears here (without subscript c) is the actual, rather than a classical value. However, the operator, $(\partial/\partial T)_p$, or $(\partial/\partial T)_V$ and $(\partial/\partial V)_T$, applied to a classical expression gives a classical expression. We therefore obtain

$$\begin{aligned}\delta C_p = 2RT[&(\partial\eta/\partial T)_V+(\partial\eta/\partial V)_T(\partial V/\partial T)_{p,c}]\\&+RT^2[(\partial^2\eta/\partial T^2)_V+(\partial^2\eta/\partial T\partial V)\\&\times\{(\partial V/\partial T)_p+(\partial V/\partial T)_{p,c}\}\\&+(\partial^2\eta/\partial V^2)_T(\partial V/\partial T)_p(\partial V/\partial T)_{p,c}\\&+(\partial\eta/\partial V)_T(\partial^2 V/\partial T^2)_{p,c}]. \quad (11)\end{aligned}$$

In the case of liquid neon, $(\partial V/\partial T)_p$ and $(\partial V/\partial T)_{p,c}$ will be nearly enough alike so it will not be necessary to distinguish between them.

II. THE EVALUATION OF THE QUANTUM CORRECTION, η

The evaluation of the quantum correction for the solid is very easy, if we assume that it obeys the Debye specific heat law. In this case we can write the expression for $\ln Q$ in the form[8]

$$\begin{aligned}\ln Q = \ln[(T/\Theta)^3 e] &-(3/40)(\Theta/T)^2\\&+(3/6720)(\Theta/T)^4-\cdots, \quad (12)\end{aligned}$$

where Θ is the Debye characteristic temperature. If we break off Eq. (12) at the second term and compare with Eq. (1) we see that this gives

$$\eta = -(3/40)e^{\frac{3}{2}}Q_c^{-\frac{3}{2}} = -0.1464Q_c^{-\frac{3}{2}}. \quad (13)$$

In many respects the liquid resembles the solid, and we shall assume that Eq. (13) holds for the liquid as well as the solid. It is true that there is a translational, as well as a vibrational, contribution to the partition function of the liquid, and there may be some complications arising from the possibility of a change in coordination number in the liquid, as indicated in the discussion following Eq. (3). However, the quantum correction will, in general, be expected to decrease as the partition function increases, and in view of the reasonably close similarity between liquid and solid, it would appear that Eq. (13) cannot be too far incorrect for the liquid.

We may now refer back to Eq. (2) to get η in terms of thermodynamic quantities. Since $A_c-E_p = E_c-TS_c-E_p = E_{t,c}-TS_c$, where $E_{t,c}$ is the classical thermal energy, we may write from Eq. (13)

$$\eta = -0.146\exp(2E_{t,c}/3RT-2S_c/3R). \quad (14)$$

Since $(\partial E_{t,c}/\partial T)_V = C_{v,c}$ and $(\partial S_c/\partial T)_V = C_{v,c}/T$, we have

$$(\partial\eta/\partial T)_V = -(2/3)\eta E_{t,c}/RT^2. \quad (15)$$

We also have

$$\begin{aligned}(\partial\eta/\partial V)_T = (2/3)\eta[&(\partial E_{t,c}/\partial V)_T/RT\\&-(\partial S_c/\partial V)_T/R]. \quad (16)\end{aligned}$$

We note that $T(\partial S_c/\partial V)_T = (\partial E_c/\partial V)_T+p$. Substituting this into Eq. (16), and remembering that $E_c = E_{t,c}+E_p$ (the zero-point energy does not occur in the classical case) we get

$$\begin{aligned}&(\partial\eta/\partial V)_T\\&\quad = -(2/3)\eta(dE_p/dV)/RT-(2/3)\eta p/RT. \quad (17)\end{aligned}$$

We will, in general, apply this with $p=0$.

To apply Eq. (11) we also need the second derivatives. In the final expressions for the second derivatives we set $p=0$.

$$\begin{aligned}(\partial^2\eta/\partial T^2)_V = (4/9)&\eta E_{t,c}^2/R^2T^4\\&-(2/3)\eta C_{v,c}/RT^2\\&+(4/3)\eta E_{t,c}/RT^3, \quad (18)\end{aligned}$$

$$\begin{aligned}d^2\eta/\partial V\partial T = (4/9)&\eta E_{t,c}(dE_p/dV)/R^2T^3\\&-(2/3)\eta(\partial E_{t,c}/\partial V)_T/RT^2, \quad (19)\end{aligned}$$

$$\begin{aligned}(\partial^2\eta/\partial V^2)_T = (4/9)&\eta(dE_p/dV)^2/R^2T^2\\&-(2/3)\eta(d^2E_p/dV^2)/RT\\&-(2/3)\eta(\partial p/\partial V)_{T,c}/RT. \quad (20)\end{aligned}$$

Equation (19) can be somewhat transformed. Using the relation at zero pressure,

$$\begin{aligned}(\partial E_c/\partial V)_T &= (\partial E_{t,c}/\partial V)_T+dE_p/dV\\&= T(\partial S_c/\partial V)_T = T(\partial p/\partial T)_{V,c},\end{aligned}$$

we have

$$\begin{aligned}\partial^2\eta/\partial V\partial T = (4/9)&\eta E_{t,c}(dE_p/dV)/R^2T^3\\&+(2/3)\eta(dE_p/dV)/RT^2\\&-(2/3)\eta(\partial p/\partial T)_{V,c}/RT. \quad (21)\end{aligned}$$

III. APPLICATION TO SOLID NEON

Application of the above results to a Debye solid should yield nothing essentially different from application of the Grüneisen equation,[9]

$$p = \Gamma(E_t+E_s)-dE_p/dV, \quad (22)$$

[8] J. E. Mayer and M. G. Mayer, *Statistical Mechanics* (John Wiley and Sons, Inc., New York, 1940), p. 255.

[9] See O. K. Rice, J. Chem. Phys. **12**, 289 (1944).

where

$$\Gamma = -\Theta^{-1} d\Theta/dV. \quad (23)$$

However, by way of illustration, it will be of some interest to apply Eqs. (7) and (11) to solid neon. In this case, we shall not use Eq. (15) or (17), but will go directly to the relation which follows from Eq. (12),

$$\eta = -(3/40)(\Theta/T)^2 + (3/6720)(\Theta/T)^4. \quad (24)$$

From this we obtain

$$(\partial\eta/\partial V)_T = \Gamma[(6/40)(\Theta/T)^2 - (12/6720)(\Theta/T)^4] \cong -2\Gamma\eta[1-0.0060(\Theta/T)^2]. \quad (25)$$

We may also write

$$(\partial V/\partial p)_{T,c} = -(\partial V/\partial T)_{p,c}/(\partial p/\partial T)_{V,c}. \quad (26)$$

$(\partial p/\partial T)_{V,c}$ is readily obtained by differentiating Eq. (22), taken for the classical case. Since Γ and dE_p/dV are independent of T this gives

$$(\partial p/\partial T)_{V,c} = C_{v,c}\Gamma = 3R\Gamma. \quad (27)$$

$(\partial V/\partial T)_{p,c}$ may be written in the form

$$(\partial V/\partial T)_{p,c} = -\Gamma^{-1}T^{-1}(\partial \ln\Theta/\partial \ln T)_{p,c}. \quad (28)$$

Using Eqs. (25) to (28) in Eq. (7), we obtain

$$\Gamma(V-V_c) = (2/3)(\partial \ln\Theta/\partial \ln T)_{p,c}\eta \times[1-0.0060(\Theta/T)^2]. \quad (29)$$

If we have a series of substances which obey the law of corresponding states, the value of $(\partial \ln\Theta/\partial \ln T)_{p,c}$ will be the same for all of them.[10] In the case of the rare gases xenon may be considered as practically classical at its melting point. The melting points are very near to being corresponding states; hence we may take the value of $(\partial \ln\Theta/\partial \ln T)_p$ given by Murphy and Rice for xenon at its melting point[11] as the $(\partial \ln\Theta/\partial \ln T)_{p,c}$ for neon at its melting point.

If we set Θ_c equal to the value of Θ at V_c, then it is seen that the left-hand side of Eq. (29) will be $-(\Theta-\Theta_c)/\Theta_{Av}$, where Θ_{Av} may be taken as the mean of Θ and Θ_c. Θ at the melting point of Ne (or rather the temperature of the corresponding point, based on the melting point of xenon, which differs by only a few tenths of a degree) may be found by a slight extrapolation in Table V of Murphy and Rice, while Θ_c may be estimated from the results with xenon. We find

$$-(\Theta-\Theta_c)/\Theta_{Av} = -(59.2-65.8)/62.5 = 0.106. \quad (30)$$

Evaluating the right-hand side of Eq. (29), using $\Theta = 59.2$ and $T = 24.9$ to calculate η, we obtain

$$(2/3)(\partial \ln\Theta/\partial \ln T)_{p,c}\eta[1-0.0060(\Theta/T)^2] = 0.667\times 0.385\times 0.410\times 0.965 = 0.101. \quad (31)$$

This is an excellent check, especially since $(\partial V/\partial p)_{T,c}$ will actually vary with volume, but is evaluated at V_c (this is effectively what is done, since the right-hand side of Eq. (28) is evaluated at V_c by the above procedure).

The value of Γ for argon has been taken as 0.18 mole cc^{-1}. For neon it can be calculated by multiplying by the inverse ratio of the critical volumes,[12] according to the law of corresponding states; it therefore is 0.325 mole cc^{-1}. This gives $V-V_c = 0.33$ cc/mole from Eq. (30). The actual volume of solid neon given by Clusius[13] is 13.98 cc/mole. If we multiply the volume of solid krypton[14] at its melting point by the ratio of the critical volumes we get 13.42 cc/mole for V_c. Similarly, from argon[15] we get 13.59 cc/mole for V_c. The calculated value of $V-V_c$ seems to agree about as well as one might expect.

We have also evaluated Eq. (11) for the solid. This requires some further differentiation, including differentiation of Eq. (28), which brings in the quantity $(\partial^2 \ln\Theta/\partial \ln T\partial T)_{p,c}$, which has been estimated as $-0.00405\times(289.8/44.8)$ from Table II, Murphy and Rice (the ratio in parentheses is the ratio of critical temperatures of xenon and neon, taken from Guggenheim). We also have to evaluate $(\partial V/\partial T)_p$ (non-classical) which is done with the aid of Table V of Murphy and Rice. We have obtained for δC_p at the melting point -2.0 cal. mole^{-1} deg.$^{-1}$. Comparison of Tables II and V of Murphy and Rice shows that this is about right.

[10] See G. W. Murphy and O. K. Rice, J. Chem. Phys. **14**, 518 (1946).

[11] We will use the calculations based on Murphy and Rice's "Curve II." These calculations do not fit the experimental data on neon and xenon perfectly, but they are reasonably good and they do exactly fit the law of corresponding states as extended by Murphy and Rice.

[12] E. A. Guggenheim, J. Chem. Phys. **13**, 253 (1945).

[13] K. Clusius, Zeits. f. physik. Chemie **B31**, 459 (1936).

[14] K. Clusius and K. Weigand, Zeits. f. physik. Chemie **B46**, 1 (1940).

[15] O. K. Rice, J. Chem. Phys. **14**, 321 (1946).

IV. APPLICATION TO LIQUID NEON

The checks obtained in Section III merely confirm the consistency of the present calculation with that of Murphy and Rice. The comparison of experimental and calculated $V-V_c$ may have some significance, but again the calculation may be handled equally well by either method. For the case of the liquid, however, only the equations of the present paper are available.

To calculate $V-V_c$, or better $(V-V_c)/V_c$, we clearly need, from Eqs. (7), (17), and (26), values of V_c, dE_p/dV, $(\partial V/\partial T)_{p,c}$, and $(\partial p/\partial T)_{V,c}$. To get δC_p we need also $E_{t,c}$, $C_{v,c}$, $(\partial^2 V/\partial T^2)_{p,c}$, and d^2E_p/dV^2. These quantities are not known for neon; they are known or may be readily calculated for argon from related quantities.[16] Since the quantities appearing in the expressions for $(V-V_c)/V_c$ and δC_p are, except for η, in a combination which is independent of the substance if the law of corresponding states holds, the values for argon should be sufficiently good. The values for the second derivatives show a rather sudden change at a molar volume equal to the molar volume at the normal melting point of argon. However, the volumes we are interested in are equal to or greater than the normal melting volume, so no ambiguity occurs here. The second derivatives can be obtained by differences from the first derivatives; the values are necessarily rough, but they fortunately do not contribute greatly to δC_p. d^2E_p/dV^2 is sufficiently small, and the terms containing it are sufficiently unimportant, so that they can be neglected.

We have yet to consider η for neon. This is to be obtained from Eq. (13). Q_c can be obtained by comparison with argon. We have previously shown that Q_c can be expressed approximately in the form[16]

$$Q_c = Q_0^3 = [(2e)^{1/3}T/\Theta + (2\pi mkT/h^2)^{1/2}2^{-1/6}(\quad - a_0)]^3. \quad (32)$$

On going from one substance to another which obeys the law of corresponding states, the two terms in the bracket transform in the same way. (For the transformation of Θ see Murphy and Rice.[10] To convert Θ from argon to neon we use f_Θ (argon) = 1.530 and f_Θ (neon) = 1.405.) Q_0 has been calculated for argon in connection with the calculations of the article cited, whence Q_0 for neon and η for neon can be obtained as indicated. The various thermodynamic quantities required and η are listed in Table I.

[16] O. K. Rice, J. Chem. Phys. 14, 324 (1946); see especially Tables V and VI.

TABLE I. Thermodynamic quantities for argon; η for argon and neon.

V	28.02 cm³ mole⁻¹
T (fusion)	83.78°K
dE_p/dV	50.5 cal. cm⁻³
$E_t/3RT$	0.7961
$C_v/3R$	0.856
$(\partial V/\partial T)_p$	0.1178 cm³ mole⁻¹ deg.⁻¹
$(\partial p/\partial T)_v$	0.556 cal. cm⁻³ deg.⁻¹
$(\partial^2 V/\partial T^2)_p$	0.00165 cm³ mole⁻¹ deg.⁻²
Q_0 (argon)	3.681
$-\eta$ (argon)	0.01080
$-\eta$ (neon)	0.1030

This table gives the values of the various quantities at the melting temperature and melting volume of argon, or, in the case of η, at the corresponding point for neon. Neon at its melting point (24.55°K), or at its corresponding temperature (24.9°, which is the temperature we have actually used), is slightly expanded beyond its corresponding volume. The errors which will be caused by this discrepancy are not sufficient to make it worth while to perform further calculations. It is easy to find from reference 16 how the various quantities involved change with volume at constant pressure. This should give the order of magnitude of the errors involved, and it is found to be of the order of 10 percent in $(V-V_c)/V_c$ and 15 percent in δC_p. However, these are probably exaggerations since the most affected quantity is η, and it will be affected considerably less at constant temperature than at constant pressure.

Use of Table I enables us to estimate $(V-V_c)/V_c$ as 0.026. Figure 2 of Guggenheim's article[12] enables one to estimate $(V-V_c)/V_c$ by comparing the ratio of density to critical density for neon and other gases. It appears that neon is about 4 to 5 percent expanded over what one might expect from the law of corresponding states. However, just the points near the melting points near the melting point for neon are a little out of line, so 4 percent expansion is probably the better estimate. Pitzer states that liquid neon has a density about 3 percent less than that of the "perfect liquid."[17] So it appears that the theo-

[17] See p. 588 of reference 3.

retical estimate of $(V-V_c)/V_c$ cannot be far out of line.

δC_p is calculated as -1.42 cal. per mole. The specific heat of liquid neon is given[13] as 8.64 near the melting point, that of argon[13] as 10.05 or[18] 10.5, that of krypton[19] as 10.6, and that of xenon[20] as 10.7. The classical values should all be the same by the law of corresponding states. It is, therefore, obvious that there is reasonably good agreement between the calculated and experimental values of δC_p.

V. TWO-PHASE SYSTEMS

We will now consider the effect of the quantum correction on the equilibrium between the solid and the liquid. We shall first consider the change in the temperature of melting at zero pressure. At zero pressure the Gibbs free energy F is equal to the Helmholtz free energy A. We can consequently use Eq. (3), substituting F for A and F_c for A_c. F_c really corresponds to $A_{c,0}$, since we should compare classical and quantum F's at the same pressure. The difference between A_c and $A_{c,0}$ is, as we have shown following Eq. (6), a second-order quantity. It is not entirely negligible for the solid, but is not important and may be neglected for our purposes.

The condition for equilibrium between two phases may be written

$$\Delta F=\Delta F_c-RT\Delta\eta=0. \tag{33}$$

If there were no quantization equilibrium would occur at a temperature T_c with $\Delta F_c=0$, while Eq. (33) holds at a temperature T where $\Delta F_c=0+(\partial\Delta F_c/\partial T)_p(T-T_c)=-\Delta S_c(T-T_c)$. Substituting this into Eq. (33), we obtain

$$T-T_c=-RT\Delta\eta/\Delta S_c. \tag{34}$$

Using the values of η for solid and liquid given in Sections III and IV, and taking for ΔS_c the entropy of melting, 3.35, of argon, we obtain $T-T_c=-4.5°$. The observed value of $T-T_c$ is about $24.55-24.9=-0.35°$. The discrepancy is very large, and quite surprising, in view of the apparently good results obtained with solid and liquid separately.

We can analyze the situation further by considering $\Delta E-\Delta E_c$ and $\Delta S-\Delta S_c$ for the fusion process. Since the melting temperature is so nearly a corresponding temperature with respect to the melting temperature of xenon, say, we can neglect any effect of change in temperature on these quantities. This means that we can calculate $\Delta E-\Delta E_c$ by applying Eq. (10) directly to both solid and liquid at 24.9°K. For the solid we apply the equations of Section III. For the liquid we apply the equations of Section II and the data of Section IV, and convert from argon to neon. We obtain $E-E_c=54.3$ cal. mole^{-1} for solid neon and $E-E_c=18.3$ for liquid neon. Thus,

$$\Delta E-\Delta E_c=-36.0 \text{ cal. mole}^{-1}, \text{ calc.}$$

From the heat of fusion of krypton[19] we get for the corresponding heat of fusion of neon 83.6 cal. mole^{-1}, while the actual heat of fusion is about 80.1 cal. mole^{-1}. Thus,

$$\Delta E-\Delta E_c=-3.5 \text{ cal. mole}^{-1}, \text{ obs.}$$

A similar discrepancy occurs for the entropy. We can write

$$\begin{aligned}\Delta S-\Delta S_c&=(\Delta E-\Delta E_c-\Delta A+\Delta A_c)/T\\&=(\Delta E-\Delta E_c)/T+R\Delta\eta\\&=-1.45+0.61=-0.84 \text{ cal. mole}^{-1}\text{ deg.}^{-1}.\end{aligned}$$

The actual value of $\Delta S-\Delta S_c$ is around -0.1 cal. mole^{-1} deg.$^{-1}$.

The results with $\Delta E-\Delta E_c$ and $\Delta S-\Delta S_c$ appear to indicate that the quantum correction for the liquid is nearly as great as for the solid. This would seem very strange in itself, but it is still more puzzling in the light of the results of Section IV. The calculation for δC_p may indeed indicate that Eq. (13) gives something of an underestimate of η; if it were increased by perhaps 40 percent a better value of C_p would result. On the other hand, it must also be noted that the derivatives of η in Eq. (11) involve the quantity dE_p/dV, which is somewhat indirectly calculated from the data. It does not appear likely, however, that this can cause appreciable error. We have[21]

$$dE_p/dV=(\partial E/\partial V)_T-(\partial E_i/\partial V)_T.$$

$(\partial E_i/\partial V)_T$ is certainly negative; therefore dE_p/dV

[13] A. Eucken and H. Hauck, Zeits. f. physik. Chemie **134**, 161 (1928).
[19] K. Clusius, A. Kruis, and F. Konnertz, Ann. d. Physik **33**, 642 (1938).
[20] K. Clusius and L. Riccoboni, Zeits. f. physik. Chemie **B38**, 81 (1937).
[21] Zero-point energy is not included because argon is essentially classical.

should be slightly larger than $(\partial E/\partial V)_T$ which at zero pressure is equal to $T(\partial p/\partial T)_V$. Now the value of dE_p/dV used is only slightly larger than $T(\partial p/\partial T)_V$; it seems likely that dE_p/dV should be increased rather than decreased, and this would actually increase $|\delta C_p|$, so that $|\eta|$ would have to be increased less. The use of values at the normal melting temperatures and volumes gives a slight overestimate for $|\delta C_p|$, which might mean that $|\eta|$ should be increased by a little more than 40 percent, but this effect is not very great.

Another quantity which occurs in the derivatives of η which is not entirely directly determined experimentally is $E_{t,c}$. We have also used the calculated rather than the experimentally determined value of $C_{v,c}$. However, it does not appear that any possible change in these quantities could clear up the discrepancy.

On the other hand, it appears likely that the discrepancy is too great to be accounted for on the basis of deviations from the law of corresponding states.

We are, therefore, forced to leave the question of the quantum correction for neon in a somewhat unsatisfactory state.

THE JOURNAL OF CHEMICAL PHYSICS VOLUME 16, NUMBER 2 FEBRUARY, 1948

The Raman Spectrum and Structure of Nickel Carbonyl*

BRYCE L. CRAWFORD, JR. AND WILLIAM HORWITZ**
School of Chemistry, University of Minnesota, Minneapolis, Minnesota

(Received November 5, 1947)

A redetermination of the depolarization factors of the Raman lines of nickel carbonyl shows the presence of only two polarized lines instead of three, as previously reported by other investigators. The data obtained not only eliminate the only evidence against the tetrahedral structure for this molecule but supply additional evidence in its favor.

ALTHOUGH the molecular structure of nickel carbonyl has been investigated several times, no clear-cut decision as to its configuration has been arrived at. The present status of the problem is well summarized by Herzberg,[1] who lists the structure of this molecule as tetrahedral, but adds in a footnote, "It must be mentioned that there is a serious discrepancy between this structure and the observed Raman spectrum in that the three strongest Raman lines are polarized whereas on the tetrahedral model there are only two totally symmetrical vibrations."

Raman spectra of nickel carbonyl were obtained by Dadieu and Schneider[2] and by Anderson,[3] but the only conclusion that could be reached from the evidence of these investigations was that the intact carbon monoxide group was present in nickel carbonyl rather than the organic carbonyl group. A more complete investigation of the Raman spectrum was performed by Duncan and Murray.[4] The data were interpreted on the basis of a planar square structure, a structure which these authors incorrectly ascribed to Pauling.[5] On the basis of the directed theory of valence, Pauling predicted that the complexes of *bivalent* nickel should have a planar configuration, but on the basis of the same theory complexes of *neutral* nickel should have a tetrahedral structure. Not only was the theoretical basis for the planar structure as used by Duncan and Murray incorrect, but, as Wilson[6] pointed out shortly afterwards, the assignment was invalid since they had

* A portion of the thesis submitted by William Horwitz in partial fulfillment of the requirements for the degree of Doctor of Philosophy at the University of Minnesota, August 1947.

** Present address: U. S. Food and Drug Administration, Minneapolis 1, Minnesota.

[1] G. Herzberg, *Infrared and Raman Spectra of Polyatomic Molecules* (D. Van Nostrand Company, Inc., New York, 1945), p. 356.

[2] A. Dadieu and F. A. Schneider, Akad. Wiss. Wein **68**, 191 (1931).

[3] J. S. Anderson, Nature **130**, 1002 (1932).

[4] A. B. F. Duncan and J. W. Murray, J. Chem. Phys. **2**, 636 (1934).

[5] L. Pauling, J. Am. Chem. Soc. **53**, 1367 (1931).

[6] E. B. Wilson, Jr., J. Chem. Phys. **3**, 59 (1935).

TABLE I. The Raman data of nickel carbonyl.*

Frequency cm^{-1}	Relative intensity	Depolarization factor	Assignment**
79±1 (10)	100	0.86±0.07 (18)	ω_3 ω_5
381±4 (8)	25	~0.01 (17)	ω_1
461±3 (4)	10	0.83±0.11 (5)	ω_4
598 (2)	3	<0.4 (1)	$2\omega_6$
2039±5 (9)	47	0.73±0.06 (18)	ω_2 ω_8
2121±7 (4)	3	<0.4 (1)	$\omega_8+\omega_5$

* Number of observations in parentheses.
** From Crawford and Cross (see reference 8). The assignment of 2121 cm^{-1} has been changed from $\omega_2+\omega_5$.

violated the selection rules for the Raman effect. Their conclusion that nickel carbonyl was planar was, therefore, also invalid. Actually their experimental data do not agree with either the tetrahedral or the square model, since either of these structures should have only two polarized Raman lines while Duncan and Murray reported the presence of three.

Brockway and Cross,[7] using electron-diffraction methods, found evidence clearly favoring a tetrahedral structure, but a surprisingly small value was found for the nickel-to-carbon distance which may tend to alter the tetrahedral structure. Crawford and Cross[8] performed an infra-red absorption study and a quantitative vibrational analysis on this molecule and found that a reasonable assignment of frequencies could not be made on the basis of the square model; a satisfactory assignment could be obtained for the tetrahedral model only if the Raman polarization data of Duncan and Murray were in error. The purpose of this investigation was to re-examine the state of polarization of the Raman lines of nickel carbonyl to determine whether Crawford and Cross were justified in rejecting the polarization data of Duncan and Murray which represent the only evidence against the tetrahedral structure for nickel carbonyl.

APPARATUS AND MATERIALS

Nickel carbonyl[9] of commercial grade was purified by several vacuum distillations. The Raman spectra and depolarization factors were obtained with the apparatus described in a previous publication.[10]

Wave-length measurements were obtained by comparison with a bracketing iron reference spectrum. Ordinary nails were used for the arc in order to supplement the iron spectrum with manganese lines in the 2000-cm^{-1} region. Measurements were made with a Bausch and Lomb spectrum measuring microscope or with a Leeds and Northrup recording microphotometer. The wave numbers (vacuum) were obtained by a linear interpolation over a limited region or by the use of the Hartmann formula over the entire spectrum. The frequencies and standard deviations are listed in Table I. The relatively low precision of these observations is the result of the use of a large number of different methods of measuring and calculating the spectra in an attempt to determine the most accurate and convenient method of frequency determinations.

The exposure time required to obtain a density of one unit for the strongest line (79 cm^{-1}) of nickel carbonyl was 2.1 minutes as compared with 30 minutes for the 459-cm^{-1} line of carbon tetrachloride and 13 minutes for the 992-cm^{-1} line of benzene. This line is one of the most intense Raman lines which has been reported, but despite this fortunate circumstance the depolarization factor is difficult to measure because it lies on the "wing" of the exciting line as shown in the microphotometer tracing of Fig. 1. When the "minimum adjacent background" method for correcting for background which was developed for the lines of carbon tetrachloride[10] was applied to this line, the impossible values for ρ of greater than 1 were obtained. The background for this line was obtained by extrapolating the estimated contour of the exciting line and taking the intersection of this curve with the position of the peak as the background density. The "minimum adjacent background" was used for the correction with the 381-cm^{-1} and 461-cm^{-1} lines while no background correction was required for the 2039-cm^{-1} line.

[7] L. O. Brockway and P. C. Cross, J. Chem. Phys. 3, 828 (1935).
[8] B. L. Crawford, Jr. and P. C. Cross, J. Chem. Phys. 6, 525 (1938).
[9] We are indebted to Mr. O. B. J. Fraser of the International Nickel Company, Inc. for this material.
[10] B. L. Crawford, Jr. and W. Horwitz, J. Chem. Phys. 15, 268 (1947).

RESULTS

The only Raman polarization data on this compound available hitherto are the qualitative results of Duncan and Murray,[4] who report the following: the 463-cm^{-1} line, depolarized; the 382-cm^{-1} line, polarized; the 82- and 2043-cm^{-1} lines, partly polarized. The quantitative depolarization factors, as determined in this investigation, are presented in Table I together with the standard deviations and the number of observations. There is no question that the 381-cm^{-1} line is highly polarized. On 16 of 17 observations there was no trace of a parallel component; on only one tracing was there any suggestion of a parallel component, and this was only a slight jog in the tracing, of the same magnitude as several other jogs of no significance (i.e., arising from grain fluctuations, spots, dust, etc.). Even if this parallel component is considered significant, the estimated degree of depolarization of this line is about 0.01, or as close to zero as it is possible to demonstrate experimentally.

These data also show that the 79-cm^{-1} line is depolarized. The fact that this line actually lies on the "wing" of the Rayleigh line with substantially different background densities on its two sides may have led Duncan and Murray[4] to the conclusion that it was partially polarized. Even under high microphotometer magnification we have been unable to confirm Duncan and Murray's classification of this line as unsymmetrical. An unsuccessful attempt was made to resolve this line into the two lines postulated by Crawford and Cross,[8] using the long focal length camera of the Steinheil spectrograph which is capable of resolving doublets with a spacing of 10 cm^{-1}.

The 461-cm^{-1} and the 2039-cm^{-1} lines were found to be depolarized and partially polarized, respectively, as reported by Duncan and Murray.[4] The latter is unsymmetrical. It too is a postulated doublet which could not be resolved with the long focal length camera.

A single measurement of the degree of depolarization of the weak lines at 598 cm^{-1} and 2121 cm^{-1} showed them to be at least partially polarized. No attempt was made to study the still weaker lines reported by Duncan and Murray,[4] since the continuous background was approaching substantial levels with the exposure time required.

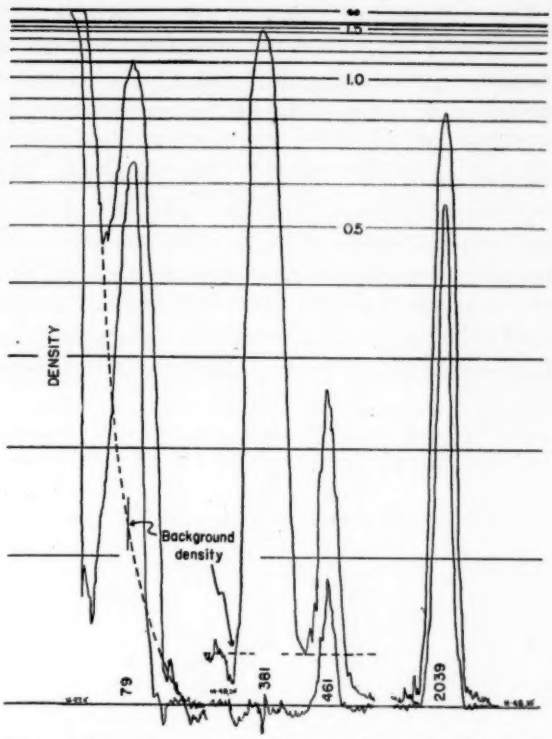

FIG. 1. Microphotometer tracing of the polarized Raman spectrum of nickel carbonyl (upper—perpendicular; lower—parallel). The Raman lines are from different plates.

The relative intensities found in this study, as shown in Table I, are in good agreement with those reported by Duncan and Murray.[4]

DISCUSSION

The present investigation reveals the presence of only two strong polarized lines, which agrees with the selection rules for either the tetrahedral or the square configuration for nickel carbonyl. The partially polarized line reported by Duncan and Murray at 82 cm^{-1} is actually depolarized. As pointed out by Crawford and Cross,[8] a polarized line in this region is unaccountable by either model. The fact that the 381-cm^{-1} line is completely polarized is in itself very strong evidence in favor of the tetrahedral structure since complete polarization is expected theoretically only for molecules of the cubic point groups. For all non-cubic point groups, which includes the planar square, the degree of depolarization of the totally symmetric Raman lines is intermediate between 0 and 6/7.

The vibrational analysis of Crawford and Cross[10] which rejected the polarization data of Duncan and Murray for the 82-cm^{-1} line, is shown, on the basis of the data presented here, to be completely justified. As a result of polarization measurements on the two weak overtone and combination lines at 598 cm^{-1} and 2121 cm^{-1} it has been necessary to change the assignment of the latter from $\omega_2+\omega_5$ to $\omega_8+\omega_5$ in order to allow for a polarized combination. The original assignment of 598 cm^{-1} as $2\omega_6$ remains unchanged, since this overtone may have a polarized component.

The tetrahedral structure for nickel carbonyl may be considered as established on the basis of the following evidence:

1. The theory of directed valence predicts a tetrahedral structure for quadricovalent neutral nickel complexes.
2. The electron-diffraction study of Brockway and Cross[7] clearly favors the tetrahedral structure.
3. As shown by Crawford and Cross,[8] a satisfactory vibrational analysis of the molecule can only be made on the basis of the tetrahedral model.
4. The present investigation supplies the Raman polarization data which indicate a tetrahedral structure and which justify the previous vibrational analysis.

Letters to the Editor

THIS section will accept reports of new work, provided these are terse and contain few figures, and especially few halftone cuts. The Editorial Board will not hold itself responsible for opinions expressed by the correspondents. Contributions to this section should not exceed 600 words in length and must reach the office of the Managing Editor not later than the 15th of the month preceding that of the issue in which the letter is to appear. No proof will be sent to the authors. The usual publication charge ($4.00 per page) will not be made and no reprints will be furnished free.

Origin of the Potential Barrier Hindering Rotation in Ethane and Related Substances

EDWIN N. LASSETTRE AND LAURENCE B. DEAN, JR.
Department of Chemistry, The Ohio State University, Columbus, Ohio
December 9, 1947

ATTEMPTS have been made by Aston, Isserow, Szasz, and Kennedy[1] to systematize the calculation of potential barriers hindering rotation around single bonds by assuming a repulsion between hydrogens which was found empirically to vary inversely as the fifth power of the distance. Since the energy of interaction of two quadrupoles varies inversely as the fifth power of the distance[2] these results have suggested to us that the barriers arise, not from the repulsion of hydrogen atoms, but from the electrostatic interaction of the charges of *one bond* with the charges of *another bond*. We have investigated the potential barrier for ethane on the basis of this model with results which are in rather satisfactory agreement with experiment and which suggest that the ideas are of general applicability. The results are briefly described below.

In considering the magnitude of interaction between bonds the following specific hypotheses are employed. (i) A single-bond charge distribution consists of a unit positive charge at each nucleus and a pair of electrons. (ii) The electron distribution of a single bond is cylindrically symmetric with respect to the internuclear axis. (iii) The charge distributions of two bonds, which have no atom in common, do not significantly overlap and, hence, exchange interactions are negligible. (iv) The electrostatic potential due to a single-bond charge distribution is sufficiently well characterized by its dipole and quadrupole moments, calculated relative to an origin midway between the nuclei. These hypotheses are in qualitative accord with the accepted ideas concerning the distribution of molecular electrons. If, however, this theory is to account satisfactorily for potential barriers, it is essential that the bond quadrupole moments have reasonable magnitudes.

In the first calculations, an approximate quadrupole moment for the negative charge of the C−H bond was calculated by assuming that the electron pair forming the bond is distributed in a localized molecular orbital which is a linear combination of atomic orbitals for carbon and hydrogen. The molecular orbital used is

$$\sigma = aN_1\tau_1 \exp -(1.62r_1)(\tfrac{1}{2}+\tfrac{3}{2}\cos\theta)+bN_2 \exp(-r_2),$$

where r_1 and r_2 are the distances, in atomic units, of an electron from the carbon and hydrogen nuclei, respectively, and θ is the angle between r_1 and the line of centers. N_1 and N_2 are normalizing constants. The factor $(\frac{1}{2}+\frac{3}{2}\cos\theta)$ is Pauling's tetrahedral orbital,[3] and the radial factor is obtained from Slater's functions and screening constants.[4] The constants a and b can be determined from the normalizing condition and the bond dipole moment (0.4 Debye). Since, however, the sign of the dipole moment is uncertain, we have preferred to vary a/b over a considerable range which includes both signs for the dipole moment. This procedure also indicates how sensitive the calculated barrier is to alterations in bond ionic character since a/b can be considered a measure of ionic character. The results are given in Table I. In Table I the second column contains

TABLE I.

a/b	$\mu\times10^{+18}$ e.s.u.	P atomic units	D-D kcal.	D-Q kcal.	Q-Q kcal.	Barrier V (stag.) kcal.	V (stag.) kcal.
1.0	−2.30	3.16	1.58	−3.33	5.63	3.88	147.1
1.5	−1.51	3.22	0.68	−2.22	5.84	4.30	96.4
2.0	−0.98	3.22	0.29	−1.45	5.84	4.68	70.3
4.0	0.03	3.13	0.00	0.05	5.52	5.57	38.3
5.75	0.40	3.07	0.05	0.56	5.30	5.91	33.1

the calculated bond dipole moment and the third column the bond quadrupole moment. The "quadrupole moment," P, is defined for a cylindrically symmetric distribution of charge density ρ by the formula

$$P=\int(r^2-3x^2)\rho d\tau,$$

where x is the coordinate perpendicular to the axis of symmetry. This is the only parameter required to characterize the quadrupole field of such a distribution. The interaction energy of the three C−H bonds of one methyl group with the three of the other methyl group was calculated for both the staggered (D_{3d}) and the eclipsed (D_{3h}) configurations. The difference between these is given in column seven and the separate dipole-dipole, dipole-quadrupole, and quadrupole-quadrupole energies are also given in columns four, five, and six, respectively. The interactions between C−C and C−H bonds need not be calculated since they remain unchanged as a methyl group is rotated around its symmetry axis.

The results may be briefly summarized as follows:

1. The staggered configuration has lower energy for every value of a/b.

2. The calculated potential barrier is larger than that observed (2750 cal.[5]), but is of the proper order of magnitude.

3. For those values of a/b which give the correct magnitude to the bond dipole moment (0.4D) the quadrupole-quadrupole interaction predominates, and hence an inverse fifth-power dependence on distance between bonds is confirmed.

4. The barrier is not very sensitive to bond ionic character.

5. In performing the calculations it was observed that,

although certain quadrupoles attract and others repel, the net interaction of methyl groups in ethane is one of repulsion both for the staggered and the eclipsed configurations.

6. The calculated potential barriers are small, being the difference between interactions in two configurations, but the total interaction energy is large. (See column eight.)

Since a considerable weight of indirect evidence now exists in favor of the staggered configuration for ethane,[3,6] the above are seen to be in as good agreement with experiment as could be expected in view of the rough approximation to the negative charge distribution which has been employed. Accurate agreement between the calculated and the experimental barrier (2750 cal.) is obtained with quadrupole moment 2.03 (atomic units) if $\mu=0.4$D and 2.35 if $\mu=-0.4$D. The calculated interaction energies are given in Table II. It is interesting to note that both of these quadrupole moments are considerably smaller than those of Table I. This implies that the actual bonding distributions overlap even less than is indicated by the rough molecular orbital used here, hence is consistent with our initial hypothesis. It seems, therefore, that the potential barrier for ethane can be accounted for by means of a quadrupole moment of reasonable magnitude, and the staggered configuration is favored. Thus far the mutual polarization of bonding distributions has been ignored. It is obvious that such polarization occurs but it is difficult to see how such interactions can stabilize the staggered configuration.

It is of interest that quadrupole moments obtained from observed potential barriers (which depend only on energy differences) may be used to calculate the force exerted by one bond on another which contains no common atom. The large energy of interaction of methyl groups in ethane (see Table II, column 7) indicates that such forces are appreciable. In this way a more quantitative treatment of the dependence of interatomic distances, hydrogenation energies, dissociation energies, etc., on bond environment, along the lines proposed by Conn, Kistiakowsky, and Smith,[6] becomes possible.

Although we have found the same dependence on *distance* for interacting bonds of small dipole moment as did Aston and collaborators, the present model also provides for dependence on the quadrupole moments of two interacting bonds as well as their orientation relative to each other and to the line joining them. Moreover, in a complex substance, such as tetramethyl methane, substantial interactions between C−H and C−C bonds are expected, and hence the similar dependence on distance may be fortuitous.

The conception of interaction of bonding distributions as constituting the source of potential barriers is essentially similar to that proposed by Kistiakowsky, Lacher, and Ransom[7] several years ago. In certain respects the present treatment may be considered as a quantitative extension of their ideas.

TABLE II.

$\mu\times10^{+18}$ e.s.u.	P atomic units	D-D kcal.	D-Q kcal.	Q-Q kcal.	Barrier kcal.	V (stag.) kcal.
0.40	2.03	0.05	0.37	2.33	2.75	14.2
−0.40	2.35	0.05	−0.43	3.13	2.75	29.0

A further investigation of the electrostatic interaction of bonding distributions is in progress along two lines: (a) A more accurate calculation of the electrostatic potential than is provided by dipole and quadrupole terms, (b) the empirical calculation of quadrupole moments from the observed potential barriers of compounds other than ethane, and the use of such moments in the prediction of other properties in order to check the accuracy of these values. The calculations will be fully reported when this investigation is complete.

[1] J. G. Aston, S. Isserow, G. J. Szasz, and R. M. Kennedy, J. Chem. Phys. **12**, 336 (1944).
[2] H. Marganau, Rev. Mod. Phys. **11**, 1 (1939).
[3] L. Pauling, *Nature of the Chemical Bond* (Cornell University Press, Ithaca, New York, 1940), p. 86.
[4] J. C. Slater, Phys. Rev. **36**, 57 (1930).
[5] G. B. Kistiakowsky, J. R. Lacher, and F. Stitt, J. Chem. Phys. **7**, 289 (1939). See also J. D. Kemp and K. S. Pitzer, J. Chem. Phys. **4**, 749 (1936).
[6] J. B. Conn, G. B. Kistiakowsky, and E. A. Smith, J. Am. Chem. Soc. **61**, 1868 (1939).
[7] G. B. Kistiakowsky, J. R. Lacher, and W. W. Ransom, J. Chem. Phys. **6**, 900 (1938).

Physical Basis of a Concept about the Mechanism of Viscosity of Liquids

R. PARSHAD
Research Laboratory of Electronics, Massachusetts Institute of Technology, Cambridge, Massachusetts
December 15, 1947

A THEORY of viscosity of liquids should explain the following: (1) decrease of viscosity with temperature; (2a) increase of viscosity with pressure; (2b) the rate of increase of viscosity increasing with increase of pressure; (3) increased viscosity of associated liquids over that of normal liquids.

The current theories of viscosity generally relate cohesion with viscosity. Cohesion may be taken as a measure of total attraction energy of molecules and is indicated in magnitude by latent heat of vaporization or inverse function of compressibility. While the relation between cohesion and viscosity is generally true, there are significant departures from this correspondence. These originate in the difference between the mechanisms of viscosity and cohesion. Viscosity arises because of the resistance to the displacement of a molecule at right angles to the intermolecular line (taking an ideal case of two molecules), and is, in general, due to the resistance offered to change of configuration of the molecules, or the resistance against changing of places of individual molecules in the same configuration, while the intermolecular distances remain unchanged. Cohesion arises due to resistance offered to a direct change of intermolecular distances, the configurations remaining the same. These differences have been discussed more fully elsewhere.[1]

We assume that viscosity, or the resistance offered to change of position of molecules, is due to the existence of potential barriers around the molecules in the liquid. The steeper these potential barriers, the more the viscosity will be. This is why liquids of anisotropic molecules have, in general, higher viscosity than liquids of more symmetrical molecules. Now we postulate that these potential

barriers are caused by the interaction of the two opposing intermolecular forces of attraction and repulsion acting individually. For high viscosity not only high attracting forces are needed but also high repulsive forces. By the interaction of these two opposite forces the molecules tend to get fixed up in space so to speak; this fact means high viscosity. The departure from complete correspondence between cohesion and viscosity arises because cohesion is a measure of difference of attractive and repulsive energies while viscosity depends individually upon both. Our concept at once explains the following pertinent facts.

(1) *Increase of viscosity with pressure.* With decrease of volume under pressure, both the attractive and repulsive forces increase, leading to an increase of viscosity. Moreover, as these forces are inverse functions of distance, their rate of increase will increase with the decrease of the intermolecular distance. Further, since the repulsive forces are of much shorter range they will, after a stage, increase much faster than the attractive forces. This leads to a rate of increase of viscosity which increases fast with pressure. On the other hand, the rate of fall of compressibility with pressure will be rapid in the beginning and slower afterwards as it is related to the difference of attractive and repulsive energies, which increases in the beginning but decreases at still higher pressures.

(2) *Viscosity and association.* It has been shown[2] that molecules of associated liquids do not only have great attractive forces but also have significant repulsive forces. This may be physically explained as being caused by the hydrogen bonds, in which the distance between two oxygen atoms of interacting molecules (O—H——O) decreases so much as to produce repulsive forces as well. This tendency is further increased due to the semipermanent nature of the hydrogen bond links, so that, due to the hindered relation of the molecules concerned, the intermolecular forces become more of a first order than second order.

(3) *Behavior of water.* Remembering that compressibility decreases with breaking of associations,[3] and that the associations break under pressure and with increase of temperature, the odd behavior of water in its change of viscosity and compressibility with pressure and temperature will be explained.

(4) *Decrease of viscosity with temperature.* This is the easiest thing to explain and also follows from the current theories. With the increase of temperature at constant volume, both the attractive and repulsive energies will increase because of the smoothing out of intermolecular distribution functions. Even if that is not so or if the effect is negligible, the increase of kT will increase the probability of jump of the potential barriers, leading to decreased viscosity.

At constant pressure, the intermolecular distances increase, leading to a more rapid decrease of both kinds of forces and so leading to a faster decrease of viscosity.

Further details of the theory and its quantitative aspects will be taken up in a later paper.

[1] For example, Andrade's Theory, Phil. Mag. **17**, 494, 698 (1934); Eyring's Theory, Glasstone, Laidler, and Eyring, *Theory of Rate Processes* (McGraw-Hill Book Company, Inc., New York, 1941).
[2] Parshad, Doctorate Thesis, Punjab University, India, 1946.
[3] Parshad, Ind. J. Phys. **19**, 47 (1945).

Small-Angle X-Ray Scattering from Metal Deposits Made by Evaporation

BENJAMIN CARROLL
The Newark Colleges, Rutgers University, Newark, New Jersey
AND
I. FANKUCHEN
The Polytechnic Institute of Brooklyn, Brooklyn, New York
December 2, 1947

THE formation of dull or black films during the evaporation of a metal has been the subject of considerable conjecture. Numerous diffraction studies of "evaporated" metal films have been reported,[1,2,3] but the small-angle scattering properties of these deposits have been overlooked. We have examined aluminum and copper deposits produced at 10^{-2} and 10^{-4} mm by means of Debye-Scherrer and small-angle diagrams, and have found that the black deposits exhibited marked small-angle scattering of x-rays (Fig. 1) and bright deposits did not; however, the Debye-Scherrer diagrams were substantially alike regardless of the wide variations in the reflectivity of the metal surface toward white light.

Aluminum was evaporated from a tungsten wire and deposited on glass surfaces at various distances from the source. In the case of copper, a tantalum heater was used permitting the evaporation of relatively large quantities of metal.[4] To minimize the possibility of compound forma-

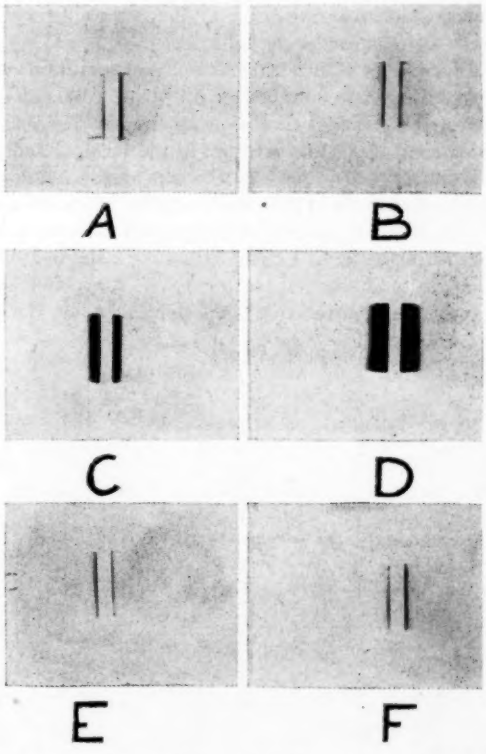

FIG. 1. Small-angle x-ray scattering of bright and dark metallic deposits. A. Bright aluminum foil made at 10^{-4} mm. B. Bright copper foil made at 10^{-4} mm. C. Aluminum black made at 10^{-2} mm. D. Copper black made at 10^{-2} mm. E. Bright aluminum foil made at 10^{-2} mm (when condensation is close to source). F. Bright copper foil made at 10^{-2} mm (when condensation is close to source).

tion for the metal deposits formed at 10^{-2} mm, the pressure in the evaporation chamber was regulated by allowing helium to leak into the system. The deposits were scrapped from the glass base and examined with filtered copper radiation. The distance between sample and photographic plate was 50 cm for the small-angle work and the method used to evaluate particle size was the same as described by Jellinek and Fankuchen.[5] The identical specimens were then used in the Debye-Scherrer camera for the purpose of observing line-broadening effects.

The Debye-Scherrer patterns of all samples showed no particular orientation effects and aside from general darkening of the background of the photograms for the black deposits, line broadening, due to small particle size was not apparent (see Fig. 2). The average particle size for aluminum and copper black as calculated from the small-angle scattering was 110A and 90A, respectively; the bright deposits formed close to the heater during the same evaporation experiment (pressure 10^{-2} mm) gave negligible scattering at small angles, indicating that the crystals were about 10^{-5} cm.

Jellinek and Fankuchen[5] showed that for fairly homogeneous specimens of γ-alumina, crystallite sizes calculated from small-angle scattering and line-breath measurements of Debye-Scherrer patterns were in good agreement. If gross inhomogenities exist in a specimen as in the case of the aluminum and copper black, small-angle scattering will indicate the presence of the fine particles or crystallites only, whereas the Debye-Scherrer diagrams will reveal the existence of the coarser crystallites.

The formation of black deposits by evaporation can be considered a general method of preparing colloidal metal particles, the colloidal condition apparently being caused by the arrival of clusters of atoms at the surface. Reorganization and crystal growth of the film depends upon the surface mobility of the condensed atoms. Since the activation energy for migration over the surface of a solid is greater for an atom in a cluster than for a single atom, on the surface of the sub-phase, we have an explanation for the invariable occurrence of black deposits when the mean free path inside the vacuum chamber was much smaller than the distance between the source and the condensing surface. The formation of bright deposits and relatively coarse crystallites close to the source when the pressure was 10^{-2} mm were probably not only due to the comparability of the mean free path and the distance from the source to the condensing surface, but also to the somewhat higher temperature that prevailed near the source.

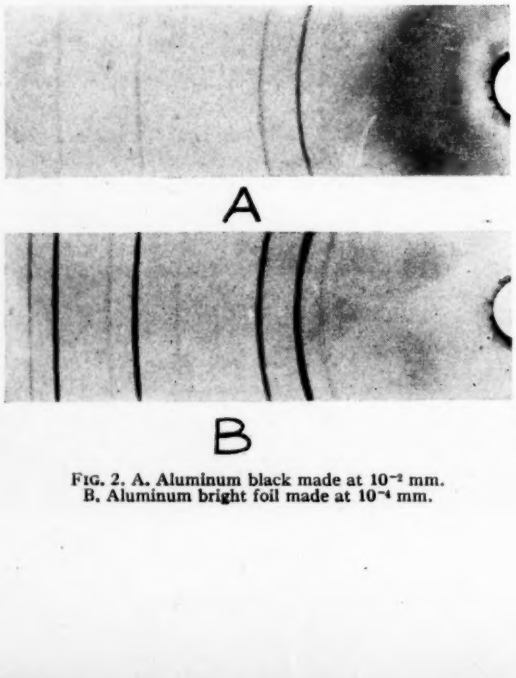

FIG. 2. A. Aluminum black made at 10^{-2} mm. B. Aluminum bright foil made at 10^{-4} mm.

[1] Andrade, Trans. Faraday Soc. **31**, 1157 (1935).
[2] Barrett, *Structure of Metals* (McGraw-Hill Book Company, Inc., New York, 1943), p. 440.
[3] Milligan and Focke, J. Phys. Chem. **45**, 107 (1941).
[4] W. C. Caldwell, J. App. Phys. **12**, 779 (1941).
[5] Jellinek and Fankuchen, Ind. Eng. Chem. **37**, 158 (1945); also see Jellinek, Solomon, and Fankuchen, *ibid.*, **18**, 172 (1946).

A New Concept about the Mechanism of Passivity of Iron in Nitric Acid

R. PARSHAD* AND L. C. VERMAN**
Physical Laboratory, Council of Scientific and Industrial Research, Delhi, India
December 19, 1947

MANY theories[1] have been advanced from time to time to explain the passivity of iron in concentrated nitric acid. In the following we offer a new concept.

In 1944 electrochemical evidence was obtained[2] showing the existence of a hydrogen or hydride film on aluminum, spaced between the well-known oxide film and the metal itself. In our view, the tenacity and strength of the oxide film is due to this hydrogen film.

We were led to believe that the passivity of iron in concentrated nitric acid might also be due to this intermediate hydrogen film, with the difference that, whereas in the case of aluminum the film could be produced in the atmosphere, on iron it would come from the acid itself, possibly as a result of an initial metal-acid interaction. This hydrogen film adsorbed on iron would, in our view, attract an oxygen or oxygen-rich film (helped in this process by the attraction of iron itself for oxygen), and the latter oxygen-rich film would stop further oxidation.

Experimentally, when a piece of iron is inserted in nitric acid, a potential due to this hydrogen film should be expected before the known noble potential due to the oxygen-rich film is recorded. A platinum electrode was dipped in concentrated nitric acid and some time later an iron electrode was at once inserted in the acid. The potentials produced right from the making of the cell were amplified by a d.c. amplifier and measured on a cathode-ray oscillograph. In acid of concentration 68.8 percent by weight at 32.6°C, the potential of the cell rose to 1.25 volts almost instantaneously, and then in 0.05 second fell to a steady potential of about 0.2 volt. During its decrease, the potential passed through a "plateau" where its rate of fall was the lowest. As concentration of acid decreased, the initial rise of potential occurred in two steps: first an almost instantaneous rise as before and then a continued slower rise through about 0.1 volt. The rate of fall of potential after it had reached the maximum also decreased. For example, in acid 45.6 percent by weight, at 32.6°C, the time taken to reach the steady low potential was one second.

We have reasons to believe that the initial potential is

due to the formation of the hydrogen film on iron and the continued rise of potential at lower concentrations indicates the continued but slower formation of the film.

The following observation is a significant support to our theory. An iron electrode, which had been kept unused for some years, took about 10 seconds of chemical action before gaining passivity in acid, 41.4 percent by weight, while the same iron, with its surface renewed by having it abraded with emery-cloth, took about 25 seconds. According to previous theories of passivity, this fact is due to the formation of a thin invisible film of iron oxide or of adsorbed oxygen on the old surface of iron. The potential measurement of the cell showed, however, a higher potential when the electrode of old iron surface was used than that obtained for the use of the fresh surface. In the older theories, the relative magnitudes of the potentials should have been in the opposite order. In our view, the greater potential of the cell for the older surface of iron was due to its adsorption of some hydrogen film from the atmosphere, which helped the iron to gain passivity in the dilute acid.

Many other phenomena associated with passivity are easily explained by the proposed mechanism. For example, the corroding action of halides is due to the affinity of the halogens for hydrogen, resulting in destruction of the film and so of passivity.

Details of the experimental data and application of the concept to behavior of stainless steels will be published elsewhere.

* Now at Research Laboratory of Electronics, Massachusetts Institute of Technology, Cambridge, Massachusetts.
** Now at Indian Standards Institution, New Delhi, India.

[1] For a review see Evans, *Metallic Corrosion, Passivity, and Protection* (Edward Arnold and Company, London, 1946); Uhlig and Wulff, Am. Inst. Min. and Met. Eng. **135**, 494 (1939).
[2] R. Parshad, Nature **154**, 178 (1944).

The Infra-Red Emission and Absorption of the Carbon Monoxide-Oxygen Flame*

S. SILVERMAN, G. A. HORNBECK, AND R. C. HERMAN
Applied Physics Laboratory, The Johns Hopkins University, Silver Spring, Maryland
December 5, 1947

RECENTLY developed combustion engines, such as rockets and jet-engines of various types, have led to a renewed interest in the infra-red emission of flames, explosions, and combustion reactions in general. Numerous investigators, beginning with Julius and Paschen in the 1890's have studied the infra-red emission of different flames and hot gases.[1] The mission bands corresponding to the well-known absorption bands of the H_2O and CO_2 molecules were observed in the Bunsen flame in the region from about 1 to 12μ. Until recently[2] the only observation of radiation in the longer wave-length region, from about 10 to 20μ, was made by Rubens and Aschkinass[3] in 1898, who found emission throughout that region from both the Bunsen flame and hot CO_2. Subsequently, investigators of the CO-oxygen flame[4] reported the strong emission bands of CO_2 at 2.8 and 4.4μ but failed to observe the fundamental at 14.95μ.

The CO-oxygen flame has been studied to determine, if possible, the vibrational excitation of the CO_2 molecules formed in this reaction. The flame employed in these investigations was obtained by burning a mixture of CO and O_2 in an ordinary torch. The CO was commercial grade and contained as its chief impurities about 1.5 percent each of H_2 and N_2, but no H_2O emission was observed in the infra-red. The iron carbonyl was removed from the CO in the usual manner. The instrument used was a Perkin-Elmer infra-red spectrometer with NaCl or KBr optics. It was flushed continuously with dry N_2 to minimize atmospheric absorption. The receiver was a bolometer using chopped radiation at 10 cycles/sec. with tuned amplification for drift-free recording purposes.

The emission spectrum of the CO-oxygen flame shows in addition to the peaks previously observed a number of rather weak emission bands between about 10 and 20μ. The two strongest bands lie at 667 and 721 cm^{-1}, and agree to within about 1 cm^{-1} with the transitions ($01^10 \rightarrow 000$) and ($10^00 \rightarrow 01^10$) of the CO_2 molecule in the ground electronic state. There are other bands in this region as shown in Fig. 1. Relative to the 4.4μ band the intensities of the bands are quite low and it is not surprising that some earlier workers were unable to detect them. We have also repeated the study of the emission of hot CO_2 gas streaming from a furnace at about 1400°K. The emission spectrum is compared to that of the flame in Fig. 1.

To determine the absorption spectrum of the flame, radiation from a Globar was modulated and passed through it. In this way the emission from the flame itself is eliminated except for random intensity variations. Absorption bands are found at 2.8, 4.4, 14.1, and 14.95μ of which only the two fundamentals are strong.

Further work on the CO-oxygen and other flames is being conducted and a more complete report will be made in the future. We wish to express our thanks to Dr. E. K. Plyler of the National Bureau of Standards who has shown us the results of similar studies on the Bunsen flame[2] and who reports finding the long wave-length bands of CO_2.

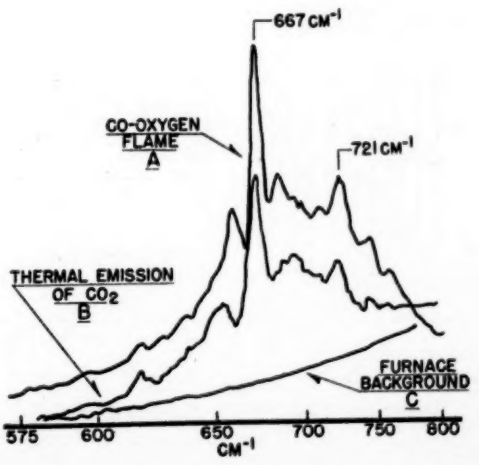

FIG. 1. Curve A: Emission from CO-oxygen flame in 15μ region. Slit width =0.3 mm. Curve B: Thermal emission from hot CO_2, uncorrected for background radiation from furnace, which is shown separately in curve C. Slit width =0.5 mm. All the curves were obtained with a KBr prism and are unsmoothed for noise variations; the maximum noise is about 2 percent of the peak deflection.

We are also indebted to Mr. B. W. Bullock for valuable help in experimental matters. In conclusion we express our appreciation to Professor D. M. Dennison and Dr. E. O. Salant for their interest and many valuable discussions.

* The work described in this letter has been supported by the Bureau of Ordnance, U. S. Navy, under Contract NOrd-7386.

[1] For an extensive bibliography, see Jean Lecomte, *Le Spectre Infrarouge* (Les Presses Universitaries de France, Paris, 1928), and A. G. Gaydon, *Spectroscopy and Combustion Theory* (Chapman Hall Limited, London, 1942).

[2] E. K. Plyler, J. Opt. Soc. Am. **37**, 984A (1947).

[3] H. Rubens and E. Aschkinass, Wied Ann. **64**, 584 (1898).

[4] W. E. Garner and C. H. Johnson, Phil. Mag. **3**, 97 (1927); C. R. Bailey and A. H. Lih, Trans. Faraday Soc. **25**, 29 (1929).

A Cylindrical Model for the Small Soap Micelle*

WILLIAM D. HARKINS

George Herbert Jones Chemical Laboratory, University of Chicago, Chicago 37, Illinois

December 16, 1947

THE model presented here (Fig. 1) is based on extensive papers on x-ray relations by Mattoon, Stearns, and Harkins,[1] and on a great deal of other work by Corrin, Oppenheimer, Mittelmann, Herzfeld, Roginsky, and Lind.

A quotation from a Cambridge University Symposium[2] (1947) is as follows:

> There are different schools of thought on these matters, for example McBain postulates two types of micelle, "ionic" and "neutral," Hartley only one, the "spherical" ionic micelle. The latter view is now generally accepted, and will be followed here.

McBain's views are expressed more accurately in his 1942 review.[3] His ionic micelle is spherical (adopted by Hartley) and his neutral micelle identical with Stauff's "Grossmizellen" or lamellar micelles.

Soap micelles are:

1. Small.

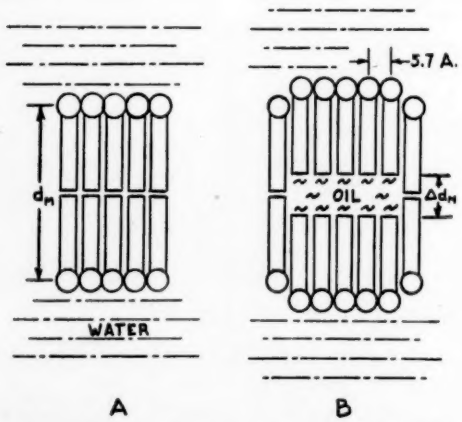

FIG. 1. Highly idealized cross section of a soap micelle. A. Without solubilized oil. B. With solubilized oil. The solubilization of an oil is found to increase the number of soap molecules in the micelle. Although a cylinder seems to represent most of the properties of the micelle as now known, it is imperfect in that it represents too large an interface at the side between hydrocarbon groups and water. Thus it seems not improbable that a model which lies between a cylinder and a cylindrical type of spheroid may be found to more perfectly represent the energy relationships. This would amount to a distortion of the side of the cylinder by means of which polar groups cover to some extent the non-polar hydrocarbon chains.

2. Not spherical and exhibit a thickness, as measured by a new x-ray *M*-band,[1a] equal to the double length of the molecule.

3. This thickness is increased by the solubilization of a non-polar oil, but not by alcohols or amines.

4. When a salt is added the critical micelle concentration is decreased, the micelle size increased by increase in the diameter of the cylinder, and the principle of ionic strength and Debye-Hückel theory becomes invalid (Corrin and Harkins[4]).

5. The number of *soap molecules* per micelle is increased by solubilization of an oil and by long chain alcohols and amines.

By diffusion Hartley[5] found the cetyl pyridinium chloride micelle to be small and to contain about 70 molecules. Our x-ray work on different detergents indicates sizes of this order, but both smaller and considerably larger.

Our earlier x-ray work appeared to favor the lamellar model of McBain and German investigators,[3b,c] which consists of 5 or 6 large double layers of soap with interlayers of water of definite thickness (τ) as calculated from our data for potassium myristate.

After a long and intensive study, in an endeavor to find a mechanism which would control the interlayer or "bound" water in this way, the writer concluded that there is no such mechanism, and that these water layers are non-existent, but instead each double layer of molecules is a micelle and moves *freely* as a large "molecule" through the solution, until a second critical concentration (*ca.* 7 percent for potassium myristate) is reached. Above this concentration each double layer is a micelle, but the micelles now come closely enough together to restrict their motion (libration or rotation) so that above this concentration the x-ray *I*-band appears. This is related to the distance between the micelles.

Calculations of the thickness (τ) of the oil layer solubilized by the micelle, as made by the writer, proved incorrect the conception of this process as related to the lamellar model. Those who developed this model assumed (McBain's review, p. 124) that the increment (Δd_I) in the long spacing due to the oil gives the thickness of the oil layer. The mean thickness (τ) should equal the volume of oil in the micelles divided by the area of the large double soap layers, which is known, since each pair of molecules occupies 28 sq.A. In calculations for *n*-heptane, triptane, and ethyl benzene the mean thickness (τ) was found at all concentrations of the oils to be only 0.4 as large as Δd_I. For example, for 3.5 percent *n*-heptane in 25 percent potassium laurate $\tau = 5.5$A but $\Delta d_I = 13.6$A or 2.5 times larger than it should be. It was concluded that Δd_I is not the distance

Percent soap	Water layer thickness τ in A
8	34
10	31.7
15	26.3
20	22.5
25	19.6
30	17.2
35	15.2

between layers in a lamellar micelle, but the change in the intermicellar distance (d_I).

With respect to solubilization, Corrin found that Hartley's spherical model gave much better agreement than this.

The cylindrical model is superior in that its height is measured by the *M*- or micelle thickness band, and it has a diameter which may be varied and can be calculated approximately at high concentrations from the *I*-band, or at low concentrations from light scattering (Debye).

In any model the energy relations make it essential to make the interface hydrocarbon chains-water as small as possible, which means that the cylinder may be somewhat distorted at the side to give coverage of the hydrocarbon chains by a few polar-ionic groups of the soap. However, the model is essentially a cylinder with these groups at the ends.

* This investigation was carried out under the sponsorship of the Reconstruction Finance Corporation, Office of Rubber Reserve, in connection with the government's synthetic rubber program.

[1a] R. W. Mattoon, R. S. Stearns, and W. D. Harkins, submitted for publication (September, 1947); [b] *ibid.* J. Chem. Phys. **15**, 209 (1947); [c] W. D. Harkins, R. W. Mattoon, and R. Mittelmann, *ibid.* **15**, 763 (1947).

[2] A. E. Alexander, *Colloid Science. A Symposium* (Chemical Publishing Company, Inc., Brooklyn, 1947), p. 43. McBain now considers the "neutral" micelle to be the somewhat ionized "large lamellar micelle."

[2a] J. W. McBain, *Advances in Colloid Science* (Interscience Publishers, Inc., New York, 1942), edited by E. O. Kraemer, p. 124, for extensive references to work on the "large lamellar micelle" see: [b] W. D. Harkins, R. W. Mattoon, and M. L. Corrin, J. Am. Chem. Soc. **68**, 220 (1946), and [c] J. Colloid Sci. **1**, 105 (1946).

[4] M. L. Corrin and W. D. Harkins, J. Am. Chem. Soc. **68**, 679, 683 (1947).

[5] G. S. Hartley and D. M. Runnicles, Proc. Roy. Soc. **A168**, 420 (1938).

The Solubility of Sodium Soap in Organic Solvents

A. Bondi
Shell Development Company, Emeryville, California
November 18, 1947

THE solubility of sodium palmitate and sodium stearate in organic solvents has been determined by several members of the Stanford Group.[1-3] These data seem rather difficult to correlate with each other or with other solubility data. The latter is usually most fruitful if the comparison is made on the basis of Hildebrand's relation:

$$\ln a_2 = -\frac{\Delta H_f}{R}\left(\frac{1}{T}-\frac{1}{T_f}\right),$$

where ΔH_f the heat of fusion (or transition) and T_f the melting (or transition) temperature.[4,5]

In view of the fact that the sodium soaps exhibit not only a melting point but a series of transition points in the solid state, the ideal solubility curve changes its slope at as many points. The transition points and the transition heats have been determined by Vold.[6] It is therefore possible to construct the ideal solubility curve of these soaps. Such a curve for sodium palmitate is shown—marked "ideal"—on Fig. 1. The other curves on the same figure are the so-called T_i curves,[7] giving the temperature at which the isotropic melt changes into an anisotropic liquid crystal. The proximity of several curves to the Raoult's law curve is rather surprising, since one usually associates "ideality" with simpler physical behavior. It should be noted that the slope of all solutions in hydroxylic compounds deviates in the low temperature (<180°C) region but little from the slope of the ideal curve, while the slope of the other solutions, particularly in hydrocarbons, is very much steeper. This suggests that the excess free energy of mixing with the alcohols consists of a negligible heat of mixing and a strongly negative entropy of mixing. The solution of soap in hydrocarbons requires on the other hand both rather large (negative) enthalpy and entropy changes. One would hardly have expected that the solubility of stearic acid in similar solvents deviates more from ideality than that of soap, as is evident from the data on Fig. 2. This applies particularly to alcoholic solutions.

In the high temperature region all solutions behave quite similarly in exhibiting solid solution phenomena, as is also apparent in visual observation of these systems. The effect of chemical structure of the solvent on the shape of the solubility curve is sometimes quite marked, as e.g., in the case of the cresols. The position of *p*-cresol solutions is given on the graph. The solubility curve of soap in *o*-cresol, on the other hand, is practically identical with that of cetyl alcohol and has, therefore, not been drawn in. In other cases there is little specificity as is exemplified by the solubility in cyclohexane and in low mole weight aromatic hydrocarbons, or cetane and white medicinal oil.

The humps in the solubility curves which are observed in soap solutions in cyclic (low molecular weight) hydrocarbons, in water, and in glycerol are somewhat reminiscent of the shape of solubility curves of systems forming two immiscible liquid phases in a certain temperature range. While presentation of the soap solubility data in the

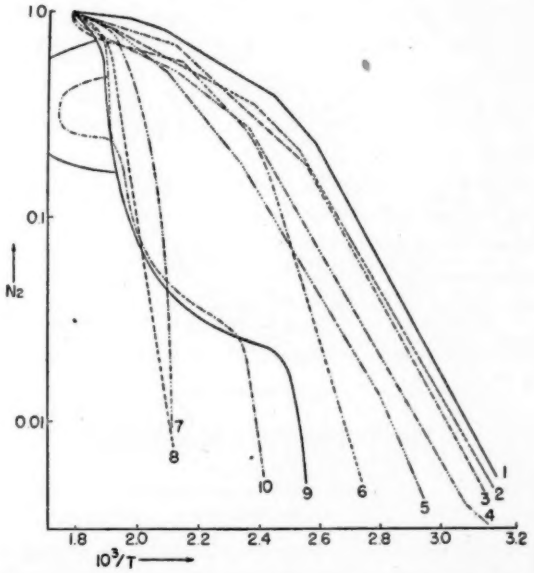

FIG. 1. Solubility of sodium palmitate in various organic solvents (from data of references 1, 2, 3) compared with ideal solubility, curve (1).

(1) Ideal solubility
(2) *p*-cresol
(3) Diethylene glycol
(4) Ethyl alcohol
(5) Cetyl alcohol
(6) *n*-butylamine
(7) *n*-cetane
(8) Nujol
(9) Cyclohexane, sodium stearate in
(10) Ethylbenzene, sodium stearate in

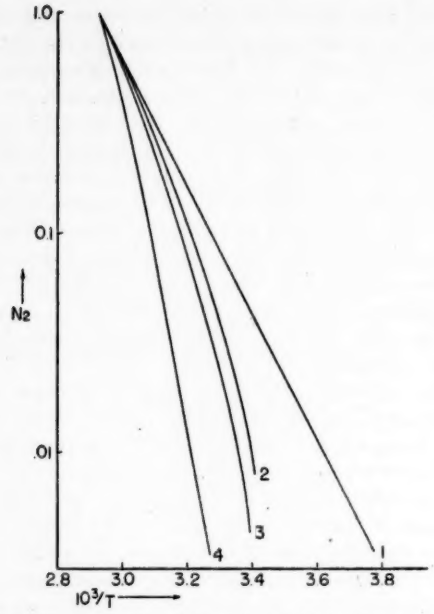

FIG. 2. Solubility of stearic acid in various organic solvents (from data of reference 8) compared with ideal solubility, curve (1).
(1) Ideal solubility
(2) Cyclohexane
(3) *n*-butyl alcohol
(4) Methyl alcohol

manner shown in Fig. 1 simplifies the discussion of these complicated systems, it leaves many phenomena still unexplained.

The writer was unable to find any solubility data of simpler compounds undergoing phase transition in the solid state, such as camphor, C_2Cl_6, and the like, to compare with the apparently more thoroughly studied soap systems.

The writer wishes to acknowledge discussions with Professor J. W. McBain and Dr. O. Redlich, which led to this work.

[1] R. D. Vold, C. W. Leggett, Jr., and J. W. McBain, J. Phys. Chem. **44**, 1058 (1940).
[2] C. W. Leggett, Jr., R. D. Vold, and J. W. McBain, J. Phys. Chem. **46**, 429 (1942).
[3] G. H. Smith, Ph.D. Thesis, Stanford, 1946.
[4] J. H. Hildebrand, *Solubility of Non-Electrolytes* (Reinhold Publishing Corporation, New York, 1936).
[5] A. Bondi, J. Phys. Chem. **51**, 891 (1947).
[6] R. D. Vold, J. Am. Chem. Soc. **63**, 2915 (1941).
[7] J. W. McBain, L. H. Lazarus, and A. V. Pitter, Zeits. physik. Chemie **A147**, 87 (1930).
[8] C. W. Hoerr and A. W. Ralston, J. Org. Chem. **9**, 329 (1944).

The Triplet State of Ethylene

D. P. CRAIG
University College, London, England
December 9, 1947

IN dealing with the separation between the ground and triplet states of ethylene, Laidler[1] has drawn attention to the remarkable agreement existing between the experimental value of 74 kcal. obtained by Lewis and Kasha,[2] and the calculated value of 72 kcal. found by Hartmann[3] by the method of antisymmetrical molecular orbitals.

It is not, however, indicated in Hartmann's paper what values were used for the various integrals that occur, and in treating the same problem by the same approximation during the course of other work, the writer has obtained a considerably greater value for the singlet-triplet separation. Using values for the integrals obtained by interpolation between the values given by Sklar and Lyddane,[4] the singlet-triplet separation comes out to be 95 kcal. or greater, the exact value depending on the assumptions made about the configuration of the triplet state. Therefore, there is probably not the good agreement between calculated and experimental values that Hartmann's value suggests. Hartmann's value for the excited singlet state, given in the same paper, appears to be in error due to the use of a wrong wave function, and the corrected value again proves to be considerably greater than the experimental.

The values for the integrals used in these calculations are so closely in agreement with those given recently by Griffing[5] that there is no need to quote them here.

[1] K. J. Laidler, J. Chem. Phys. **15**, 712 (1947).
[2] G. N. Lewis and M. Kasha, J. Am. Chem. Soc. **66**, 2100 (1944). These authors commented that Hartmann's value was improbably low.
[3] H. Hartmann, Zeits. physik. Chemie **B53**, 96 (1943).
[4] A. L. Sklar and R. H. Lyddane, J. Chem. Phys. **7**, 374 (1939).
[5] V. Griffing, J. Chem. Phys. **15**, 421 (1947).

Erratum: Infra-Red Spectrum and Depolarization Factors of the Raman Lines of Spiropentane and the Raman and Infra-Red Spectra of 1,1-Dimethylcyclopropane, 1-Methylcyclobutene, and Methylenecyclobutane

FORREST F. CLEVELAND
Department of Physics, Illinois Institute of Technology, Chicago 16, Illinois
AND
M. J. MURRAY AND W. S. GALLAWAY
Universal Oil Products Company, Chicago, Illinois

[J. Chem. Phys. **15**, 742 (1947)]

DUE to a faulty distillation and an oversight, the infrared spectrum of methylenecyclobutane reported in Table IV of the above paper contains spurious bands at 782, 990, 1051, and 1155 cm^{-1}, which correspond to the prominent bands of spiropentane. If these are deleted, the remaining bands are those of methylenecyclobutane. (It should also be noted that the strongest band of spiropentane is nearly coincident with the 877-cm^{-1} band of methylenecyclobutane.) The Raman data, however, were obtained with another sample which was pure enough not to show the strongest line of the spiropentane.

This correction of the experimental data necessitates the following changes in the assignments for eight of the weak bands: the combination or overtone frequencies whose values are given in the last column of Table IV as 801, 1509 or 1510, 1883, 2013, 2061 or 2063, 2118 or 2109, 2177 or 2188, 2310, and 2416 should be deleted; they may be replaced by the combination frequencies $1167-373=\mathbf{794}$, $354+1167=\mathbf{1521}$, $728+1167=\mathbf{1895}$, $954+1070=\mathbf{2024}$, $895+1167=\mathbf{2062}$, $954+1167=\mathbf{2121}$, $1029+1167=\mathbf{2196}$, and $1029+1395=\mathbf{2424}$. Thus eight of the nine carbon skeleton frequencies and eighteen of the twenty-four C−H frequencies are now tentatively assigned.

An Equation of State for Gases at Extremely High Pressures and Temperatures from the Hydrodynamic Theory of Detonation

STEWART PATERSON
Imperial Chemical Industries Limited, Explosives Division, Stevenston, Scotland
December 1, 1947

THE thermal equation of state for any two-parameter substance is included in the general form:

$$pv = nRT + p\alpha(v, T),$$

where p, v, T, n, R represent pressure, specific volume, temperature, number of moles per g, and gas constant per mole, respectively. In attempting to determine the equation of state for gases at high pressures and temperatures from the observed velocities of detonation (D) of explosive compounds, at various densities (Δ), P. Caldirola[1] has assumed that the "covolume" $\alpha(v, T)$ can be regarded under such conditions as a function of v alone. This assumption, criticized by S. R. Brinkley,[2] finds support in a recent valuable paper by M. A. Cook[3] on the same topic. Cook's arguments in favor of the temperature independence of α are partly of an *a posteriori* nature, deduced from the coincidence of the $\alpha(v)$ curves for explosives yielding widely different calculated detonation temperatures, and as such appear to carry considerable weight. The relative constancy of the theoretical second virial coefficient between, say, 2000 and 6000°K provides independent support for the same view, which is largely shared by the writer.

Cook, however, also claims to have evaluated α directly from the experimental detonation velocities, not only on the assumption that $\alpha = \alpha(v)$, but also by an independent and exact method which allows for possible variation with T. If this were so, it would of course enable one to dispense with extraneous and *a posteriori* arguments regarding the temperature dependence of α. However, it does not seem that Cook has in fact carried out such an "exact" solution, nor indeed that it is possible to do so on the basis of experimental velocities for one explosive alone. For since $\alpha(v)$ can evidently be determined to fit the observed velocities for one explosive, these velocities alone do not allow us to discriminate between such a solution and any alternative solution, e.g., Kistiakowsky and Wilson's[4] in which α depends also on T.

Cook's position is somewhat obscured by the large number of interdependent equations which he writes down. The solution depends, in fact, upon Cook's Eqs. (2), (6), (9), and (16), together with *any two* of (10), (11), (12), and (13); for these last four are not independent, any two being immediately deducible from the remaining two. Cook ignores Eq. (9), which amounts to discarding the Chapman-Jougnet condition. Then, since W appears only in (2) and p_2 only in (6), we can get these equations also aside, leaving (16) and *any two* of (10), (11), (12), and (13) to be solved for T_2, v_2, α, β.

These are apparently the equations from which it is proposed to deduce T_2, v_2, α, β by successive approximation. Cook evaluates α from (13) and then v_2 from (12), thereafter calculating β from (11). Since (11) follows at once from (12) and (13), this process would clearly not be expected to define a unique solution. On the other hand, if Cook commenced these "successive approximations" with the values of β given by "method b" which as he says preceded "method a" in the development of the theory, it seems natural that method b should be confirmed.

As indicated above the clearest proof that Cook has not accomplished an exact solution, and that such is not possible on the basis of the experimental velocities for one explosive alone, is given by the fact that equations of state markedly different from his own are capable of giving good agreement with observed velocities. Since Cook's analysis is based solely on the $D(\Delta)$ relation, it is clear, therefore, that this relation alone cannot lead to a unique equation of state. If it does not provide proof that Kistiakowsky and Wilson's equation, for example, is not correct, it evidently cannot prove that an alternative equation is correct.

Regarding "method b" itself, a further point may be made. It is stated by Caldirola, and seems implied by Cook, that one can "unequivocally" determine $\alpha(v)$ from the known $D(\Delta)$ relation. One of the five equations available to define v_2, p_2, T_2, W, and α is however a differential equation in α, and the solution therefore would be expected, in general, to embrace not one only but an entire family of $\alpha(v)$ curves. That this is in fact the case may be confirmed by a step-by-step integration, as distinct from the method of successive approximation used by Cook, which should and does lead to the envelope of the family. Physical considerations certainly appear to favor this singular solution, but the point seems to deserve attention.

[1] P. Caldirola, J. Chem. Phys. **14**, 738 (1946).
[2] S. R. Brinkley, J. Chem. Phys. **15**, 113 (1947).
[3] M. A. Cook, J. Chem. Phys. **15**, 518 (1947).
[4] G. B. Kistiakowsky and E. B. Wilson, OSRD Report 69.